Evaluation of Steric Repulsion at *peri*-Positions as Non-Electronic Activation on Aromatic Rings

by

Annisa Indah Reza

Student ID Number: 1256001

A dissertation submitted to the
Engineering Course, Department of Engineering,
Graduate School of Engineering,
Kochi University of Technology,
Kochi, Japan

in partial fulfillment of the requirements for the degree of
Doctor of Philosophy

Assessment Committee:

Supervisor: Nagatoshi Nishiwaki
Co-Supervisor: Kazuya Kobiro,
Co-Supervisor: Akitaka Ito
Committee Member's Name: Shotaro Hayashi
Committee Member's Name: Toshiyuki Kawaharamura

March 2025

Acknowledgments

I sincerely acknowledge every support and help I received during my study and the preparation of this dissertation.

Foremost, my deepest gratitude is granted to my supervisor, Prof. Nagatoshi Nishiwaki, for showing faith and patience in guiding me from the beginning of this journey. His encouragement, ideas, recommendations, and warm gestures have manifested positively, allowing me to be more confident in whatever challenges I encounter. I cannot express how lucky I am to have met, joined, and advised by you for the past four years.

I am deeply grateful to my co-supervisors, Prof. Kazuya Kobiro and Prof. Akitaka Ito, whose ideas and comments have remarkably opened room for improvement in my research. I also thank Prof. Shotaro Hayashi and Prof. Toshiyuki Kawaharamura for their valuable feedback on my research.

My warm thanks and appreciation also go to everyone in Nishiwaki Laboratory. Dr. Kento Iwai, who, through many discussions with him, has assisted me during confusing times. For my fellow master's and bachelor's students who shared the same moments with me, I could not ask for better companionship than what you have offered by surrounding me with support, laughter, and cherishable memories.

I am also thankful to I-House and Indonesian members in Kochi for their companionship and good friendship. The same goes for all International Relations Section staff (IRC) staff. Their excellent dedication to work has made daily inquiries and academic assistance full of pleasurable conversations.

Finally, I thank my family and friends in Indonesia for their love and prayers, which must have miraculously contributed to my studies. Special thanks to my sister, Nurul Gayatri Indah Reza, who, through all her words, I dare to start, endure, and finish this journey.

Disclaimer

I hereby declare that the work in this dissertation was carried out following the Regulations of Kochi University of Technology. The dissertation contains no materials previously published or written by other people except where references are applied. Any views expressed in the dissertation belong to the author and do not necessarily represent those of Kochi University of Technology. The passages in some chapters in this dissertation have been quoted verbatim from the previous publications that were initially written by the author, listed as follows:

Journal Papers:

1. **Reza, A. I.**; Iwai, K.; Nishiwaki N.

   A Study of the Correlation between the Bulkiness of the *peri*-Substituents and the Distortion of a Naphthalene Ring.

   Molecules **2023**, *28*, 5343 (13 pages).

2. **Reza, A. I.**; Iwai, K.; Nishiwaki N.

   Non-Electronic Activation of Anthracenes Using Steric Repulsion of the 9-Substituent with Chloro Groups at the *peri*-Positions.

   Asian Journal of Organic Chemistry **2024**, e202400381 (5 pages).

Proceeding:

3. **Reza, A. I.**; Iwai, K.; Nishiwaki N.

   Evaluation of the Bulkiness of *peri*-Substituents Distorting 1,8-Dimethylnaphthalene Framework.

   The 8th International Symposium on Frontier Technology (ISFT), pp. 2–12

   July 27th – 28th **2024**, Kami, Kochi, Japan

Conferences:

1. **Reza, A. I.**; Iwai, K.; Nishiwaki N.

   Steric Repulsion between *peri*-Substituents Distorting Naphthalene Ring.

   The 103rd Annual Meeting of the Chemical Society of Japan

   March 22nd – 25th **2023**, Chiba, Japan.

2. **Reza, A. I.**; Iwai, K.; Nishiwaki N.

   Non-Electronic Activation on Anthracene Ring by Steric Repulsion between Substituents.

   The 104th Annual Meeting of the Chemical Society of Japan

   March 18th – 21st **2024**, Chiba, Japan.

3. **Reza, A. I.**; Iwai, K.; Nishiwaki N.

   Evaluation of the Bulkiness of *peri*-Substituents Distorting 1,8-Dimethylnaphthalene Framework.

   8th International Symposium on Frontier Technology

   July 27th **2024**, Kochi, Japan

4. **Reza, A. I.**; Iwai, K.; Nishiwaki N.

   Non-Electronic Activation using Steric Repulsion on *peri*-position between Substituents and Chloro groups: 1,8-Dichloroanthracene Framework.

   26th IUPAC International Conference on Physical Organic Chemistry (ICPOC)

   August 18th – 22nd **2024**, Beijing, China.

The author originally wrote all the quoted sources.

[Supplementary]

Review Article:

1. **Reza, A. I.**; Iwai, K.; Nishiwaki N.

   Recent Advances in Synthesis of Multiply Arylated/Alkylated Pyridines.

   The Chemical Record **2022**, *22*, e202200099 (20 pages).

   Selected as a Front Cover

Abstract

The chemical and physical properties of organic molecules are always influenced by a series of steric rules (steric effects) alongside electronic effects. Even in a modest implementation of valence shell electron pair repulsion (VSEPR) theory, the geometric shape of the sp^3 hybridized carbon node is normalized as a tetrahedral, following how much electron repulsion from hydrogen as substituents can be minimized. When substituents in a molecule, either atoms or groups of atoms, are at a proximate distance, the repulsion force and consequence become more intense, disturbing the energetically minimized bond angles. Eventually, the steric effects determine not only molecular shapes but also molecular conformation, stereochemistry, and potential reaction preferences, as they influence physical and chemical properties even without electronic influences.

Six-membered aromatic rings, such as benzene, are well-known for their aromaticity features, such as rigidity, planarity, structural simplicity, low stereochemical diversity, and high stability. As a result, a significant amount of research has been dedicated to enhancing aromatic frameworks, leading to the development of more complex structures. For this purpose, activating the aromatic ring accompanied by de-aromatization is a key step. While the most used approach is an electronic activation, limited efforts have been made to study de-aromatization related to non-electronic force in highly strained molecules, presumably due to the synthesis of such compound is not easily achieved. Fairly, when a sterically demanding group is introduced in an aromatic ring, out-of-plane deformation may distort aromaticity, generating new physical and chemical properties that can be quantified and evaluated, which is one of the still challenging projects.

In this study, I examined the steric repulsion between *peri*-substituents. These *peri*-substituents are situated at a closer distance from one another than those at the *ortho*-position. Consequently, enhancing the bulkiness of the *peri*-substituents serves as an effective strategy for inducing ring distortion, ultimately resulting in non-electronic activation of the aromatic ring.

In the first case, horizontal and vertical distortions occurred when the **1,8-dimethylnaphthalene framework** was adjusted with a bulky bromo atom. As the bulkiness increased, the vertical distortion by torsion angle was prominently detected over horizontal ones, such as elongation and suppression of bond length corresponding to that steric interaction (Figure 2-3). Despite the change in geometrical features, reactivity evaluation under hydrogenation and nitration reaction was partially correlated to the experienced ring deformation of each evaluated naphthalene derivative.

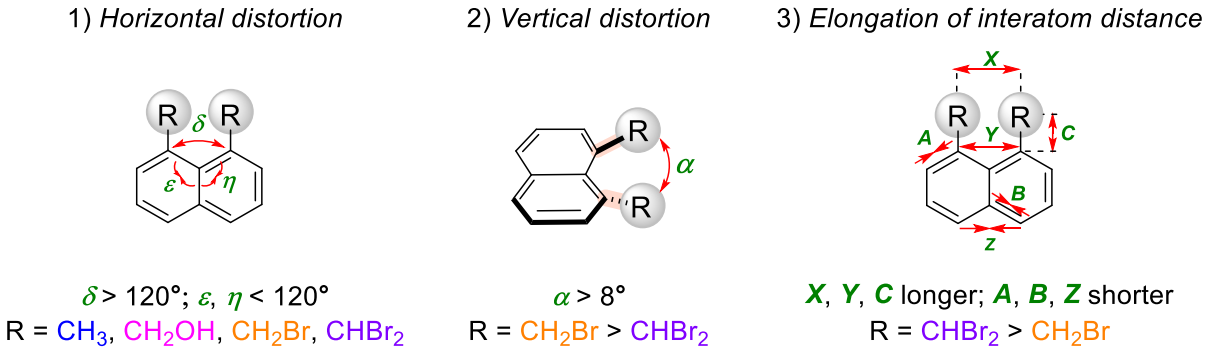

Figure 2-3. Three observed types of distortion of the naphthalene ring.

To further extend the concept of *peri*-interaction into the three-ring aromatic system of anthracene, the 9-substituted **1,8-dichloroanthracene framework** was selected. An intense repulsion with the two chloro atoms created geometrical distortions of the central ring by embedding bulkier substituents at the 9-position. As expected, the strain released by steric repulsion in a series of 1,8,9-substituted anthracenes gave a massively elevated out-plane deformation along with horizontal distortions. Regarding non-electronic activation, the

reactivity test under a Diels–Alder reaction showed a linear increase that resembled the degree of vertical distortions, emphasizing the initial proposition where geometrical deformation influenced de-aromaticity. These results indicated that steric repulsion between crowded 1,8,9-substituents disrupts the coplanarity of the central ring of anthracene, reducing its aromaticity and leading to the creation of more activated compounds compared to 1,8,10-substituted anthracenes (Figure 3-9).

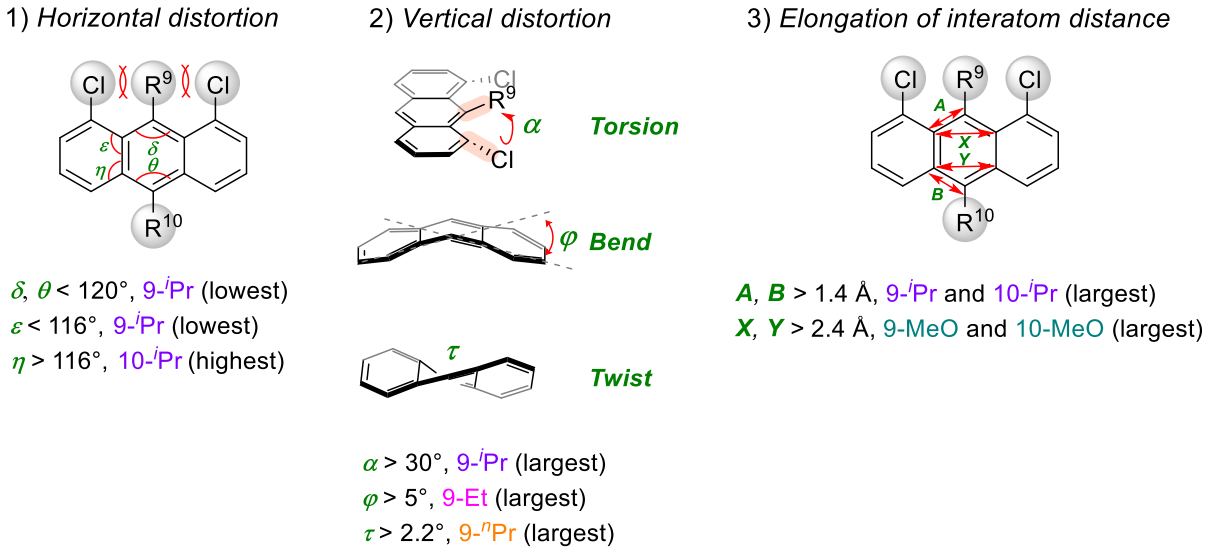

Figure 3-9. Three observed types of distortion of the anthracene ring.

Content

Chapter 1: General Introduction

Part I: Non-planar Aromatic and Aromaticity

1. Origin of Non-Planar Aromatic Compounds

In a prevalent understanding of chemistry, aromatic compounds are often characterized to fit criteria with structures that appear as cyclic, conjugated, and planar systems with [4n+2] π-electrons according to the Hückel rule, which is perfectly adapted by benzene. However, at the advanced level of study, some mentioned characters cannot be fully adapted by existing structures, especially where heterocyclic and organometallic compounds are involved.[1] Particularly in the geometry aspect, some benzenoids in higher analogs of polycyclic aromatic hydrocarbons (PAHs) exist despite being unshared in the same ring plane, leading to the widely acknowledged term of "non-planar aromatic".[2]

Synthetically, there are two common strategies to obtain non-planar PAHs: (1) insertion of the inner ring into a hexagonal aromatic system, reforming in-plane shape to a bowl-shaped C–C bond, and (2) introduction of steric strain by peripheral atom crowding.[3] The first strategy found in the circulene class where the inner ring ranged from four-membered as found in quadrannulene,[4a] five-membered as in corranulene,[4b] six-membered as in coronene[4c] or hybrid-membered ring such as summanene[4d,e] (Figure 1-1a). Secondly, disturbing planarity in planar aromatic PAH systems is achievable by allowing non-bonding interaction between spatially close substituents, promoting bending or twisting structures as recorded for naphthalenes,[5a] anthracene,[5b] and helicene[5c] (Figure 1-1b).

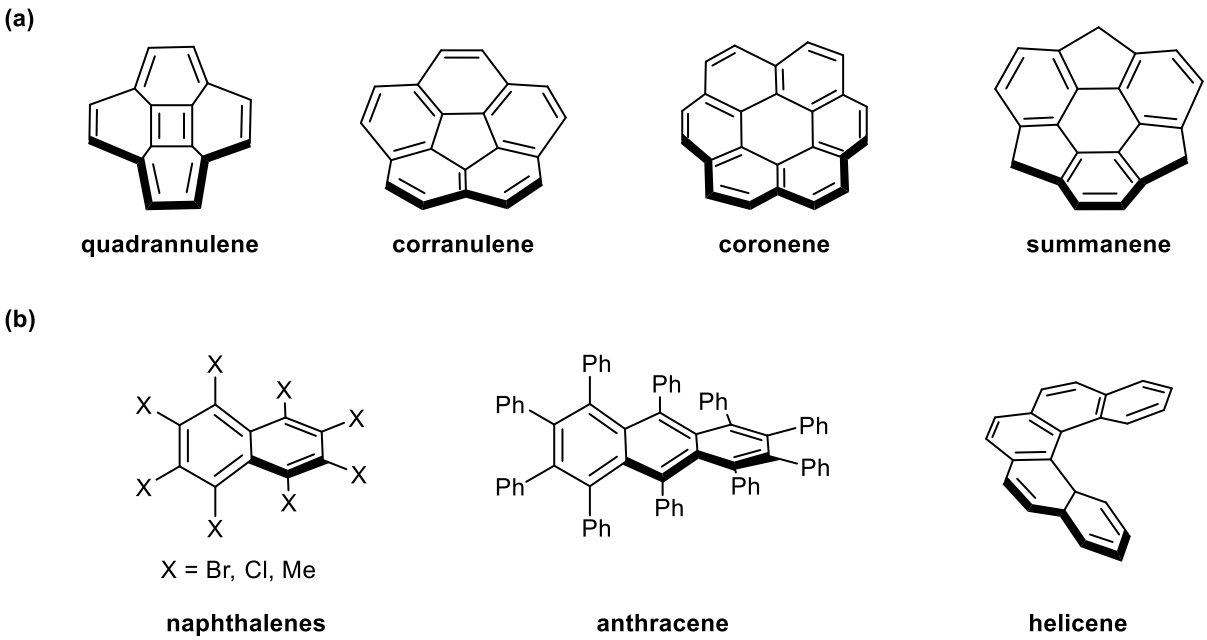

Figure 1-1. Geometry of non-planar polycyclic aromatic hydrocarbons (PAHs).

2. Aromaticity and De-aromaticity

Since the discovery of benzene by Faraday in 1825,[6] enumerative studies have been conducted to expand the definition, concept, and evaluation of aromaticity that deviates from the classic benzene ring.[7] However, the definition of aromaticity remains debatable following the massive surge of novel organometallic and inorganic compounds. According to the IUPAC definition,[8] *"The concept of the spatial and electronic structure of cyclic molecular systems displaying the effects of cyclic electron delocalization which provide for their enhanced thermodynamic stability (relative to acyclic structural analogs) and tendency to retain the structural type in the course of chemical transformations. A quantitative assessment of the degree of aromaticity is given by the value of the resonance energy. It may also be evaluated by the energies of relevant isodesmic and homodesmotic reactions. Along with energetic criteria of aromaticity, important and complementary are also a structural criterion (the lesser the alternation of bond lengths in the rings, the greater is the aromaticity of the molecule) and a magnetic criterion (existence of the diamagnetic ring current induced in a conjugated cyclic*

molecule by an external magnetic field and manifested by an exaltation and anisotropy of magnetic susceptibility). Although originally introduced for the characterization of peculiar properties of cyclic conjugated hydrocarbons and their ions, the concept of aromaticity has been extended to their homoderivatives (see homoaromaticity), conjugated heterocyclic compounds (heteroaromaticity), saturated cyclic compounds (σ-aromaticity) as well as to three-dimensional organic and organometallic compounds (three-dimensional aromaticity). A common feature of the electronic structure inherent in all aromatic molecules is the close nature of their valence electron shells, i.e., double electron occupation of all bonding molecular orbitals (MOs) with all antibonding and delocalized nonbonding MOs unfilled".

With this long-covered explanation of aromaticity, the quantitative accepted features for evaluating aromaticity primarily include the following assessments:[9]

a. Geometric, discuss geometrical deviation such as bond length and planarity
b. Magnetic, discuss proton chemical shift, magnetic susceptibility, and ring currents
c. Energetic, discuss resonance energy (RE) and the aromatic stabilization energy (ASE)
d. Electronic, discuss electron localization function (ELF) and electron sharing indices (ESI)
e. Reactivity, lower reactivity, tendency of electrophilic aromatic substitution than addition reaction

Determining which parameter to prioritize in defining and evaluating aromaticity is challenging. Zhu has suggested that electronic indices should be given prominence, as electron delocalization comes first in the definition and is undeniable evidence in all aromatic compounds.[10] However, electron delocalization is arduous to observe experimentally, making magnetic and geometric criteria preferable since NMR and X-ray crystallography can quickly determine them.[11] Still, some magnetic and geometric cases were inconsistent with thermodynamic stabilization energy criteria. On the other hand, chemical reactivity in aromatic compounds may be implicated by various factors such as strain, molecular orbital energy level

boundaries, and oxidation states, making it puzzling to establish one single trend. Eventually, the term aromaticity is not directly observable, but the consequences or properties related to it are, either experimental or theoretical. Interestingly, providing multidimensional equivalent explanations of aromaticity for one structure is considered unrealistic.[12]

Despite the extended definition by IUPAC on aromaticity, neither de-aromatization nor de-aromaticity exists, although everybody seems to understand what that term refers to. De-aromatization is often used to describe the loss of aromaticity properties when aromatic systems are transformed to partially unsaturated or completely saturated system.[13] Significant progress in developing and utilizing de-aromatization techniques cover metal-mediated,[14] photochemical,[15] nucleophilic reactions,[16] radical dearomatizations,[17] and even enzymatic approaches.[18] In fact, the de-aromatization of simple benzene rings into diverse alicyclic structures has evolved sophisticatedly over the last centuries. The challenge has now shifted to creating pharmaceutical-oriented structures, natural-product-like structures, and other fine chemicals that remain attractive (Figure 1-2).[19]

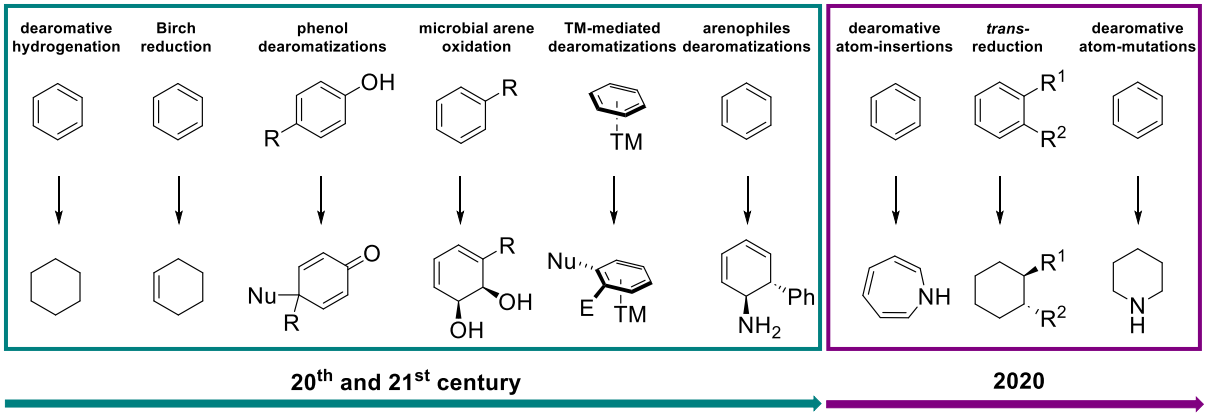

Figure 1-2. The representative evolvement of de-aromatization in the benzene ring.

2.1. Geometry Criterion

The technique for determining molecular structure, X-ray diffraction, was developed in the 1920s and remains the primary method for studying the geometry of aromatic compounds. An abundance of structural data has led scientists to create quantitative descriptors of

aromaticity based on experimental bond lengths, which are now comparable with computationally obtained molecular geometries. A notable property of aromatic systems is their tendency to equalize bond lengths, as evidenced when comparing non-aromatic and aromatic systems such as butadiene, benzene, and cyclopentadiene (Figure 1-3). The alteration of bond length can effectively be used to evaluate the decrease of aromaticity in cyclic systems.[20]

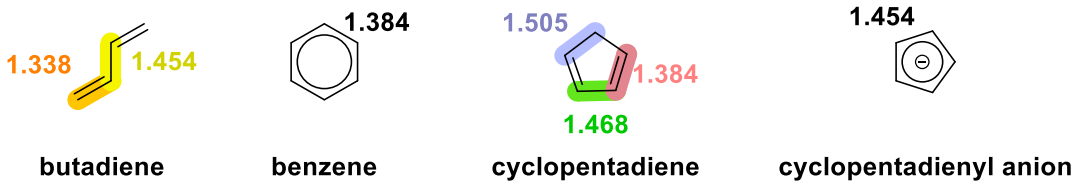

Figure 1-3. Bond length (Å) in butadiene (experimental),[21] benzene (D_{6h} symmetry, experimental),[21] cyclopentadiene, and cyclopentadienyl anion (computed at B3LYP/6-311++G (d,p)).

When geometry criterion is considered in evaluating non-planar geometry and non-rigidity of polycyclic aromatic system, it directly correlates with the interaction between substituents. Due to high conformational flexibility, the aromatic ring's deformability of six-membered polycyclic conjugated systems is inclined to experience out-of-plane deformation.[22a] Consequently, a decrease in aromaticity degree corresponds to increased ring flexibility. In fact, several computational and experimental studies demonstrate that the aromaticity of a cyclic conjugated system is firmly bound to the deformability of the ring found in benzene, naphthalene, anthracene, and phenanthrene rings.[22b]

2.2. Magnetic Criterion

Molecules with cyclic conjugated π-electron systems, such as benzene and PAHs, exhibit more diamagnetic susceptibility than noncyclic conjugated π-systems. The most popular method for quantifying aromatic compounds' magnetic properties is granted to the nucleus-independent chemical shift (NICS) method. Schleyer introduced NICS in 1996 and described

it as the negative value of the computed total isotropic shielding at a chosen point in space.[23] The significantly negative (i.e., magnetically shielded) NICS values in the interior positions of rings or cages indicate the presence of induced diatropic ring currents or "aromaticity." In contrast, positive values (i.e., deshielded) at each point are close in denoting paratropic ring currents or "antiaromaticity".[24] The representation of the NISC values on the benzene ring corresponds to its magnetic character within the range distance above the ring (distance in Å), shown in Figure 1-4.

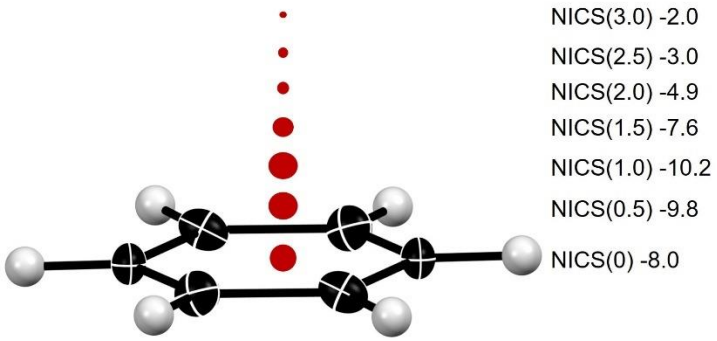

Figure 1-4. The NICS values are computed at the GIAO-B3LYP/6-311+G*// B3LYP/6-311+G* level). The red dots denote a diatropic character whose dot size is linear with the NICS magnitude. Image is reprinted with permission. Copyright (2024) from American Chemical Society.[24]

The NICS(0) value contains the local paramagnetic character from both σ-C−C and C−H of the ring, contributing to the value being more negative, which would be an insufficient descriptor of aromaticity (Figure 1-5a). Hence, $NICS_{zz}$ (the out-of-plane component of NICS) corresponds to the principal axis perpendicular to the ring plane, either above $(NICS(1)_{zz})$ or below $(NICS(-1)_{zz})$ geometric center of the ring came up as the preferred measure of the aromaticity of aromatic system. $NICS(1)_{zz}$ assumes that the effect of the local circulations and the s-framework is negligible at 1 A˚ above the ring plane, while the contribution of p-electrons is maximized at this height (Figure 1-5b).[25] In addition, measuring $NICS_{zz}$ covering a particular distance in a scanning manner is beneficial to visualize the strength of diatropic or paratropic

currents (Figure 1-5c).[26]

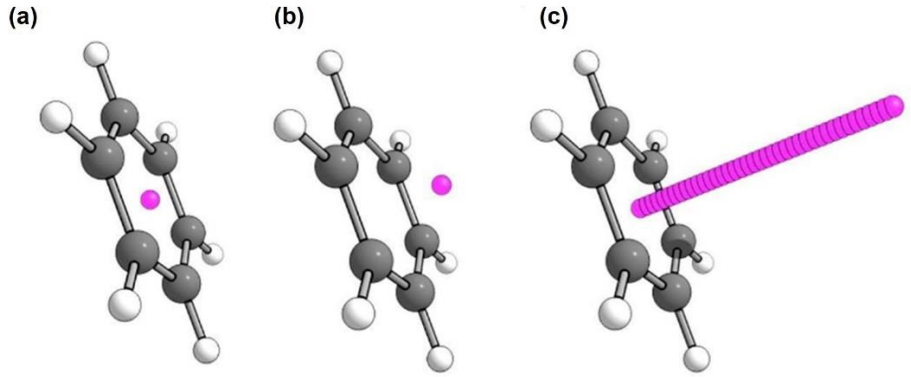

Figure 1-5. Comparison of different NICS probe placements for benzene: a) NICS(0); b) NICS(1); c) NICS-Scan (a series of NICS probes along a line perpendicular to the geometric center of the molecule, spaced at 0.1 Å intervals). Image is reprinted with permission from Elsevier Science (License Number: 5934590014505).[27]

All NICS values describe only local aromaticity (local ring current) for a particular ring where the probe atom or "dummy" atom is positioned. Therefore, NICS could not simultaneously predict the whole aromaticity of PAHs in an entire ring system. Another shortcoming is that NICS is an entirely theoretical concept with non-experimental properties, making it greatly dependent on the level of theory applied.[28] Despite this, NICS is still widely recognized as a valuable tool for assessing aromaticity. It allows for a modest review of critical features such as ring size, electronic structure, and the nature of the involved atoms that significantly influence aromaticity.[29]

2.3. Energetic Criterion

In 1933, Pauling and Sherman proposed the first quantitative description of aromaticity with a thermodynamic concept called resonance energy (RE).[30] RE is described as the energy that causes the π-delocalized compound to be more stable than its hypothetical olefin analog, in which the latter appeared as electrons fully localized in alternating single and double bonds. The most conventional RE explanation is illustrated as the disparity of hydrogenation energy

between hypothetical 1,3,5-cyclohexatriene that fits the Kekulé structure and the actual aromatic structure of benzene (Figure 1-6).[31] According to the experimental change on enthalpy (ΔH) for cyclohexene (ΔH_1) and benzene (ΔH_4) to cyclohexane in a hydrogenation reaction, 1,3,5-cyclohexatriene (ΔH_3) can be theoretically calculated. Since this hypothetical structure could not be prepared as it would immediately transform into benzene, thus, the estimation of how much benzene gains stabilization/resonance energy due to the delocalization of the π electron is still popularly taught as $\Delta H_{RE} = 36$ kcal/mol.[32]

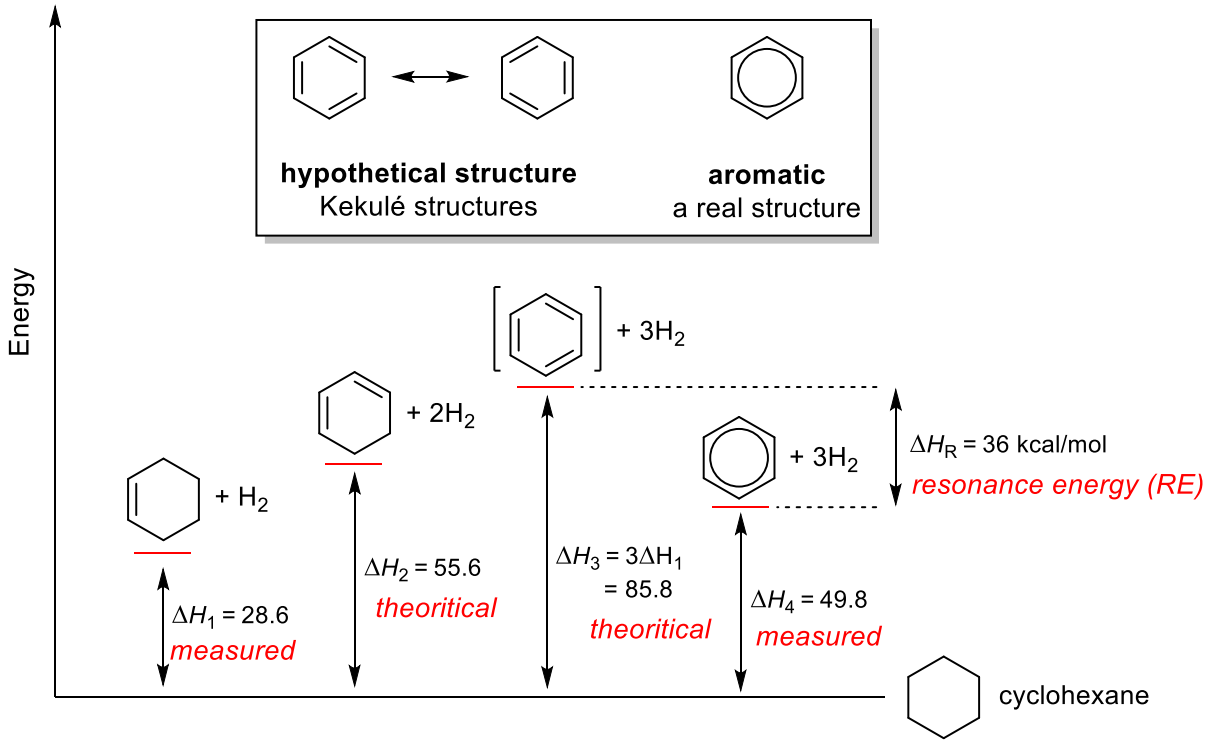

Figure 1-6. The empirical RE comparison is based on the heat of hydrogenation of benzene to assess the aromaticity by energy. Image is adapted with permission. Copyright (2024) from American Chemical Society.[31]

However, the approach based on heats of hydrogenation as proposed in Figures 1-6, is insufficient due to the negligence of steric strain energy contributions and impractical for application in more aromatic systems, especially those that are heteroaromatic.[33] Therefore, in the modern study, RE has been replaced by more precisely defined reference systems called aromatic stabilization energy (ASE).[34] According to this approach, reference systems are the

proposed reactions (which could be experimental or computational) chosen to extract only the energy related to the aromatic character of a target molecule. For instance, several conceptual reaction models resulting in ASE ranged from 19 to 67 kcal/mol for a benzene molecule that undergoes different types of reactions (Table 1-1). Consequently, the choice of reaction design is critical because the transformation from reactant to product covers the changes in conformation, hybridization, and ring stress.[34]

Table 1-1. Several ranges of aromatic stabilization energies (ASE) for benzene were obtained experimentally and calculated at B3LYP/6-311+G** (+ZPE) level.[34]

Reaction Scheme	ASE/kcal/mol
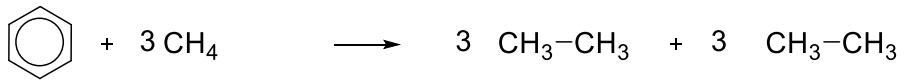	61.1 – 66.9
	48.7 – 55.3
	35.6 – 37.5
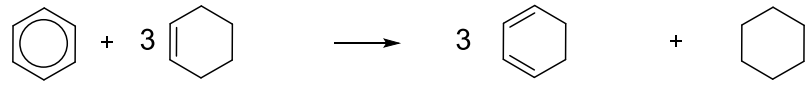	30.5 – 32.4
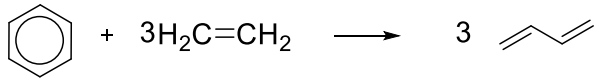	20.6 – 23.2
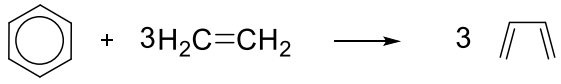	34.1 – 33.6
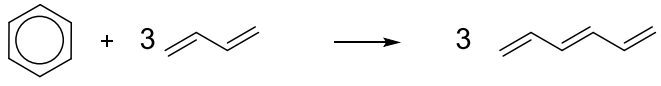	19.3 – 22.5

2.4. Electronic Criterion

The less common parameter from aromaticity interpretation is electronic-based measures of aromaticity. Since aromaticity stems from π-electron conjugation and ring currents, several

methods aim to estimate aromaticity involving electron density analysis or electronic wave function. Electron delocalization pathways can be observed through sophisticated experimental instruments or computational methods. For instance, direct imaging under scanning tunneling microscopy (STM) was able to capture the intramolecular rearrangement of 1,2-bis((2-ethynyl phenyl)ethynyl) benzene under thermally induced (Figure 1-7a).[35a] On the other hand, computational aromatic delocalization pathways are also envisaged as currents induced by an external magnetic field using the electron density of delocalized bonds (EDDB), gauge including magnetically induced current (GIMIC), or anisotropy of the induced current density (ACID) methods as presented for [18]annulene (Figure 1-7b).[35b]

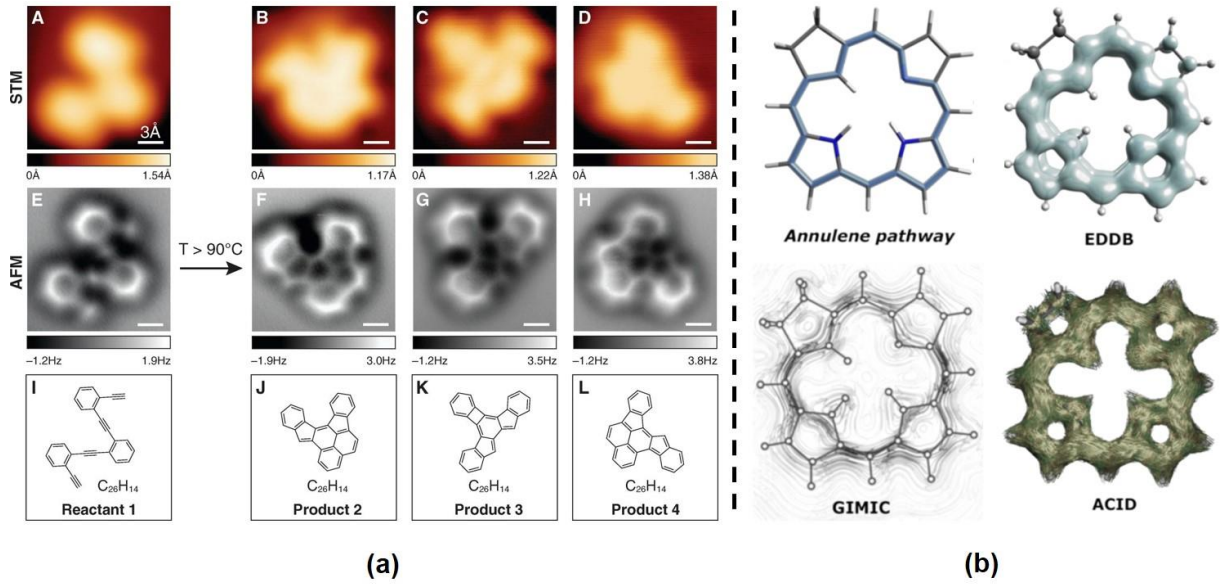

Figure 1-7. Visualization of electron pathway: (a) Direct STM images with the schematic representation of reactant undergoing experimental intramolecular transformation; (b) various computational imaginary tools in delivering electron delocalization pathway of [18]annulene. Image is reprinted with permission. Copyright (2024) from AAAS.[35a]

Despite those sophisticated approaches mentioned above, the HOMO–LUMO energy gap, the absolute and relative hardness, the electrostatic potential, and the polarizability are still employed to predict electronic criteria as well.[36] Another widely used tool for aromaticity

observation by electronic criteria is the para-delocalization index (PDI). It is calculated as an average value of delocalization indices between all *para*-related atoms of the ring, which, unfortunately, can only be used to estimate the local aromaticity of six-membered rings (since it possesses the *para*-position). However, a correlation between NICS and PDI parameters once showed similar results with some tolerations, despite both being addressed each different physical manifestations of aromaticity.[37]

2.5. Reactivity Criterion

Aromatic compounds reliably undergo electrophilic substitution reactions with greater ease than addition reactions. Thus, aromatic compounds tend to retain their initial π-electron structure. This criterion, however, is not a property of the ground state of a system but relies on the energy difference between the ground state and a transition state, leading to an intermediate.[24] Meanwhile, the kinetics aspect depends on the energies of the ground, transition, and intermediate states, with the possibility of subsequent reactions leading to stable products. Consequently, formulating a comprehensive and quantitative criterion for aromaticity based on reactivity seems speculative. Despite this, theoretical attempts (primarily for benzenoid hydrocarbons) exist to address this issue.

Typically, reactivity discussion is closely related to the frontier molecular orbital (FMO) as Highest Occupied Molecular Orbital (HOMO) and Lowest Unoccupied Molecular Orbital (LUMO) energies. The idea of absolute hardness,[38] the HOMO–LUMO gap,[39] and relative hardness (the difference between the hardness of a molecule and some hypothetical reference structure) is still popularly employed as a criterion of chemical reactivity and stability.[40] It should be emphasized that, despite being a non-ground-state property, reactivity is still attractive to explore in its corresponding to aromatic property.

3. Research purpose

It is possible to evaluate the aromaticity among investigated structures by studying the de-aromatization profile of an aromatic compound without converting it to an entirely new non-aromatic structure. It should be noted that aromaticity criteria, as mentioned earlier, cannot be equally implemented in the evaluation of the aromaticity of a compound. This is because multidimensional equivalent explanations may complicate the more relatable or the more desired observation. Hence, this study is set with geometric (both provided by experimental and theoretical data), magnetic (NICS(1) and NICS(-1)), and electronic (HOMO-LUMO energy gap) as tools to evaluate how distortion inflicted by steric repulsion in the *peri*-position influence dearomaticity, which later promote non-electronic activation.

4. References

1. (a) Pozharskii, A. F.; Soldatenkov, A.; Katritzky, A. R. "The Origin of Heterocycles". In *Heterocycles in Life and Society Second Ed.* Wiley, **2011**, pp: 325–326; (b) Joule, J. A.; Mills, K. "Structures and Spectroscopic Properties of Aromatic Heterocycles". In *Heterocyclic Chemistry Fifth Ed*. Wiley, **2009**, pp: 5–8.
2. Bodwell, G. J.; Bridson, J. N; Cyrañski, M. K. Kennedy, J. W. J. *J. Org. Chem*. **2003**, *68*, 2089–2098.
3. (a) Martin, J. W.; Slavchov, R. I; Yapp, E. K. Y.; Akroyd, J.; Mosbach, S.; Kraft, M. *J. Phys. Chem. C*. **2017**, *121*, 27154–27163; (b) Rieger, R.; Müllen, K. *J. Phys. Org. Chem*. **2010**, *23*, 315–325.
4. (a) Bharat, R. B.; Bally, T.; Valente, A.; Cyrańnski, M. K. *Angew. Chemie. Int. Ed*. **2010**, *49*, 399–402; (b) Barth, W. E.; Lawton, R. G. *J. Am. Chem. Soc*., **1971**, *23*, 1730–1745; (c) Christoph, H.; Grunenberg, J.; Hopf, H.; Dix, I.; Jones, P. G.; Scholtissek, M.; Maier, G. *Chem. Eur. J*. **2008**, *14*, 5604–5616; (d) Sakurai, H.; Daiko, T.; Sakane, H.; Amaya, T.; Hirao, T. *J. Am. Chem. Soc*. **2005**, *127*, 11580–11581; (e) Higashibayashi, S.; Sakurai, H.

Chem. Lett. **2011**, *40*, 122−128.

5. (a) Brady, J. H.; Redhouse, A. D.; Wakefield, B. J. J. *J. Chem. Res*. **1982**, *137*, 1541−128; (b) Qiao, X.; Padula, M. A.; Ho, D. M.; Vogelaar, N. J.; Schutt, C. E.; Pascal, R. A. *J. Am. Chem. Soc*. **1996**, *118,* 741−745; (c) Shen, Y.; Chen, C. F. *Chem. Rev*. **2012**, *112*, 1463−1535.
6. Faraday, M. *Philos. Trans. R. Soc.* **1825**, *115*, 440−128.
7. (a) Liu, Y.; Kilby, P.; Frankcombe, T. J.; Schmidt, T. W. *Nat. Commun*. **2020**, *11*, 1−5; (b) Fowler, P. W.; Gibson, C. M.; Bean, D. E. *Proc. R. Soc. A. Math. Phy.s Eng. Sci*. **2014**, *470*, 1−18; (c) Pandey, S. K.; Manogaran, D.; Manogaran, S.; Schaefer, H. F. *J. Phys. Chem. A*. **2016**, *120*, 2894−2901; (d) Solà, M. *Front. Chem*. **2017**, *5*, 1−5.
8. Minkin, V. I. "Glossary of Terms Used in Theoretical Organic Chemistry." In *Pure Appl. Chem*. Great Britain, **1999**, *71*, pp: 1923−1924.
9. (a) Krygowski, T. M.; Czarnocki, M. K.; Häfelinger, G.; Katritzky, A. R. *Tetrahedron* **2000**, *56*, 1783−1796; (b) Solà, M.; Boldyrev, A. I.; Cyranski, M. K.; Krygowski, T. M.; Merino, G. "Descriptors of Aromaticity." In Aromaticity and Antiaromaticity. John Wiley & Sons, **1994**, pp: 77-165.
10. Zhu, Q.; Chen, S.; Chen, D.; Lin, L.; Xiao, K.; Zhao, L.; Solà, M. *Fundam. Res*. **2023**, *3*, 926−938.
11. Krygowski, T.M,; Szatylowicz, H. *Chem. Texts*. **2015**, *1*, 1−12.
12. (a) Merino, G.; Solà, M.; Fernández, I.; Nejad, C. F.; Lazzeretti, P.; Frenking, G.; Anderson, H. L.; Sundholm, D.; Cossion, F. P.; Petrukhina, M. A.; Wu, J.; Wu, J. I.; Restrepo, A. *Chem. Sci*. **2023**, *14*, 5569−5576; (b) Agranat, I. *Struc. Chem.* **2024**, *35*, 715−720.
13. Wertjes, W. C.; Southgate, E. H.; Sarlah, D. *Chem. Soc. Rev*. **2018**, *47*, 7996−8017.
14. (a) Pape, A. R.; Kaliappan, K. P.; Kündig, E. P. *Chem. Rev*. **2000**, *100*, 2917−2940; (b) Rosillo M.; Domínguez. G.; Pérez-Castells, J. *Chem. Soc. Rev*. **2007**, *36*, 1589−1604; (c) Liebov, B. K.; Harman, W. D. *Chem. Rev*. **2017**, *117*, 13721−13755.

15. (a) Streit, U.; Bochet, C. G. *Beilstein J. Org. Chem*. **2011**, *7*, 525–545; (b) Remy, R.; Bochet, C. G. *Chem. Rev*. **2016**, *116*, 9816–9849.
16. Ortiz, F. L.; Iglesias, M. J.; Fernández, I.; Sánchez, C. M. A.; Gómez, G. R. *Chem Rev*. **2007**, *107*,1580–1681.
17. (a) Crich, D.; Patel, M. *Tetrahedron* **2006**, *62*, 7824–7837; (b) Flynn, A.; McDaniel, K. A.; Hughes, M. E.; Vogt, D. B.; Jui, N. *Chem. Rxiv*. **2019**, *1*, 1–25.
18. Lan, P.; Ye, S.; Banwell, M. G. *Chem. Asian J*. **2019**, *14*, 4001–4012.
19. Huck, C. J.; Sarlah, D. *Chem*. **2020**, *6*, 1589–1603.
20. Szatylowicz, H.; Wieczorkiewicz, P. A.; Krygowski, T. M. *Sci*. **2022** , *4*, 24.
21. Allen, F. H.; Kennard, O.; Watson, D. G.; Brammer, L.; Orpen, A. G.; Taylor, R. *J. Chem. Soc. Perkin. Trans. 2*. **1987**, *12*, 1–19
22. (a) Zhigalko, M. V.; Shishkin, O. V.; Gorb, L.; Leszczynski, J. *J. Mol. Struc*. **2004**, *693*, 153–159; (b) Shishkin, O. V.; Pichugin, K. Y.; Gorb, L.; Leszczynski, J. *J. Mol. Struc*. **2002**, *616*, 159–166.
23. Schleyer, P. R.; Maerker, C.; Dransfeld, A.; Jiau, H.; Hommes, N. J. R. **1996**, *118*, 6317–6318.
24. Chen, Z.; Wannere, C. S.; Corminboeuf, C.; Puchta, R., Schleyer, P. R. *Chem. Rev*. **2005**, *105*, 3842–3888.
25. Schleyer, P. R.; Jiao, H.; Hommes, N. J. R.; Malkin, V. G.; Malkina, O. L. *J. Am. Chem. Soc*. **1997**, *119*, 12669–12670.
26. Foroutan-Nejad, C.; Shahbazian, S.; Rashidi-Ranjbar. P. *Phys. Chem. Chem. Phys*. **2010**, *12*, 12630–12637.
27. Gershoni-Poranne, R.; Stanger, A. "NICS-nucleus independent chemical shift". In *Aromaticity: Modern Computational Methods and Applications*. Elsevier Science, **2021**, pp: 99–154.
28. Krygowski, T. M.; Cyrański, M. K. *Chem. Rev*. **2001**, *101*, 1385–1419.

29. Jiménez-Halla, J. O. C.; Matito, E.; Robles, J.; Solà, M. *J. Organomet. Chem*. **2006**, *691*, 4359–4366.
30. Pauling, L.; Sherman, J. *J. Chem. Phys*. **1933**, *1*, 606–617.
31. Katritzky, A. R.; Jug, K.; Oniciu, D. C. *Chem. Rev*. **2001**, *101*, 1421–1449.
32. Kistiakowsky, G. B.; Ruhoff, J. R.; Smith, H. A.; Vaughan, W. E. *J. Am. Chem. Soc*. **1936**, *58*, 146–153.
33. Lewis, D.; Peters, D. *Facts and Theories of Aromaticity.* The Macmillian Press Ltd, **1975**, pp: 97–104.
34. Cyrański, M. K. *Chem. Rev*. **2005**, *105*, 3773–3811.
35. (a) De Oteyza, D.G.; Gorman, P.; Chem, Y. C.; Wickenburg, S.; Riss, A.; Mowbray, D. J.; Etkin, G.; Pedramrazi, Z.; Tsai, H. Z.; Rubio, A. *Sci.* **2013**, *340*, 1434–1437; (b) Homepage: D.W. Szczepanik—EDDB. Available online: http://www.eddb.pl/runeddb/gallery/ (accessed on 10 October 2024).
36. Proft, F.; Geerlings, P. *Chem. Rev*. **2001**, *101*, 1451–1464.
37. Poater, J.; Fradera, X.; Duran, M.; Solà, M. *Chem. Eur. J*. **2003**, *9*, 400–406.
38. Zhou, Z.; Parr, R. G.; Garst, J. F. *Tetrahedron Lett*. **1988**, *29*, 4843–4846.
39. Parr, R. G.; Chattaraj, P. K. *J. Am. Chem. Soc*. **1991**, *113*, 1854–1855.
40. De Proft. F.; Geerlings, P. *Phys. Chem. Chem. Phys*. **2004**, *6*, 242–248.

Part II: The Origin of Steric Effect in Organic Molecules

1. Steric Effect and Strain

The steric effects frequently interact synergistically with electronic effects derived from electronegativity, such as dipoles, donor-acceptor interactions, inductive effects, conjugation, aromaticity, resonance, hyperconjugation, and tautomerism.[1a] According to the quantum theory, the Pauli exclusion principle forbids two electrons with the same spin from occupying the same position. As a result, atoms cannot come close together without forming covalent bonds, creating strain when there are conflicts between molecular and electron density geometry.[1a] Eventually, molecular strains arise from the electron-electron repulsion of atoms when they are too close to each other. This strain can be identified as angle (Baeyer strain), torsion (Pitzer strain), and steric (van der Walls strain) strain (Figure 1-8).

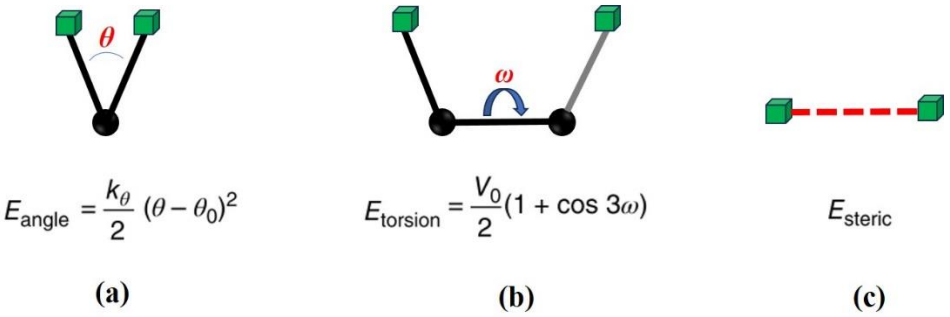

Figure 1-8. Different types of strain and their corresponding formula.

Angular strain represents an actual bond angle that is different from the ideal angles of geometry, while torsion angle reflects the resistance of the respective bonds to be twisted. On the other hand, the steric strain has a non-bonded basis since the interacting moieties cannot be linked directly or are at least four bonds away from each other.[1b] Strain level within similar molecules can be rationalized by evaluating its substituents. When the substituent is an atom,

comparing measured atomic radii (covalent or van der Waals radius) is sufficient to predict how severe the strain will be since the closer the atomic radii, the larger the strain. Finally, when the impact of this steric effect is considered in the designing molecular geometry, the outcome on intermolecular interactions, reactivity and assembly, electromagnetic behaviors, physicochemical properties, and bioactivity can also be estimated.[1a]

2. Steric Effect and Reactivity

In organic synthetic chemistry, steric effects mostly lead to these outcomes: (1) preventing access for a vital group due to steric hindrance, (2) controlling the conformational preferences of products due to steric effects, (3) protecting the active site from getting nucleophilic attack by an embedding bulky group, and (4) changing the electronic resonance of a π-bonded substituent due to out-of-plane repulsion.[2] Therefore, the steric effect may be favorable or unfavorable in any reaction. Moreover, there is no definitive rule that dictates which specific term for denoting the steric effect, making both "steric hindrance" and "steric strain/repulsion" interchangeably used to convey the typical underlying concept involving a geometrical aspect of the viewed molecule.

2.1. Retardation

From a spatial perspective, if two or more functional groups are positioned too closely together within a molecule, repulsive forces might hinder molecular motion and prevent certain reactions from occurring, in which the steric effect plays a role in retarding the reaction.[3] For instance, the first report on the hetero Diels–Alder cycloaddition in the formation of isoindoloquinolines **3** suggests that steric repulsion between substituents in the aryl group of **1** prevents the approach of *N*-vinylpyrrolidone **2** (Scheme 1-1).[4]

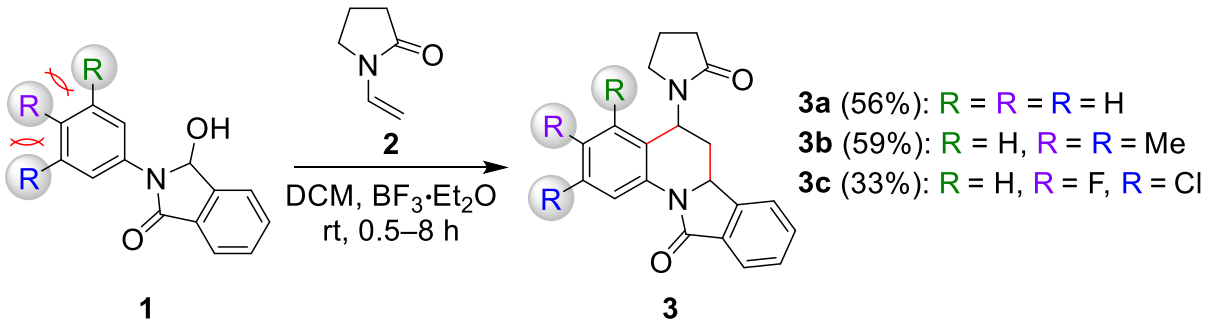

Scheme 1-1. Sterically controlled formation of isoindoloquinolines **3** by Diels-Alder reaction.

The product variation drastically changes depending on steric interaction in promoting suitable conformers in the reaction between *N*-substituted 2-vinylpyrroles **4** with dimethyl acetylenecarboxylate (**5**). The *transoid* conformation **4a** inhibits (4π+2n) cycloaddition, affording only Michael's addition **6a** and **6b**. Conversely, sufficient interaction adopted *cisoid* conformer leads to a single dihydroindole **7** product (Scheme 1-2).[5]

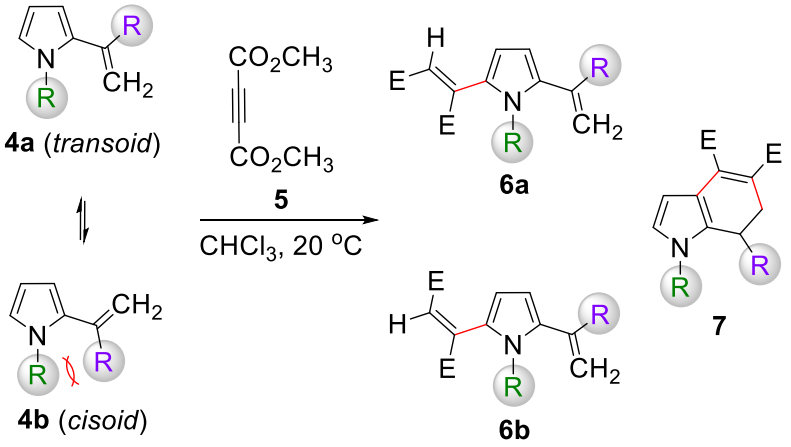

Pyrrole		Reaction Time/d	Yield/%		
R	R		**6a**	**6b**	**7**
Me	Me	3	22	17	0
Me	^{t}Bu	20	26	18	0
Me	Ph	7	35	27	0
Ph	H	4	0	0	21
Ph	Me	10	0	0	60

E = CO_2CH_3

Scheme 1-2. Sterically controlled on *N*-substituted 2-vinylpyrroles **4**.

The yield decreases when bulkier substituents on the 6-position are embedded because of repulsion between the *N*-Me group and the alkyl group, which undergoes decarboxylative *cine*-substitution at the 4-position of 2-pyridone **8** regioselectively with styrene (**9**) to afford alkenylated product **10** (Scheme 1-3).[6] Even though being far away from the reactive site, the steric repulsion between the adjacent substituents considerably influences the reactivity.

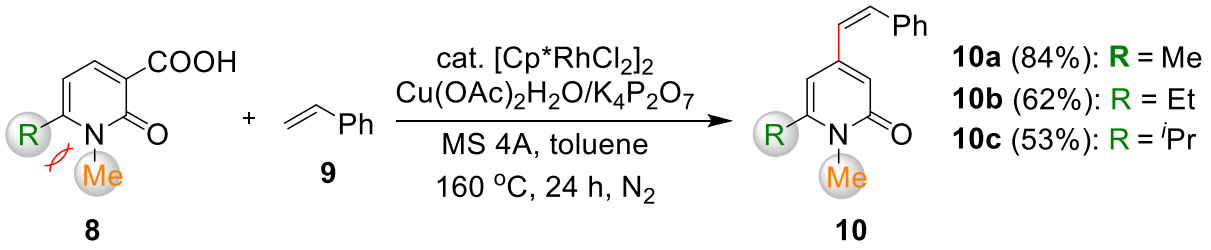

Scheme 1-3. Sterically controlled C-4 alkenylation on 2-pyridone **8** by peripheral bulkiness.

2.2. Acceleration

A limited amount of literature was collected portraying the opposite impact of the steric effect causing acceleration.[7] Still, they may help the reactivity by aiding the conformational restriction of specific structures. As illustrated, steric buttress support restrained the conformational space of *N*-[(2-allyloxy)benzyl]-3-oxidopyridinium **11**, allowing intramolecular cycloaddition **12** to proceed smoothly (Scheme 1-4a).[8] Similarly, it was a steric enhancement that aided cycloaddition on oximes **13** to produce cycloadduct **14** under different temperature conditions (Scheme 1-4b).[9]

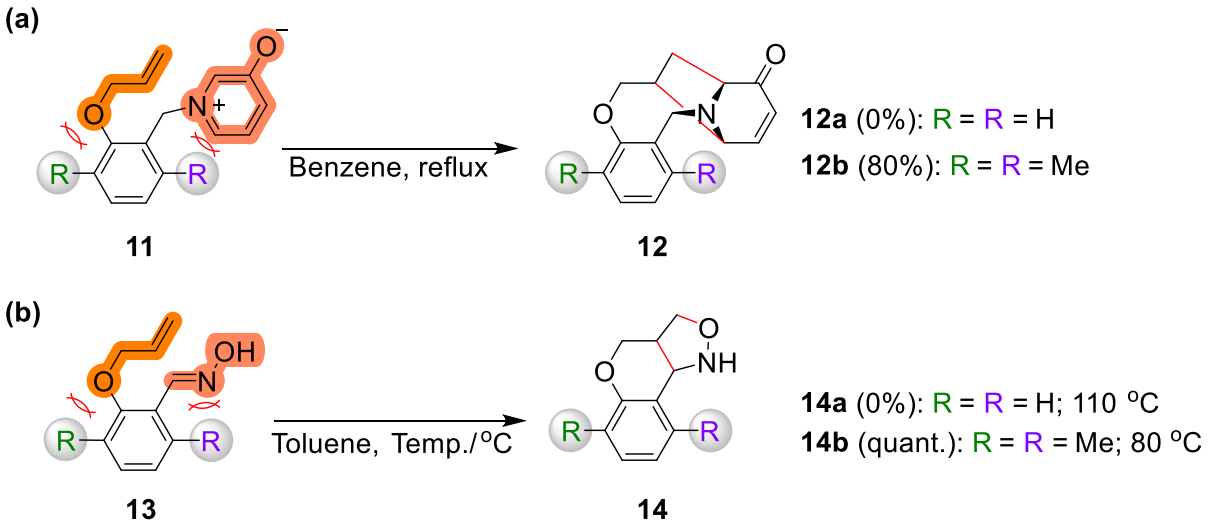

Scheme 1-4. Enhanced intramolecular cycloaddition by steric buttresses in *ortho*-position.

The bulky trityl-protected-*N,N*-disallylamine **15** possessed steric buttress that aids intramolecular, uncatalyzed *ene* reaction leading to *cis*-pyrrolidine **16** as a single isomer almost

quantitatively. At the same time, the unsubstituted parent amine under the same conditions was unfruitful (Scheme 1-5).[10]

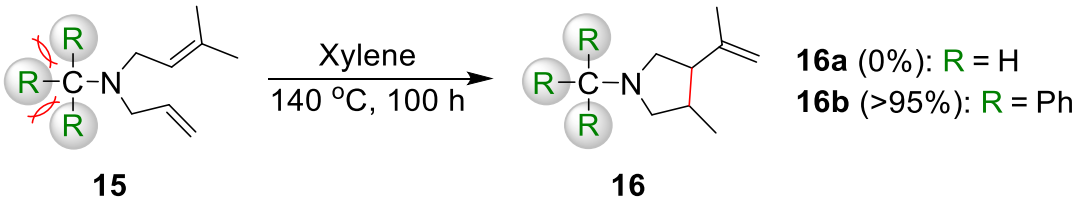

Scheme 1-5. Steric buttressness assists ring closure on the *ene* reaction.

The bulkiness of the substituent elevates the ring closure of oxazepinones **17** to benzoxazepinones **18** due to the rotational restriction of the C–N bond in amine (Scheme 1-6a). In an extended work, the modification of **17** into **19** by introducing a triazole ring combined with steric repulsion from two methyl groups has raised reactivity 140000 times higher on the formation of product **20** (Scheme 1-6b).[11]

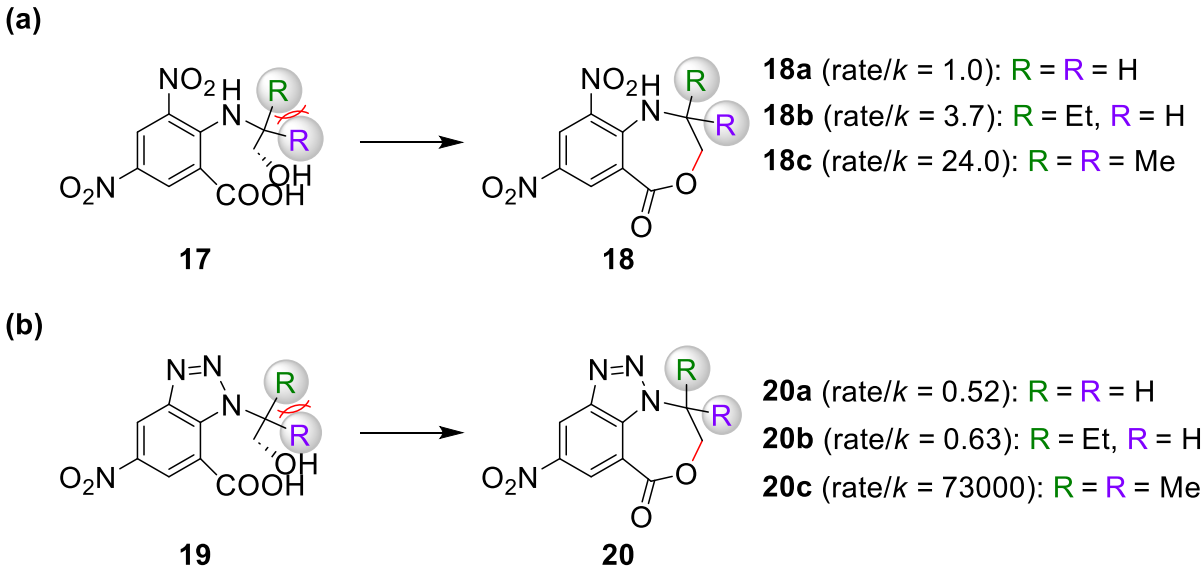

Scheme 1-6. Ring closure employs steric repulsion from the dialkyl group.

3. Steric Effect between Molecular Substituents at *peri*-Positions

Since the steric effect is strongly correlated to the geometry and topology of the molecular framework, the general discussion on this matter falls into several framework, such as an open

chain framework, aromatic unsaturated framework, and cyclic framework.[1] Regarding the latter, the *peri*-position of naphthalene brings closer proximity of substituents (in this case, hydrogen atoms) than the *ortho*-position of benzene but slightly higher than the *bay*-position distance of phenanthrene (Figure 1-9) amongst arenes. Due to the limited space available, the rigid, planar geometry of naphthalene will strain any other (*i.e.,* non-hydrogen) *peri*-atoms, compelling the two *peri*-atoms to form sub-van der Waals contacts.[12] Thus, the attractiveness of *peri-position* geometry in naphthalene has been discussed in several areas covering aromaticity,[13] chelation assembly,[14] and mechanophore.[15]

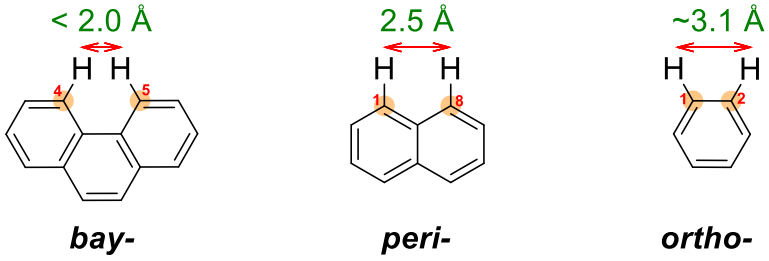

Figure 1-9. Graphical geometry of *bay*-, *peri*-, and *ortho*-position in arenes.

The stability of the non-planar naphthalene ring comes from the unseparated cooperation of strain repulsion and π-electron delocalization effects within the system. The steric strain from bulky substituents alone can be manifested into four forms: (a) bond's stretching, (b) in-and-out plane deflection angles of the substituent, (c) twisted of planar torsion angle, and (d) distortion or conceding of the core ring.[16] Consequently, the molecules are expected to alter their geometrical status, proposing new properties and/or reactivity as a worthy subject to observe.[17]

Unfortunately, the correlation between steric repulsion in *peri*-positions increased de-aromaticity and influence reactivity has been limited for study. The first study found an unusually high reactivity of 1-methyl-3,6,8-trinitro-2-quinolone (**21**) when allowed to react with 2,4-pentanedione **22**. The *cine*-substituted product **23** efficiently proceeded on the pyridone moiety when the bulkier substituents were embedded at the C8 positions. Conversely,

a small substituent as hydrogen atoms failed to complete the reaction even after increasing the temperature (Scheme 1-7).[18]

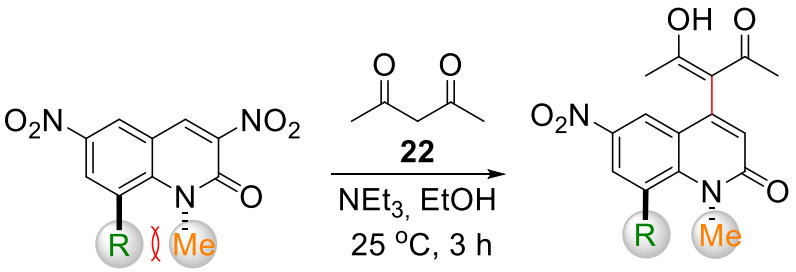

21	[a]Torsion	23
R	angle/ °	Yield/ %
H	0.9	0[b]
Me	2.9	92
NO_2	30.9	98

[a]Dihedral angle between N1-Me and C8-R bonds
[b]Temperature was 80 °C

Scheme 1-7. Steric repulsion-dependent reactivity on quinolone **21** framework.

Since the 8-position was distant from the reaction site, and the electronic properties of the 8-substituent did not affect the reaction; thus, steric repulsion between substituents was presumed crucial. Evidence supporting the role of steric repulsion in the de-aromatization of the ring was obtained through X-ray crystallography, revealing a significant difference in the dihedral angle due to steric interactions between the N1–Me group and the C8–R substituents in substrates **21**.

Inspired by these results, a systematic study on the correlation between steric repulsion and reactivity was performed using 8-alkylated 1-methyl-quinolinium salts **24** (Scheme 1-8).[19] As the C8-substituent becomes bulkier, the dihedral angles between the N1–Me and C8–R bonds become larger, inducing distortion of the quinoline ring. As expected, the highly distorted quinolinium salts underwent fast reactions with sodium tri(acetoxy)borohydride (monitored by reaction rate *k*) corresponding to their distortion in forming adduct **25**. The de-aromaticity of

quinolinium salts frameworks was also supported by a computational study on its magnetic (NICS(1)) and electronic (HOMO–LUMO gap) profiles.

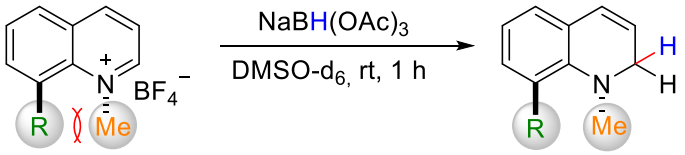

24 **25**

24 R		[a]Torsion angle/ °	[b]NICS(1)/ ppm	ΔHOMO-LUMO/ eV	Reactivity *k*
H	**a**	0.9°	-9.65	4.32	1.0
Me	**b**	3.1°	-9.60	4.11	2.8
Et	**c**	7.5°	-9.40	4.11	4.6
^{n}Pr	**d**	15.6°	-9.16	4.07	4.8
^{i}Pr	**e**	24.8°	-8.92	4.00	7.5
^{t}Bu	**f**	57.0°	-8.41	3.98	28.2

[a]Dihedral angle between N-Me and C8-R bonds
[b]NICS(1) on pyridine ring

Scheme 1-8. Steric repulsion-dependent reactivity on 8-alkylated 1-methylquinolinium salts **24**.

The steric repulsion between *peri*-substituents in the typical rigid planar aromatic naphthalene ring was recently investigated. The transformation of 1,8-diiodonaphthalene (**26**) showed various reactivities to undergo a homocoupling reaction, leading to iodo-rearranged products **27** and **28** (known as Halo-Jacobsen rearrangement or halogen dance reaction) and binaphthyl **29** by simply relying on its non-electronic activation revoked by steric repulsion (Scheme 1-9).[20] Surprisingly, the uncrowded with lower steric effect nature of 1,5-diiodonaphthalene (**28**) remained intact under the same conditions.

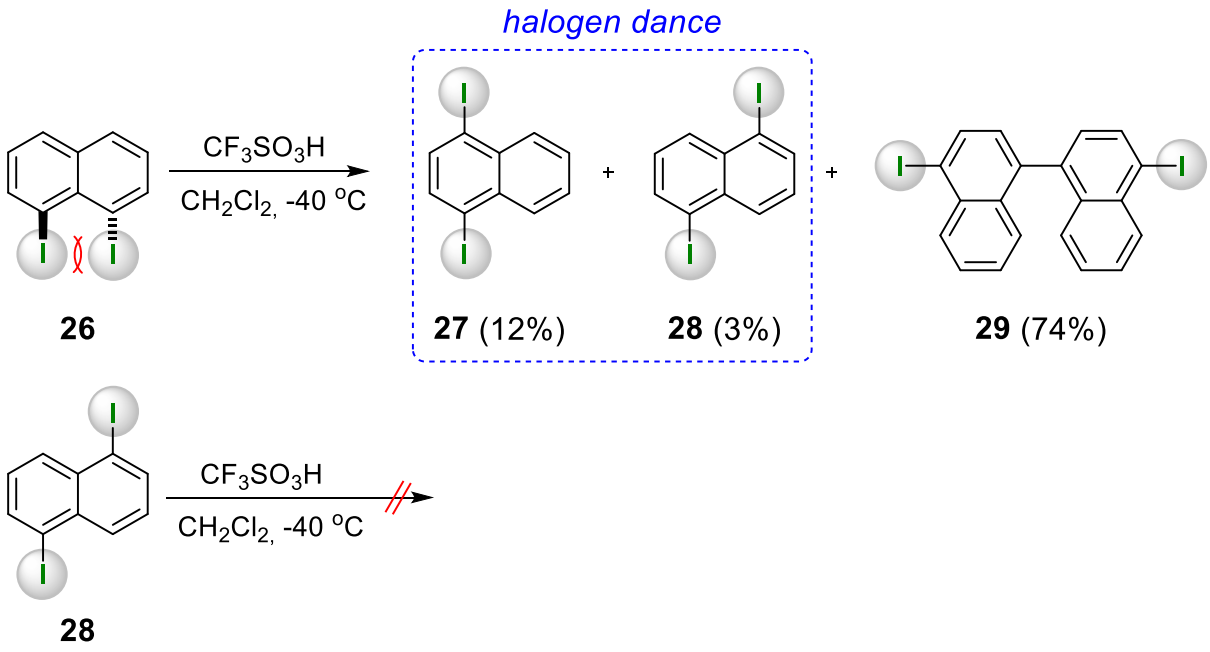

Scheme 1-9. Steric repulsion-dependent reactivity between 1,8-diiodonaphthalene **26** and 1,5-diidonaphthalene **28**.

4. Research Purpose

The study under the premise of steric strain and de-aromaticity mostly revolved around a computational approach because a series of strained substrates are not readily available. Meanwhile, aromaticity criteria provide an estimation to quantify how deviations from planarity in an aromatic system reduce the aromatic character in the π-electron system. Combining the fact that steric repulsion between the *peri*-substituents in PAHs is the modest way to impose out-of-plane distortion of planarity that exclusively correlates to the geometrical aspect of aromaticity, I investigate this topic intending to understand how distorted aromatic structures enhance the reactivity of stable and planar aromatic rings such as naphthalene and anthracene and propose the non-electronic activation as the sole reason for reactivity behavior it may cause.

5. References

1. (a) Yang, L.; Xie, L.; Wei, Y.; Liu, Y. "Steric Strain in Molecular Organics." In *Ency. Phy. Org. Chem.* Wiley, **2017**, 1–55; (b) Brown, W.H.; Iverson, B.L.; Anslyn, E.; Foote, C. In *Organic Chemistry. Fourth Ed*. Salt Lake City, **2009**.
2. Wipf, P.; Skoda, E. M.; Mann, A. "Conformational Restriction and Steric Hindrance in Medicinal Chemistry." In *Prac. Med. Chem. Fourth Ed.* Academic Press, **2015**, 279–299.
3. Voronenkov, V. V.; Osokin, Y. G. *Russ. Chem. Rev*. **1972**, *41*, 616–629.
4. Jha, A.; Chou, T. Y.; Jaroudi, Z.; Ellis, B. D.; Cameron, T. S. *Beilstein J. Org. Chem*. **2014**, *10*, 848–857.
5. Jones, R. A.; Saliente, T. A.; Arques, J. S. *J. Chem. Soc. Perkin Trans. 1*. **1984**, 2541–2543.
6. Hazra, S.; Hirano, K.; Miura, M. *Org. Lett*. **2021**, *23*, 1388–1393.
7. Brown, F.; Davies, T.D.; Dostrovsky, I.; Evans, O. J.; Hughes, E. G. *Nat*. **1951**, *167*, 987–1988.
8. Orlek, B. S.; Sammes, P. G.; Weller, D. J. *J. Chem. Soc. Chem. Commun*. **1993**, *18*, 1412–1413.
9. Orlek, B. S.; Sammes, P. G.; Weller, D. J. *J. Chem. Soc. Chem. Commun*. **1993**, *7*, 607–608.
10. Choony, N.; Sammes, P. G.; Smith, G.; Ward, R. W. *Chem. Commun*. **2001**, *20*, 2062–2063.
11. (a) Turk, J.; Haney, W. M., Heid, G.; Barlow, R. E.; Clapp, L. B. *J. Het. Chem*. **1971**, *8* 149–151; (b) Milstien, S.; Cohen, L. A. *Proc. Nat. Acad. Sci*. **1970**, *67*, 1143–1147.
12. Kilian, P.; Knight, F. R.; Woollins, J. D. *Coord. Chem. Rev*. **2011**, *255*, 1387–1413.
13. (a) Schweizer, W. B.; Procter, G.; Kaftory, M.; Dunitz, J. D. *Helv. Chim. Acta*. **1978**, *61*, 2783–2808; (b) Schumann, H.; Dechert, S.; Hummert, M.; Lange, K. C. H.; Schutte, S.; Wasserman, B. C.; Köhler, K.; Eichhorn, J. *Z. Anorg. Allg Chem*. **2004**, *630*, 1196–1204; (c) Pla, D.; Sadek, O.; Cadet, S.; Mestre-Voegtlé, B.; Gras, E. *Dalton Trans.* **2015**, *42*, 18340–18346; (d) Wannebroucq, A.; Jarmyn, A. P.; Pitak, M. B.; Coles, S. J.; Wallis, J. D. *Pure Appl. Chem*. **2016**, *88*, 317–331.

14. (a) Dobrowolski, M. A.; Cyrański, M. K.; Wróbel, Z. *Phys. Chem. Chem. Phys*. **2016**, *18*, 11813−11820; (b) Bristow, J. C.; Naftalin, I.; Cliff, S. V. A.; Yang, S.; Carravetta, M.; Heinmaa, I.; Stern, R.; Wallis, J. D. *Cryst. Eng. Comm*. **2020**, *22*, 6783−6795.

15. (a) Hoefelmeyer, J. D.; Schulte, M.; Tschinkl, M.; Gabbaï, F. P. *Coord. Chem. Rev*. **2002**, *235*, 93−103; (b) Kilian, P.; Knight, F. R.; Woollins, J. D. *Chem. Eur. J*. **2011**, *17*, 2302−2328; (c) Yang, J.; Horst, M.; Werby, S. H.; Cegelski, L.; Burns, N. Z.; Xia, Y. *J. Am. Chem. Soc*. **2020**, *142*, 14619−14626.

16. Balasubramaniyan, V. *Chem. Rev*. **1966**, *66*, 567−641.

17. Sarkar, S.; Row, T. N. G. *IUCrJ*. **2017**, *4*, 37−49.

18. (a) Nishiwaki, N.; Tanaka, C.; Asahara, M.; Asaka, N.; Tohda, Y.; Ariga, M. *Heterocycles.* **1999**, *51*, 567−574; (b) Chen, X.; Kobiro, K.; Asahara, H.; Kakiuchi, K.; Sugimoto, R.; Saigo, K.; Nishiwaki, N. *Tetrahedron* **2013**, *69*, 4624−4630.

19. Iwai, K.; Asahara, H.; Nishiwaki, N. *Bull. Chem. Soc. Jpn*. **2020**, *93*, 50−57.

20. (a) Iwai, K.; Nishiguchi, N.; Nishiwaki, N. *J. Org. Chem.* **2023**, *88,* 9409−9412; (b) Iwai, K.; Nishiwaki, N. *J. Org. Chem.* **2024**, *89,* 78439−7847.

Chapter 2. Steric Repulsion between *peri*-Substituents of 1,8-Dimethylnaphthalene Derivatives

1. Introduction

As the modest acene groups, the flatness and rigid structure of unsubstituted naphthalene are considerably facile enough to be distorted by introducing bulky substituents to its boundary.[1] Using a 1,8-dimethylnaphthalene framework where the bulkiness of substituents is introduced by replacing one hydrogen atom of the methyl group with bulky substituents such as the hydroxy and bromo group, the distortion imposed by steric repulsion is evaluated, including the response of substrates under selected reactivity test (Figure 2-1).

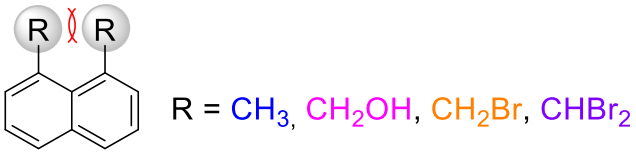

Figure 2-1. Selected substrates to study bulkiness in *peri*-naphthalene framework.

2. Synthesis and Crystal Study

The 1,8-disubstituted naphthalenes **1**–**4** were synthesized in a stepwise manner from 1,8-naphthalic anhydride (**6**) (Scheme 2-1). First, **6** was reduced with lithium aluminum hydride in the presence of zinc chloride to produce bis(hydroxymethyl) derivative **2**.[2] The hydroxy groups were then efficiently converted to bromomethyl groups by heating with phosphorous tribromide, resulting in 1,8-bis(bromomethyl) derivative **3**. The subsequent reduction of **3** with sodium borohydride yielded 1,8-dimethylnaphthalene **1** quantitatively.[3] Additionally, bromination at the benzyl position of **3** by *N*-bromosuccinimide (NBS) produced the bulkier structure, 1,8-bis(dibromomethyl) derivative **4**.[4] However, attempts to isolate the tribrominated structure **5** were unsuccessful because intermediately formed instable **5** was immediately converted to the

highly stable structure of **3** and **4** in any three possible routes using **1–3** as substrate. Nevertheless, four derivatives of the *peri*-substituted naphthalene framework were in hand, and the single crystal of **1–4** obtained from recrystallization using chloroform as the solvent was then put into X-ray crystallography to understand the intermolecular interactions caused by its molecular packing system and to know the distortion degree caused by steric repulsion between *peri*-substituents. It is essential to get X-ray crystallography data since their structural information can be closely compared to the optimized structure determined computationally under the selected level of theory, which secures the reliability of calculated data.[5] Some selected crystal parameters for naphthalene derivatives are presented in Table 2-1.

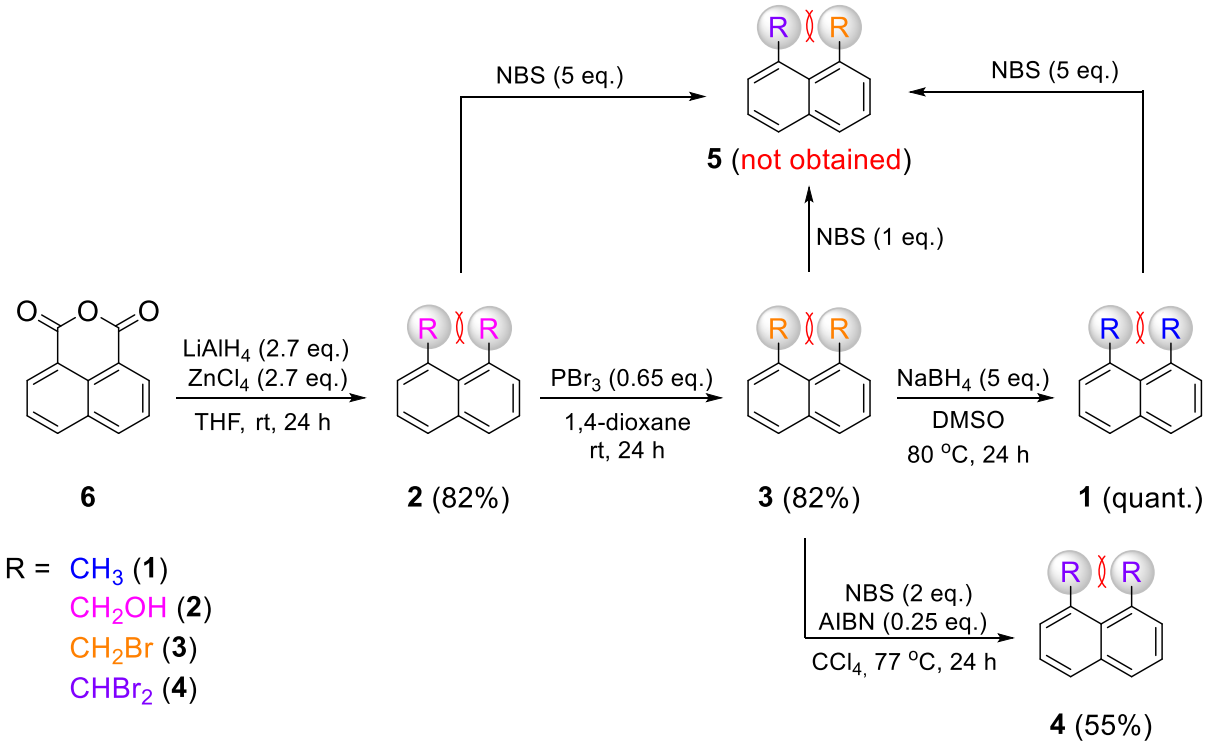

Scheme 2-1. Synthesis procedure of *peri*-substituted derivatives using naphthalic anhydride **6**.

Table 2-1. Selected crystallographic information for crystal structures **1–4**.

	1 (R = CH_3)	**2** (R = CH_2OH)	**3** (R = CH_2Br)	**4** (R = $CHBr_2$)
Empirical formula	$C_{12}H_{12}$	$C_{12}H_{12}O_2$	$C_{12}H_{10}Br_2$	$C_{12}H_8Br_4$
Crystal system	Monoclinic	Monoclinic	Monoclinic	Monoclinic
Space group	$P2_1/n$	$P2_1/n$	$C2/c$	$P2_1/n$
a (Å)	9.5783(6)	8.4875(4)	23.3250(11)	10.1755(4)
b (Å)	6.8687(4)	4.8113(2)	7.5802(3)	6.7237(2)
c (Å)	13.2814(10)	22.4730(9)	12.3748(6)	19.3037(8)
α (°)	90	90	90	90
β (°)	92.066(7)	94.379(4)	95.479(4)	100.207(4)
γ (°)	90	90	90	90
Z	4	4	8	4
GOF	1.051	1.098	1.097	1.031
R indices	$R_1 = 0.054$, $wR_2 = 0.160$	$R_1 = 0.041$, $wR_2 = 0.110$	$R_1 = 0.036$, $wR_2 = 0.107$	$R_1 = 0.048$, $wR_2 = 0.132$
ORTEP	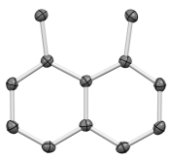	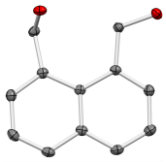	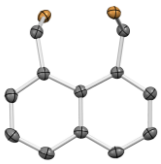	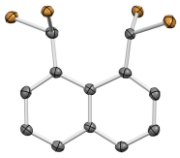

3. Evaluation of Distortions

The distortion on the naphthalene ring for each compound is evaluated under geometric and magnetic criteria. For the geometric profile, three parameters, (a) horizontal distortion, (b) bond distance and atom distance, and (c) vertical distortion, are key points to address in their relation to ring distortion.[6] The similarity values between X-ray crystallography and optimized structures calculated at the B3LYP/6-31G(d,p) level are compared. Next, NICS values obtained from the same optimized structure will represent the magnetic evaluation.

3.1. Geometric

3.1.1. Horizontal Distortions

Deformability by horizontal evaluation focuses on bond angles and bond stretching/compressing in the surrounding area, which is significantly impacted by steric repulsion from *peri*-substituents. Bond angles cornering the C8a position shown in Table 2-2

are reviewed to compare the degree of distortion since the sum of three angles in planarity must equal 360°. As a result, three atoms connected to C8a carbon remain in-plane, albeit the angles are not equally divided. However, all compounds have wider angles δ (outer ring) than the standard sp^2 bond angle (120°), while the other two angles ε and η (inner ring) are narrower. This indicates that the angle pushed C1 and C8 apart by steric repulsion between the *peri*-substituents. Accordingly, the outside angle θ at the opposite side (C4–C4a–C5 angle) tends to be smaller.

Table 2-2. Bond angles around the C8a and C4a carbons in **1–4**.[a]

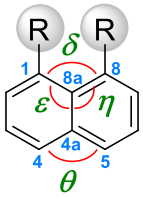

R		δ/ °	ε/ °	η/ °	θ/ °
CH_3	**1**	126.3(1)/125.5	116.6(9)/117.1	117.1(9)/117.3	118.2(1)/118.8
CH_2OH	**2**	126.3(2)/126.3	117.1(2)/116.9	116.7(2)/116.9	118.5(3)/118.4
CH_2Br	**3**	128.4(6)/126.2	115.1(5)/116.7	116.5(5)/117.1	117.6(2)/118.5
$CHBr_2$	**4**	125.5(1)/128.4	117.2(1)/115.1	117.3(1)/116.4	118.8(2)/117.6

[a]Measured values/Calculated values. Calculated values are from optimized structures at B3LYP/6-31G(d,p) level of theory.

Notably, each compound exhibited similar bond angle tendencies regardless of the bulkiness of the substituents. This result suggests that the first distortion occurs horizontally by absorbing repulsive energy when the *peri*-substituents become bulky. This energy is the manifestation of steric strain energy (van der Waals strain) due to the size variation of embedded substituents in *peri*-position.

Steric repulsion between *peri*-substituents should affect not only bond angles but also bond distances and interatom distances. Some selected bond lengths and interatom distances are shown in Tables 2-3 and Table 2-4, respectively. While bond lengths of **1**–**4** resemble each

other, some partial stretch of the inner bond length (C1–C8a) of bis(dibromomethyl)naphthalene **4** is observed as the largest than any other naphthalenes **1**–**3**. Adversely, several outer bond lengths (C1–C2, C2–C3, C4–C4a) of **4** appear shorter than the rest. Indeed, the bulkier the structure, the more prominent the bond length alternation, as shown by naphthalene **4**.

Table 2-3. Bond lengths (Å) in the naphthalene ring in **1**–**4**.[a,b]

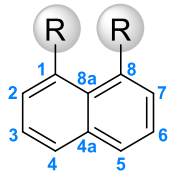

	1 (R = CH_3)	**2** (R = CH_2OH)	**3** (R = CH_2Br)	**4** (R = $CHBr_2$)
C1–C2	1.375(2)/1.377	1.380(2)/1.384	1.380(4)/1.380	**1.370(1)**/1.373
C2–C3	1.407(2)/1.409	1.407(2)/1.408	1.404(4)/1.404	**1.380(1)**/1.377
C3–C4	1.358(2)/1.358	1.364(2)/1.370	1.358(4)/1.358	**1.370(1)**/1.372
C4–C4a	1.419(2)/1.418	1.421(2)/1.420	1.423(4)/1.422	**1.407(9)**/1.407
C4a–C8a	1.442(2)/1.442	1.435(1)/1.445	1.430(4)/1.430	1.434(9)/1.434
C8a–C1	1.445(2)/1.444	1.447(2)/1.443	1.446(4)/1.446	**1.481(9)**/1.481
C4a–C5	1.418(2)/1.419	1.422(2)/1.420	1.422(4)/1.422	**1.414(9)**/1.414
C5–C6	1.358(2)/1.358	1.361(2)/1.370	1.360(5)/1.360	**1.340(1)**/1.338
C6–C7	1.409(2)/1.407	1.407(2)/1.409	1.400(5)/1.400	**1.410(1)**/1.410
C7–C8	1.377(2/1.375	1.380(2)/1.384	1.382(4)/1.382	**1.370(1)**/1.371
C8–C8a	1.444(2)/1.445	1.446(2)/1.443	1.446(4)/1.446	**1.434(9)**/1.434

[a]Measured values/Calculated values. Calculated values are from optimized structures at B3LYP/6-31G(d,p) level of theory.

[b]Values in **bold** show the prominently affected bond length amongst the naphthalenes.

On the other hand, the atomic distance between C4 and C5 on the bottom side of the ring is also triggered. The larger C1–C8, the shorter C4–C5 of naphthalene **4** compared to the other derivatives, due to compression force, is transferred through the ring. The C11–C12 distance was found to be longer in naphthalenes **3** than **4**, suggesting that its *peri*-substituents repel more severely from each other to accommodate the adjacent C1–C8 (Table 2-4). This anomaly will

later be reflected in larger vertical distortions of **3** than **4**. In conclusion, when the relaxation of steric energy reaches its limits, the naphthalene scaffold is distorted since it must reform the bond angle and bond length to some extent to provide spatial convenience for vertical distortion.

Table 2-4. Selected interatom distances (Å) in **1**–**4**.[a,b]

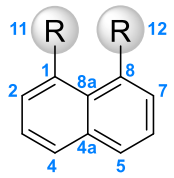

	1 (R = CH_3)	**2** (R = CH_2OH)	**3** (R = CH_2Br)	**4** (R = $CHBr_2$)
C1–C8	2.569(2)/2.568	2.580(2)/2.575	2.580(4)/2.580	**2.625(9)**/2.625
C2–C8a	2.429(2)/2.432	2.444(2)/2.444	2.440(4)/2.440	**2.459(9)**/2.459
C4–C5	2.442(2)/2.442	2.440(2)/2.440	2.445(5)/2.445	**2.413(9)**/2.412
C11–C12	2.961(2)/2.962	2.984(2)3.001	**3.058(4)**/3.058	2.990(1)/2.986

[a]Measured values/Calculated values. Calculated values are from optimized structures at B3LYP/6-31G(d,p) level of theory.

[b]Values in **bold** show the prominently affected bond distance amongst the naphthalenes.

3.1.2. Vertical Distortions

Vertical distortion of the naphthalene framework is estimated by comparison of three dihedral angles α–γ (Table 2-5). Referring to previous works,[7] dis-planarity was initially addressed using only a torsion angle α formed between C1–C11 and C8–C12 bonds. However, the tilting angles on the naphthalene backbone, either that runs across the central bridging carbon (β) or in the same ring system (γ) formed by respective bonds, can be entangled as vertical distortions.[8]

In the case of naphthalene **1**, the torsion angle α = 0.7°, indicating that the coplanarity remains. Introducing a hydroxy group to the methyl groups somewhat distorted the naphthalene **2** ring (α = 4.6°). Next, the larger bromo groups distorted the naphthalene ring to a greater degree, as seen with the dihedral angle α reaching 11.0° for **3**. Interestingly, bis(dibromomethyl)naphthalene **4** (α = 8.3°) is vertically less distorted than **3**, although two

bromine atoms are introduced to the methyl group. As previously mentioned, the atomic arrangement made the C1–C8 distance in **4** smaller than **3** to accommodate convenience in spatial interaction between substituents. The ideal conformation allows four bromo atoms in **4** to be mutually pointed out in different directions to minimize overcrowding. As for **3**, the arrangement of two bromo atoms is close enough to cause intense resistance of bonds to be twisted, resulting in higher α. While the dihedral angle β and γ of naphthalene **1** are undoubtedly slight (β = 0.5° and γ = 0.1°), those values of other naphthalenes **2**–**4** increase depending on the bulkiness of substituents. Overall, both β and γ of **4** showed the same tendency compared to compound **3**.

Table 2-5. Comparison of dihedral angles α (between C1–R and C8–R bonds), β (between C1–C8a and C4a–C5 bonds), and γ (between C1–C8a and C4–C4a bonds) in naphthalene **1**–**4**.[a]

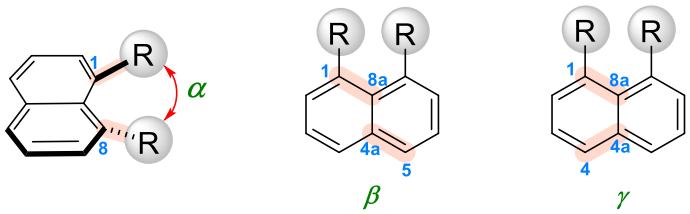

R		α/ °	β/ °	γ/ °
CH_3	**1**	0.7/0.7	0.5/0.6	0.1/0.2
CH_2OH	**2**	4.6/4.2	2.1/1.7	1.5/1.6
CH_2Br	**3**	11.0/10.9	4.1/4.9	4.9/4.1
$CHBr_2$	**4**	8.3/8.3	3.5/3.2	3.1/3.2

[a]Measured values/Calculated values. Calculated values are from optimized structures at B3LYP/6-31G(d,p) level of theory.

3.2. Magnetic Properties by NICS

NICS calculations are carried out to estimate the degree of aromaticity for naphthalenes **1**–**4** (Table 2-6). A clear example illustrating the inadequacy of NICS(0) for determining aromaticity is seen in compound **2**. In this case, π-electrons from adjacent oxygen atoms contribute to the ring currents, resulting in a considerably more negative value (−10.1 ppm) and

a higher aromaticity character compared to the other naphthalenes. To minimize the electronic effects, particularly from the bromo group positioned orthogonally to the ring plane, NICS(-1) for **Ring A** and NICS(1) for **Ring B** at a 1 Å distance are examined to assess the loss of aromaticity. Consequently, the aromaticity rankings from lowest to highest for **Ring A** are **1**, **2**, **3**, **4**, whilst for **Ring B** as **1**, **3**, **4**, **2**. This magnetic evaluation indicates that compound **1** is somehow losing its aromaticity even though it is less distorted than a prominent non-planar ring of **3** and **4**. Additionally, a comparison of NICS(1) and NICS(-1) shows an up-field shift for compound **3** compared to compound **4**, likely related to the more substantial vertical distortion in compound **3**.

Table 2-6. NICS calculation for **1**–**4**.[a]

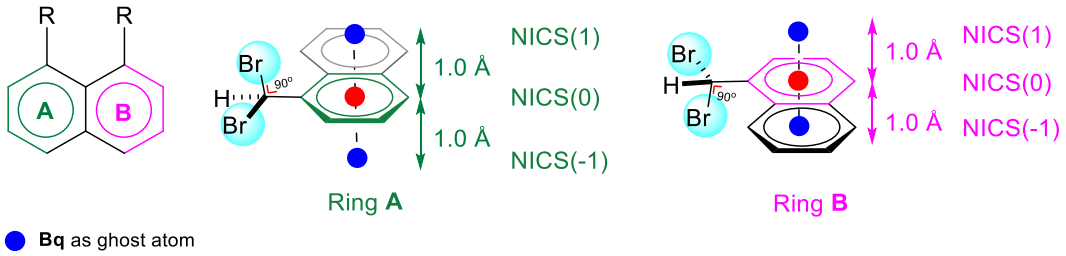

R		Ring A			Ring B		
		NICS(-1)	NICS(0)	NICS(1)	NICS(-1)	NICS(0)	NICS(1)
CH_3	**1**	−11.1	−9.0	−11.1	−11.1	−9.0	−11.1
CH_2OH	**2**	−11.2	−10.1	−12.0	−11.5	−10.0	−12.0
CH_2Br	**3**	−11.6	−9.9	−11.1	−11.1	−9.9	−11.6
$CHBr_2$	**4**	−11.7	−9.3	−10.7	−10.6	−9.3	−11.7

[a]NICS are performed using the GAIO method at B3LYP-6-31G(d,p) level of theory.

4. Reactivity

4.1. Nitration Reaction

The nitration reaction, one of the representative electrophilic aromatic substitutions, was selected to evaluate the reactivity due to the prior study that stated a congested C4–C4a–C5 position (here showed by θ angle in Table 2-2) as a direct effect from crowded *peri*-positions would cause a difficulty forming 4-nitration than 2-nitration.[9] Therefore, since derivatives **1**–**4**

are considered horizontally distorted on the opposite parts of the *peri*-position, the nitration product is proposed to follow the same stipulation. However, the outcomes are not entirely linear with the hypothesis when naphthalene **1** appeared almost comparable 1:1 of **1A** and **1B** products, while **2** gave nitronic acid ester (32%) (Table 2-7). Presumably, the substituents' electronic effect still rules the product's formation in **1** and **2** rather than merely non-electronic influencing as proposed.

Table 2-7. Nitration of 1,8-disubstituted naphthalenes **1–4**.

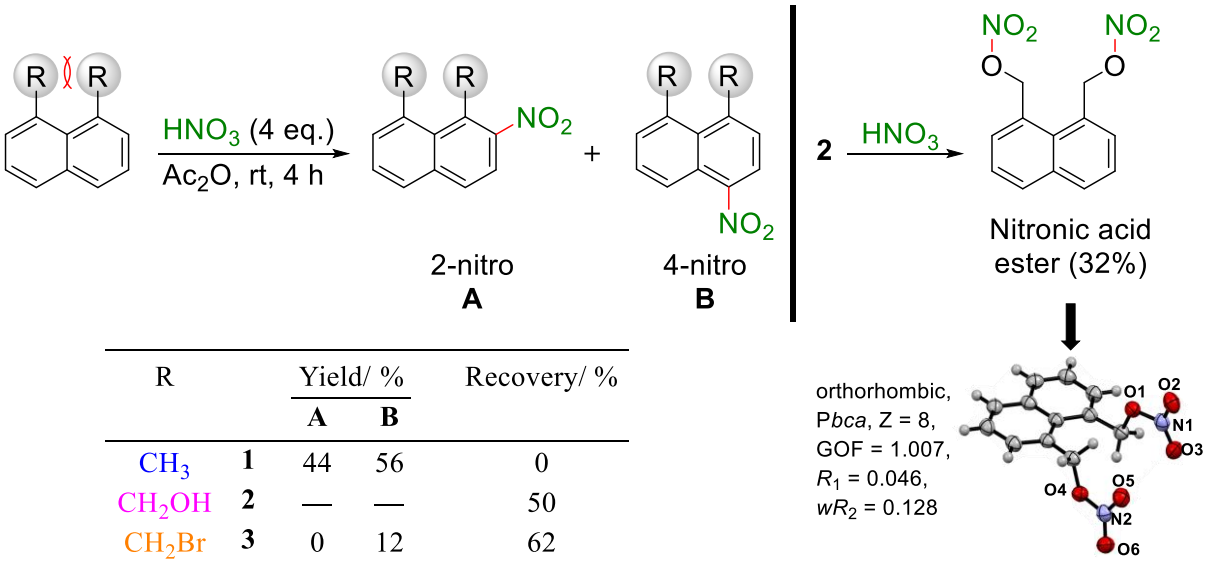

R		Yield/ %		Recovery/ %
		A	**B**	
CH_3	**1**	44	56	0
CH_2OH	**2**	—	—	50
CH_2Br	**3**	0	12	62
$CHBr_2$	**4**	0	0	61

In contrast, compound **3** produced 4-nitro products **3B** at 12%, while compound **4** was unproductive. This result partially supports the earlier proposition where **3**'s lower θ value than **4** indicates greater steric congestion for the upcoming nitro group. However, the struggle to form 2-nitro in these brominated derivatives, especially in compound **4**, could be because the crowded *peri*-position hindered the reaction.

4.2. Hydrogenation Reaction

Another approach to reactivity is catalytic hydrogenation, which was selected due to the expectation that the electronic effects of the substituents would be less significant. Naphthalene

derivatives were stirred under hydrogen at atmospheric pressure in the presence of a Pd/C catalyst in ethanol at room temperature for 1 h (Table 2-8). While naphthalenes **1**, **2**, and **4** remained unchanged under these conditions, naphthalene **3** underwent the debromination reaction, yielding **1** (68%). Although the focus of the response was primarily on the substituents (specifically the methyl group) rather than the unsaturated ring, the high reactivity of **3** is intriguing, especially when compared to the inertness of **4**, which was subjected to the more aggressive conditions.

Table 2-8. Hydrogenation on 1,8-disubstituted naphthalenes **1–4**.[a]

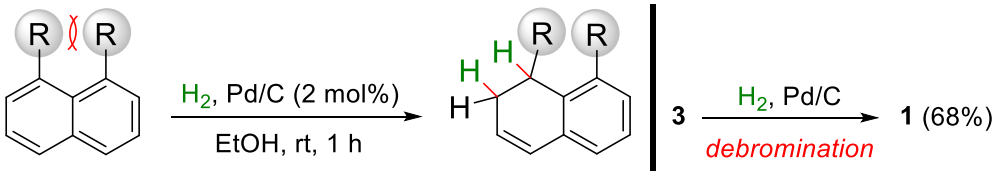

R		Yield/%	Recovery/%
CH_3	**1**	0	99
CH_2OH	**2**	0	98
CH_2Br	**3**	0	21
$CHBr_2$	**4**	0	99[a]

[a]Reaction conditions: 40 °C, cat. 20 mol%, 1 h.

4.3. Electronic Evaluation

Among the *peri*-substituted naphthalenes **1**–**4**, only compound **3** that demonstrates significant reactivity in nitration and hydrogenation reactions. From the standpoint of vertical distortion, dibrominated naphthalene **3** is more distorted than **4**, while **4** primarily experiences more horizontal distortions. To gain further insight, I performed structural evaluations and density functional theory (DFT) calculations for compounds **1**, **3**, and **4** at the B3LYP/6-31G(d,p) level, excluding naphthalene **2** due to its high influence from electronic effects in both experimental and computational observations. The calculated structural parameters closely align with the actual parameters observed through crystallography (Table 2-9).

Table 2-9. Comparison of C–C and C–Br bond length (Å) in **1**, **3**, and **4**.

Side view of crystal structures

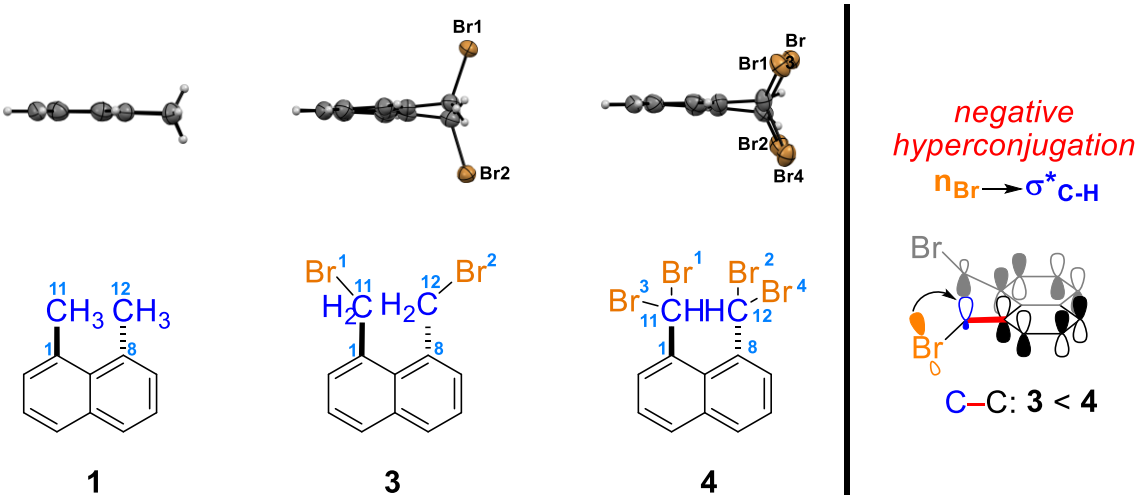

Parameters		C11–Br1	C11–Br3	C12–Br2	C12–Br4	C1–C11	C8–C1 2
CH_3	crystal	—	—	—	—	1.507(2)	1.513(2)
	calc.	—	—	—	—	1.517	1.517
CH_2Br	crystal	1.981(3)	—	1.996(3)	—	1.499(4)	1.489(4)
	calc.	2.020	—	2.021	—	1.496	1.496
$CHBr_2$	crystal	1.986(8)	1.956(7)	1.977(7)	1.947(8)	1.510(1)	1.490(1)
	calc.	1.996	1.976	1.996	1.976	1.502	1.502

The bond lengths between the substituents and ring carbons (C1–C11 and C8–C12) in compound **3** are shorter than in compounds **1** and **4**, indicating double-bond characteristics. In the brominated naphthalenes **3** and **4**, the carbon–bromine bonds (C11–Br1 and C12–Br2) are orthogonal to the rings and elongated, while the second bonds (C11–Br3 and C12–Br4) in compound **4** are shorter. During the nitration reaction, the shorter carbon–bromine bonds may have subsequently interacted with the naphthalene system after allowing electron delocalization to anti-bonding orbital (σ*) due to the negative hyperconjugation effect,[10] resulting in compound **3** appearing more reactive. However, an increase in the number of bromo atoms creates steric hindrance; thus, following the same preposition is complicated for compound **4**. Conclusively, **4** appeared more inert in the nitration reaction.

For the hydrogenation reaction, the HOMO-LUMO comparison declares how naphthalene **4** should have been more reactive than **1** and **3** due to the lower energy gap (Figure 2-2). Still, the prominent decrease of LUMO level in **4** is due to the merrier electron withdrawing bromo group instead of relying on the geometric distortions **4** had. The relationship between frontier energy and the experimental outcomes does not entirely account for the observed results, which prompts another alternative explanation. Furthermore, the catalytic surface may be less accessible for compound **4** than for compound **3** during the hydrogenation reaction since steric hindrance is imposed by the bulky dibromomethyl group. This condition can obstruct the approach of certain molecules to the catalytic site, thereby influencing the reaction efficiency.

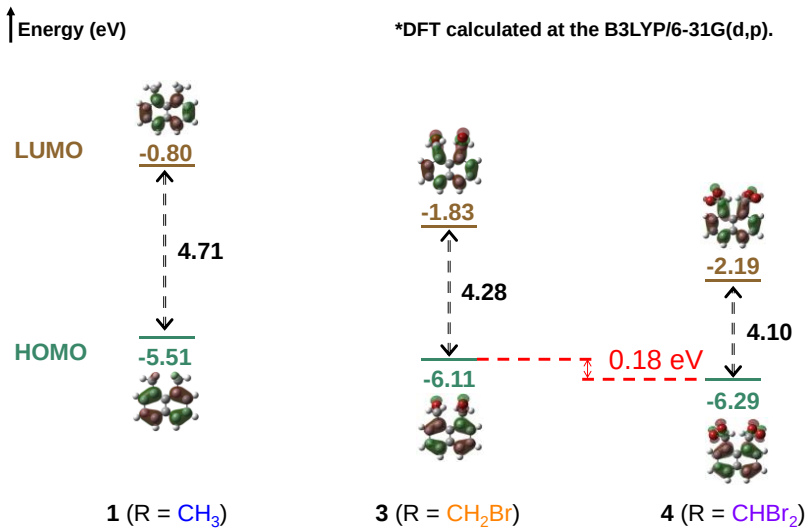

Figure 2-2. HOMO and LUMO levels (eV) of **1**, **3**, and **4**.

5. Conclusion

To summarize the discussions above, the ring distortion occurs in the following order: 1) horizontal distortion, 2) vertical distortion, and 3) elongation of the bond and interatom distances as their bulkiness increases (Figure 2-3). In detail, when two substituents exist at the *peri*-positions, the outside-ring angles around C9 δ become more prominent than the sp^2 standard angle (120°), while the inside-ring angles ε and η become smaller (horizontal

distortion). During this distortion, coplanarity has remained for all compounds. Later on, upon replacing one hydrogen atom in the methyl group with bulkier substituents such as hydroxy and bromo groups, a larger steric repulsion started to disturb the coplanarity of the naphthalene ring, notifying by dihedral angle ***α*** as vertical distortion. In addition, as the substituent becomes bulkier, interatom distances ***X*** and ***Y*** become longer, and bond length ***C*** also elongates due to the steric repulsion between *peri*-substituents (elongation of bond and interatom distances). Furthermore, the bond lengths represented by ***A*** and ***B***, along with the interatomic distance denoted by ***Z*** on the opposite side, experience a reduction in length due to compression.

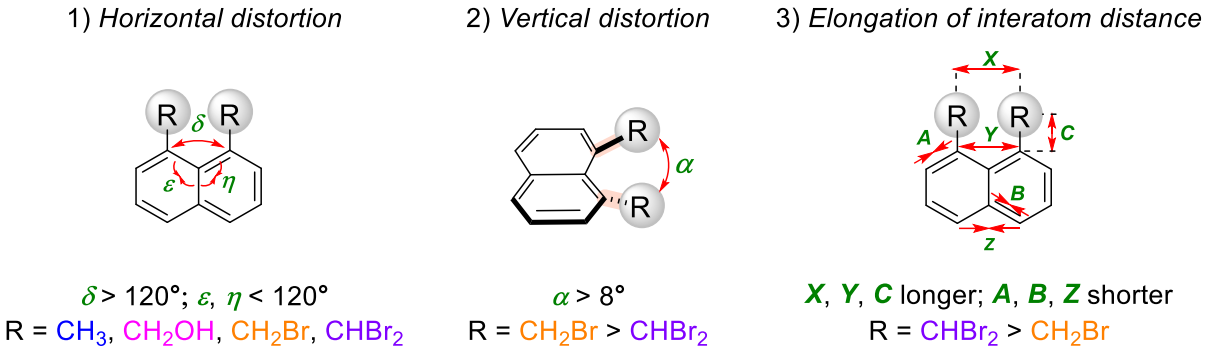

Figure 2-3. Three observing distortions of the naphthalene ring.

A systematic evaluation method for non-electronic activation is not established because the inductive electron-withdrawing and steric hindrance are still influenced. Although it is necessary to investigate further in evaluating the reactivity, the correlation between the bulkiness of the *peri*-substituents and distortion of the naphthalene ring will be useful information for researchers who study the physical properties of aromatic compounds, especially those who aim to modify them.

6. Experimental Section

All reagents were purchased from commercial sources and used without further purification. TLC on commercial aluminum-backed plates of silica gel 60 F254 was used to

monitor the progress of the reactions. ^{1}H and ^{13}C-NMR spectra were recorded on a Bruker DPX-400 spectrometer (400 MHz and 100 MHz, respectively) in $CDCl_3$ using TMS as an internal standard. The assignments of the ^{13}C-NMR were reassured by DEPT experiments. The order of aromatic proton of naphthalenes was confirmed with 2D-NOESY. IR spectra were recorded with a JASCO FT/IR-4200 spectrometer equipped with an ATM detector. The melting points were recorded on an SRS-Optimelt automated melting point system. Diffraction data were collected at 103 K under a cold N_2-gas stream on a Rigaku XtaLAB Synergy-S/Mo system (λ=0.71073 Å (Mo-Kα)). High-resolution mass spectra (HRMS) were obtained from a Bruker compact mass spectrometer set at APCI-positive mode.

A single crystal for each naphthalene was prepared using the slow evaporation method. Approximately 10 mg of the compound was dissolved in chloroform (1 ml) and placed in a clean dry glass vial.

All related calculations were performed using the Gaussian 09 package.[11] Geometries of anthracenes were optimized using B3LYP/6-31G(d,p) level of theory and the structures were verified to be minima via frequency. GIAO NMR shifts were employed to extract NICS values.

a. Preparation of 1,8-naphthalenedimethanol (**2**)

To a suspension of lithium aluminum hydride (2.6 g, 68 mmol) in tetrahydrofuran (200 mL), zinc chloride (2.2 g, 68 mmol) was added at -20 °C. Then, 1,8-naphthalic anhydride (**6**) (5 g, 25 mmol) was slowly added, and the resulting mixture was stirred at room temperature for 1 d. After quenching the reaction with water (20 mL), the pH was adjusted to 4–5 with 1 M hydrochloric acid. After the removal of THF and extraction with ethyl acetate (30 mL × 3), the organic layer was washed with brine (30 mL), dried over magnesium sulfate, and concentrated under reduced pressure. The residue was washed with diethyl ether (50 mL) to afford 1,8-bis(hydroxymethyl)naphthalene (**2**) (3.85 g, 20.5 mmol, 82%) as colorless needles. ^{1}H NMR (400 MHz, $CDCl_3$) δ 7.87 (dd, J = 8.2, 1.6 Hz, H), 7.56 (dd, J = 7.0, 1.6 Hz, 2H), 7.45 (dd, J =

8.2, 7.0 Hz, 2H), 5.30 (s, 4H). Formation of **2** was confirmed by comparison of spectroscopic data with those in the literature.[2]

b. Preparation of 1,8-bis(bromomethyl)naphthalene (**3**)

To a solution of naphthalene **2** (3.0 g, 16 mmol) in 1,4-dioxane (30 mL), phosphorous tribromide (1 mL, 10.5 mmol) was slowly added, and the mixture was stirred at room temperature for 1 d. After the addition of water (10 mL), the mixture was stirred for 1 h, and colorless precipitates were collected *via* filtration and dried under vacuum to furnish 1,8-bis(bromomethyl)naphthalene (**3**) (4.0 g, 12.7 mmol, 82%). ^{1}H NMR (400 MHz, $CDCl_3$) δ 7.89 (dd, J = 8.2, 1.6 Hz, 2H), 7.63 (dd, J = 7.1, 1.6 Hz, 2H), 7.46 (dd, J = 8.2, 7.1 Hz, 2H), 5.31 (s, 4H). Formation of **3** was confirmed by comparison of spectroscopic data with those in the literature.[2]

c. Preparation of 1,8-dimethylnaphthalene (**1**)

To a solution of 1,8-bis(bromomethyl)naphthalene (**3**) (1.6 g, 5 mmol) in dimethyl sulfoxide (20 mL), sodium borohydride (970 mg, 25 mmol) was added, and the mixture was stirred at 80 °C for 1 d. Water (20 mL) was added, producing white precipitation, and continued stirring for 1 h. The white precipitates were collected *via* filtration and purified by column chromatography (eluted by Hexane/EtOAc = 9/1), the purified white needles product gave quantitively **1** (0.78 g, 5 mmol, quant.) as colorless needles. ^{1}H NMR (400 MHz, $CDCl_3$) δ 7.67 (d, J = 8.0 Hz, 2H), 7.31–7.23 (m, 4H), 2.94 (s, 6H). Formation of **1** was confirmed by comparison of spectroscopic data with those in the literature.[3]

d. Preparation of 1,8-bis(dibromomethyl)naphthalene (**4**)[4]

To a solution of bis(bromomethyl)naphthalene **3** (2.0 g, 6.4 mmol) in carbon tetrachloride (40 mL), were added *N*-bromosuccinimide (2.3 g, 13 mmol) and azobis(isobutyronitrile) (260 mg, 1.58 mmol), and the mixture was heated under reflux for 1 d. After the addition of water (25 mL), the mixture was extracted with ethyl acetate (30 mL × 3). The organic layer was dried over magnesium sulfate and evaporated, and the residue was treated *via* column

chromatography on silica gel to afford 1,8-bis(dibromomethyl)naphthalene (**4**) (1.65 g, 3.5 mmol, 55%, eluted by hexane/EtOAc = 9/1) as pale-yellow crystals. mp 106–109 °C; ^{1}H NMR (400 MHz, $CDCl_3$) δ 8.52 (dd, *J* = 7.5, 1.3 Hz, 1H), 7.85 (dd, *J* = 8.1, 1.3 Hz, 1H), 7.66–7.56 (m, 2H), 7.66 (s, 2H); ^{13}C NMR (100 MHz, $CDCl_3$) δ 137.1 (C), 134.3 (CH), 133.5 (C), 132.0 (CH), 126.1 (CH), 123.5 (C), 40.2 (CH_2); IR (KBr/cm^{-1}) 672; HRMS (APCI–TOF) calculated for $[M+H^+–Br]^+$ $C_{12}H_8Br_3$: 390.8150, found: 390.8200.

e. Nitration reaction for *peri*-substituted naphthalenes

To a solution of *peri*-substituted naphthalene (0.3 mmol) in chloroform (3 mL), a solution of nitric acid HNO_3 (d = 1.42, 53 μL, 1.2 mmol) in acetic anhydride (1.5 mL) was added. After stirring the resultant mixture at room temperature for 4 h, water (10 mL) was added, and the mixture was extracted with chloroform (20 mL × 3). The organic layer was washed with 2 M sodium hydrogen carbonate aqueous solution (10 mL), dried over magnesium sulfate, and evaporated. The residue was treated *via* column chromatography on silica gel to afford nitrated products (eluted by hexane/EtOAc = 9/1).

1A: (26 mg, 0.13 mmol, 44%). ^{1}H NMR (400 MHz, $CDCl_3$) δ 7.72 (dd, *J* = 11.2, 8.2 Hz, 2H), 7.61 (d, *J* = 8.2 Hz, 1H), 7.48–7.38 (m, 2H), 2.94 (s, 3H), 2.88 (s, 3H). The formation of **1A** was confirmed by a comparison of spectroscopic data with those in the literature.[2]

1B: (34 mg, 0.17 mmol, 56%). ^{1}H NMR (400 MHz, $CDCl_3$) δ 8.22 (dd, *J* = 8.8, 1.3 Hz, 1H), 7.88 (d, *J* = 7.1 Hz, 1H), 7.50 (dd, *J* = 8.8, 7.8 Hz, 1H), 7.40 (d, *J* = 7.1 Hz, 1H), 7.31 (dd, *J* = 7.8, 1.3 Hz, 1H), 2.99 (s, 3H), 2.96 (s, 3H). Formation of **1B** was confirmed by comparison of spectroscopic data with those in the literature.[2]

3B: (13 mg, 0.03 mmol, 12%). mp 114-117 °C; ^{1}H NMR (400 MHz, $CDCl_3$) δ 8.30 (dd, *J* = 8.8, 1.4 Hz, 1H), 7.94 (d, *J* = 8.0 Hz, 1H), 7.76 (dd, *J* = 7.2, 1.4 Hz, 1H), 7.69 (dd, *J* = 8.0 Hz, 1H), 7.67 (dd, *J* = 8.8, 1.4 Hz, 1H); ^{13}C NMR (100 MHz, $CDCl_3$) δ 149.8 (C), 139.3 (C), 134.5 (CH), 131.1 (CH), 130.1 (C), 128.7 (CH), 127.4 (C), 125.6 (CH), 124.9 (C), 122.1 (CH), 36.1 (CH_2),

35.1 (CH_2); IR (KBr/cm^{-1}) 1526, 767; HRMS (APCI–TOF) Calcd. for $[M+H]^+$ $C_{12}H_9Br_2NO_2$: 359.9053, found 359.9103.

f. Hydrogenation reaction for *peri*-substituted naphthalenes

To a solution of *peri*-substituted naphthalene (0.3 mmol) in ethanol (8 mL), 5 wt% Pd/C (10 mg, 2 mol%) was added. After bubbling hydrogen gas for 1 min, the test tube was sealed and stirred at room temperature for 1 h. After filtration using celite, the filtrate was concentrated, and the residue was subjected to proton ^1H NMR analysis.

7. References

1. Pascal, R. A. *Chem. Rev*. **2006**, *106*, 4809–4819.
2. (a) Luo, H.; Zeng, Q.; Liu, Z.; Wei, Y.; Li, B.; Wang, F. *Syn. Comms*. **2004**, *34*, 2269–2275; (b) Kamada, T.; Gama, Y.; Wasada, N. *Bull. Chem. Soc. Jpn.* **1989**, *62*, 3024–3025.
3. Nagao, Y.; Yoshida, T.; Arimitsu, K.; Kozawa, K. *Heterocycles* **2010**, *80*, 1197–1213.
4. Hauptmann, S.; Hunger, P.; Blaskovits, A. *J. Prakt. Chem*. **1986** *37*, 72–77.
5. Deschamps, J. R. *Life Sci*. **2010**, *86*, 585–589.
6. Balasubramaniyan, V. *Chem. Rev*. **1966**, 66, 567–641.
7. (a) Chen, X.; Kobiro, K.; Asahara, H.; Kakiuchi, K.; Sugimoto, R.; Saigo, K.; Nishiwaki, N. *Tetrahedron* **2013**, *69*, 4624–4630; (b) Iwai, K.; Yokoyama, S.; Asahara, H.; Nishiwaki, N. *Bull. Chem. Soc. Jpn.* **2020**, *93*, 50–57.
8. Michl, J. "Organic Chemical Systems, Theory". In *Encyclopedia of Physical Science and Technology Third Ed.* Academic Press. **2003**, pp: 435–457.
9. Davies, A.; Warren, K. D. *J. Chem. Org. Soc. B.* **1969**, 873–878.
10. Alabugin, I. V.; Kuhn, L.; Krivoshchapov, N. V.; Mehaffy, P.; Medvedev, M. G. *Chem, Soc. Rev*. **2021**. *50*, 10212–10252.
11. Gaussian 09, Revision A.02, M. J. Frisch, G. W. Trucks, H. B. Schlegel, G. E. Scuseria, M. A. Robb, J. R. Cheeseman, G. Scalmani, V. Barone, B. Mennucci, G. A. Petersson, H.

Nakatsuji, M. Caricato, X. Li, H. P. Hratchian, A. F. Izmaylov, J. Bloino, G. Zheng, J. L. Sonnenberg, M. Hada, M. Ehara, K. Toyota, R. Fukuda, J. Hasegawa, M. Ishida, T. Nakajima, Y. Honda, O. Kitao, H. Nakai, T. Vreven, J. A. Montgomery Jr., J. E. Peralta, F. Ogliaro, M. Bearpark, J. J. Heyd, E. Brothers, K. N. Kudin, V. N. Staroverov, T. Keith, R. Kobayashi, J. Normand, K. Raghavachari, A. Rendell, J. C. Burant, S. S. Iyengar, J. Tomasi, M. Cossi, N. Rega, J. M. Millam, M. Klene, J. E. Knox, J. B. Cross, V. Bakken, C. Adamo, J. Jaramillo, R. Gomperts, R. E. Stratmann, O. Yazyev, A. J. Austin, R. Cammi, C. Pomelli, C. Ochterski, J. W. Martin, R. L. Morokuma, K. Zakrzewski, V. G. Voth, P. Salvador, J. J. Dannenberg, S. Dapprich, A. D. Daniels, O. Farkas, J. B. Foresman, J. V. Ortiz, J. Cioslowski, D. J. Fox, Gaussian, Inc., Wallingford CT, **2016**.

Chapter 3. Steric Repulsion between *peri*-Substituents of 1,8-Dichloroanthracene Derivatives

1. Introduction

Bending and twisting angles are widely used to create planarity distortion in polycyclic aromatic hydrocarbons (PAHs).[1] Due to strain distribution, different geometry is produced on the acene framework; bending introduces greater distortion in the central rings (Figure 3-1, left), while uniform distortion is formed in the case of end-to-end twists along the acene framework (Figure 3-1, right). Controlling and isolating these distortions is challenging when the goal is to obtain specific electronic, magnetic, and optical properties in products.[2] Nevertheless, several experimental studies and computational evaluations have linked features of dis-planarity and aromaticity, yielding insightful results in the acene framework. Some state that chemical reactivity increases following bending than twisting deformations.[3] Furthermore, the frontier molecular orbital, HOMO–LUMO gap, decreases slightly as the ring distortion increases,[2] which is similar to the behavior of π-electron delocalization on the evaluated ring.[4]

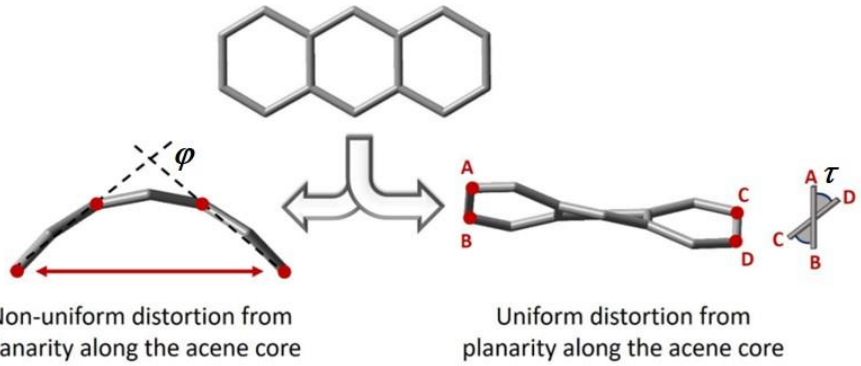

Figure 3-1. Schematic illustration of bending and twisting feature in an acene ring. Image is reprinted with permission to modify from John Wiley & Sons (License Number: 5933431452926).[1]

Several studies on deformation and aromaticity evaluation have been conducted in fully substituted anthracenes such as decaphenylanthracene,[5] and decachlroanthracene.[6] However, no report currently focuses on steric repulsion by bulkiness only on the *peri*-position. Hence, ring distortion and reactivity are evaluated using 1,8-dichloroanthracene, where bulkiness is introduced at the 9-position by various alkyl groups. To demonstrate how significant ring distortion reduces aromatic properties, the corresponding 10-substituted anthracenes are also prepared as a comparison (Figure 3-2).

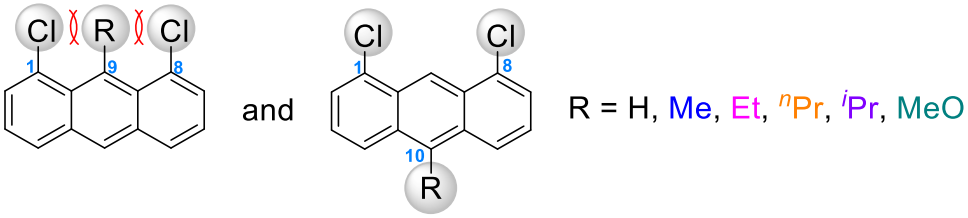

Figure 3-2. Selected substrates to study bulkiness in the *peri*-anthracene framework.

2. Synthesis and Crystal Study

According to the reported methods,[7-10] 9- and 10-substituted 1,8-dichloroanthracenes **4** and **5** were prepared in a stepwise manner (Scheme 3-1). First, the treatment of 1,8-dichloroanthraquinone **1** with tin(II) chloride underwent a single reduction to afford a mixture of regioisomeric anthrones **2A** and **2B**, while a double reduction led to unsubstituted 1,8-dichloroanthracene **3** upon treatment of **1** with sodium borohydride. Two subsequent steps were used to introduce the alkyl groups: alkylation using Grignard reagents on the carbonyl group and dehydration using thionyl chloride. To confirm the possibility that the electronic effect of the substituent may influence the reactivity, methoxy derivatives showing electron-donating resonance effect were also prepared by *O*-methylation of anthrones **2A** and **2B** using dimethyl sulfate in the presence of sodium hydride.

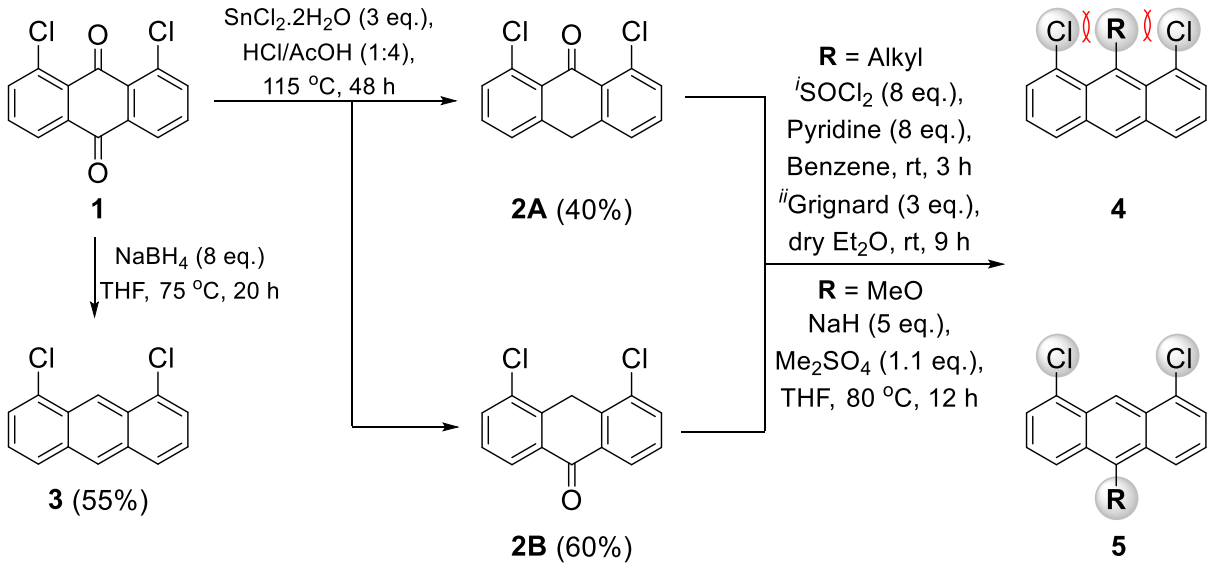

Anthracenes		Yield/%	
R		**4**	**5**
Me	**a**	76	51
Et	**b**	49	88
^{n}Pr	**c**	70	52
^{i}Pr	**d**	quant.	65
MeO	**e**	quant.	63

Scheme 3-1. Synthesis procedure of anthracene derivatives using 1,8-dichloroanthraquinone **1**.

Crystals for X-ray crystallography analysis were grown in a slow-evaporation-recrystallization process surveying certain solvents as hexane for **4b**, and chloroform for **4e**, **5b**, **5c**, **5d**, and **5e** besides for previously reported data of **3**,[11a] **4a**,[11b] and **5a**[11b] (Table 3-1). However, a suitable single crystal could not be obtained for **4c** and **4d** despite relentless recrystallization efforts because of instability for air oxidation. When optimized structures in a gas phase were calculated for all anthracenes using the B3LYP-D3/6-311G+(d,p) level of theory, the results were in a comparable agreement between the computed structure and the observed ones for all anthracenes (see Table 3-2, Table 3-3, and Table 3-4). Hence, the missing blanks for **4c** and **4d** can be tolerated using their calculated data.

Table 3-1a. Selected crystallographic information for crystal structures **3**–**4**.

	3 (R = H)	**4a** (R = Me)	**4b** (R = Et)	**4e** (R = MeO)
Empirical formula	$C_{14}H_8Cl_2$	$C_{15}H_{10}Cl_2$	$C_{16}H_{12}Cl_2$	$C_{15}H_{10}Cl_2O$
Crystal system	Monoclinic	Monoclinic	Monoclinic	Orthorhombic
Space group	$P2_1/c$ (#14)	$P2_1/n$ (#14)	$P2_1/c$ (#14)	*Pnma* (#62)
a (Å)	19.0070(14)	10.15040(18)	7.8986(5)	7.1998(4)
b (Å)	3.9621(3)	8.46384(14)	11.8645(5)	19.0743(10)
c (Å)	15.1370(11)	26.8184(5)	13.6224(7)	8.8574(5)
α (°)	90	90	90	90
β (°)	107.4103(15)	94.3324(17)	102.460(5)	90
γ (°)	90	90	90	90
Z	4	8	4	4
GOF	1.146	1.093	1.061	1.151
R indices	$R_1 = 0.0278$, $wR_2 = 0.0827$	$R_1 = 0.0396$, $wR_2 = 0.1065$	$R_1 = 0.0347$, $wR_2 = 0.0945$	$R_1 = 0.0582$, $wR_2 = 0.1705$
ORTEP	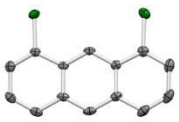	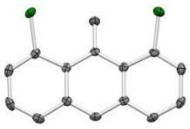		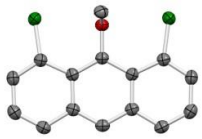

Table 3-1b. Selected crystallographic information for crystal structures **5**.

	5a (R = Me)	**5b** (R = Et)	**5c** (R = ^{n}Pr)	**5d** (R = ^{i}Pr)	**5e** (R = MeO)
Empirical formula	$C_{15}H_{10}Cl_2$	$C_{16}H_{12}Cl_2$	$C_{17}H_{14}Cl_2$	$C_{17}H_{14}Cl_2$	$C_{15}H_{10}Cl_2O$
Crystal system	Orthorhombic	Monoclinic	Triclinic	Monoclinic	Monoclinic
Space group	*Pnma* (#62)	$P2_1/c$ (#14)	*P*-1 (#2)	$P2_1/c$ (#14)	$P2_1/c$ (#14)
a (Å)	15.2621(9)	5.1457(2)	10.2371(5)	10.2232(8)	3.9754(3)
b (Å)	18.8630(11)	14.9861(7)	10.2662(4)	11.8221(7)	14.3545(13)
c (Å)	3.8738(2)	16.6489(7)	14.6413(7)	12.2349(8)	20.965(2)
α (°)	90	90	79.915(4)	90	90
β (°)	90	93.336(4)	76.524(4)	111.114(8)	91.266(8)
γ (°)	90	90	64.289(5)	90	90
Z	4	4	2	4	4
GOF	1.154	1.059	1.069	1.033	1.036
R indices	$R_1 = 0.0747$, $wR_2 = 0.2023$	$R_1 = 0.0361$, $wR_2 = 0.0889$	$R_1 = 0.0359$, $wR_2 = 0.0942$	$R_1 = 0.0510$, $wR_2 = 0.1546$	$R_1 = 0.0523$, $wR_2 = 0.1474$
ORTEP	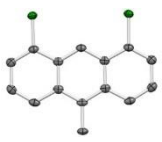	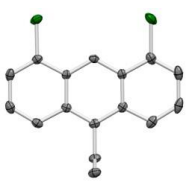	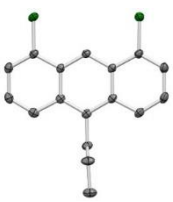	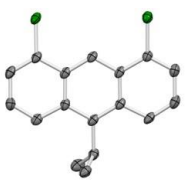	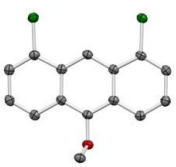

3. Evaluation of Distortions

The distortion on the anthracene ring for each compound is still evaluated under geometric and magnetic criteria. For distortion based on geometric profile, two significant parameters such as (a) horizontal distortion, consisting of bond length, atomic distance, and bond angles, and (b) vertical distortion, including torsion, bending, and twisting angles, will be discussed thoroughly. Additionally, the data will be accompanied by a summary in graphs to facilitate the observation of trends in distortions as bulkiness increases. Finally, NICS values obtained from the same optimized structure are provided for the magnetic evaluation.

3.1. Geometric

3.1.1. Horizontal Distortions

For horizontal review, only one side from each related parameter was displayed in Figure 3-3 because both sides exhibited almost the same values as shown in Table 3-2. The bond length of C9–C9a/ ***A*** increases particularly in the case of 9-isopropyl derivative **4d,** accompanied by a decline in C10–C4a/ ***B***. In the case of the 10-substituted anthracene **5** series, a reversed pattern was observed for the same parameter because of the opposite substitution position, where the bond length of C10–C4a becomes longer while C9–C9a becomes shorter (Figure 3-3a). Regarding interatomic distance, methoxy substituted **4e** has a notably high value for its C9a–C8a/ ***X*** compared to those of other alkyl substituted derivatives because the oxygen atom of **4e** is located nearly in-plane with two chloro atoms (Figure 3-3b). Consequently, an intense horizontal distortion causes an enlarging distance between C9a and C8a on **4e**. Among alkyl-substituted anthracenes, methyl and isopropyl derivatives **4a** and **4d** have similarly high values. The interatomic distance for C4a–C10a/ ***Y*** of **5d** and **5e** was longer than that of the others; however, the difference is insignificant.

On the other side, the inner bond angles where an alkyl or a methoxy group is attached (C8a–C9–C9a/ δ and C4a–C10–C10a/ θ for **4** and **5**, respectively) become narrow when the bulkiness of the substituent increases (Figure 3-3c). The narrow bond angle suggested a remarkable shift to the s-character of C9 and C10 for the bulkier **4d** (117.7°) and **5d** (119.5°) due to a bigger deviation from planarity.[12] Inner bond angles, C1–C9a–C4a/ ε and C4–C4a–C9a/ η, in the fused ring were also affected by substituent repulsion, where these angles become smaller as enlargement of the alkyl substituent, whereas the angle of **5d** shows the opposite trend (Figure 3-3d).

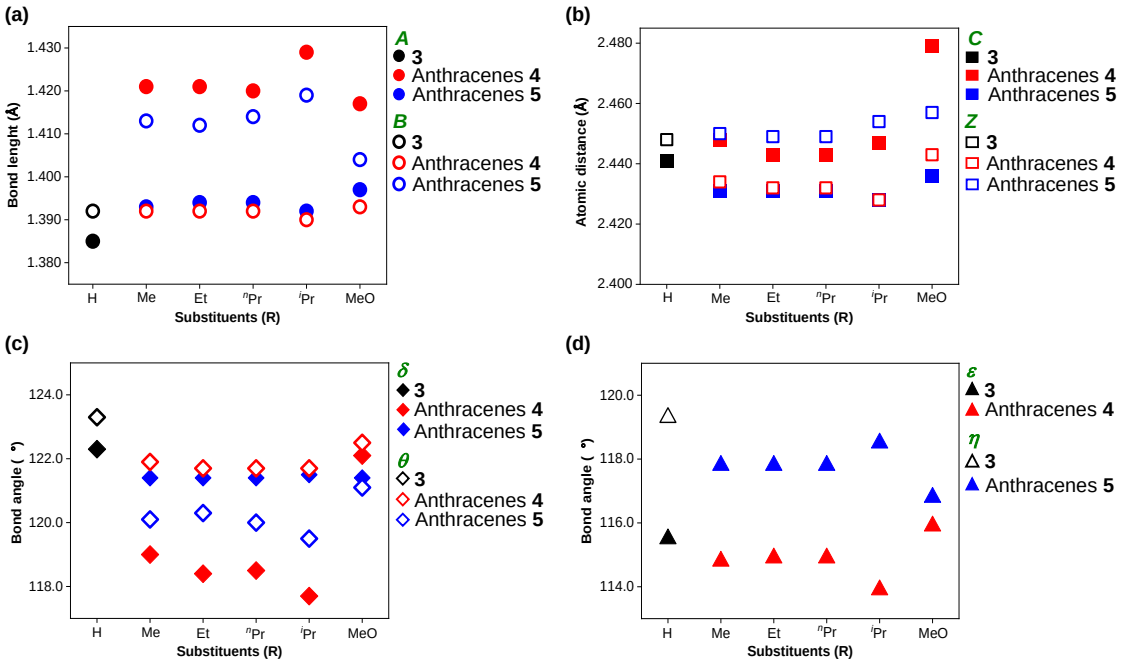

Figure 3-3. Summary of horizontal distortion's trend as bulkiness increases in *peri*-position of anthracenes **3**–**5**.

Table 3-2a. Selected parameters evaluating horizontal distortions on anthracene **3**–**4**.[a]

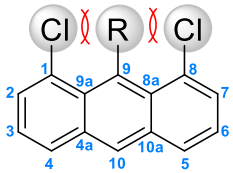

R	
Me	**a**
Et	**b**
^{n}Pr	**c**
^{i}Pr	**d**
MeO	**e**

3 (R = H) and **4**

Parameters		**3**	**4a**	**4b**	**4c**	**4d**	**4e**
Bond length (Å)	C9–C9a/ ***A***	1.397(1) 1.398	1.418(3) 1.421	1.419(2) 1.421	— 1.420	— 1.429	1.413 1.417
	C9–C8a	1.399(2) 1.398	1.423(3) 1.421	1.423(2) 1.423	— 1.423	— 1.429	1.413 1.417
	C10–C4a/ ***B***	1.400(2) 1.398	1.395(3) 1.392	1.386(2) 1.392	— 1.392	— 1.390	1.391 1.393
	C10–C10a	1.398(1) 1.398	1.389(3) 1.392	1.392(2) 1.393	— 1.393	— 1.390	1.391 1.393
Atomic distance (Å)	C9a–C8a/ ***X***	2.433(1) 2.441	2.448(3) 2.448	2.442(2) 2.443	— 2.443	— 2.447	2.475(2) 2.479
	C4a–C10a/ ***Y***	2.444(1) 2.448	2.433(3) 2.434	2.492(2) 2.432	— 2.432	— 2.428	2.437(3) 2.443
Bond angle (°)	C8a–C9–C9a/ δ	120.9(1) 121.6	119.0(2) 119.0	118.5(1) 118.4	— 118.5	— 117.7	122.4 122.1
	C4a–C10–C10a/ θ	121.7(1) 122.2	121.8(2) 121.9	122.0(1) 121.7	— 121.7	— 121.7	122.3 122.5
	C1–C9a–C4a/ ε	117.1(9) 117.0	114.6(2) 114.8	114.2(1) 114.9	— 114.9	— 113.9	115.8(2) 115.9
	C8–C8a–C10a	116.9(9) 117.0	114.9(2) 114.8	120.7(1) 120.7	— 120.7	— 121.5	120.3(2) 120.6
	C4–C4a–C9a/ η	119.7(1) 119.6	120.8(2) 120.9	114.3(1) 114.8	— 114.8	— 113.7	115.8(2) 115.9
	C5–C10a–C8a	119.6(1) 119.6	120.7(2) 120.9	121.1(1) 120.9	— 120.9	— 121.4	120.3(2) 120.6

[a]Measured and calculated values are shown as upper and lower rows, respectively.

Table 3-2b. Selected parameters evaluating horizontal distortions on anthracene **5**.[a]

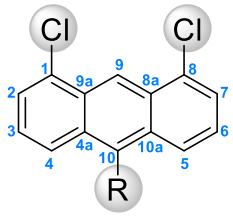

5

R	
Me	**a**
Et	**b**
^{n}Pr	**c**
^{i}Pr	**d**
MeO	**e**

Parameters		**5a**	**5b**	**5c**	**5d**	**5e**
Bond length (Å)	C9–C9a/ ***A***	1.391 1.393	1.391(2) 1.394	1.394(2) 1.394	1.385(3) 1.392	1.394(3) 1.397
	C9–C8a	1.391 1.394	1.393(2) 1.394	1.399(2) 1.394	1.395(3) 1.391	1.392(4) 1.397
	C10–C4a/ ***B***	1.414 1.413	1.409(2) 1.412	1.416(2) 1.414	1.415(3) 1.419	1.399(4) 1.404
	C10–C10a	1.414 1.415	1.416(2) 1.414	1.416(2) 1.414	1.417(3) 1.422	1.399(3) 1.404
Atomic distance (Å)	C9a–C8a/ ***X***	2.420(3) 2.431	2.422(2) 2.431	2.430(2) 2.431	2.424(3) 2.428	2.425(3) 2.436
	C4a–C10a/ ***Y***	2.453(3) 2.450	2.445(2) 2.449	2.447(2) 2.449	2.443(3) 2.454	2.451(3) 2.457
Bond angle (°)	C8a–C9–C9a/ δ	120.9 121.4	120.9(1) 121.4	120.9(1) 121.4	121.4(2) 121.5	121.1(2) 121.4
	C4a–C10–C10a/ θ	120.3 120.1	120.0(1) 120.3	119.6(1) 120.0	119.2(2) 119.5	122.4(2) 122.1
	C1–C9a–C4a/ ε	117.1(2) 117.9	117.9(1) 117.8	117.8(1) 117.8	118.4(1) 118.4	116.5(2) 116.8
	C8–C8a–C10a	117.1(2) 117.8	117.7(1) 118.1	117.8(1) 118.1	116.4(2) 117.1	119.5(2) 120.0
	C4–C4a–C9a/ η	118.3(2) 117.8	117.7(1) 117.8	118.1(1) 117.8	118.3(2) 118.5	116.4(2) 116.8
	C5–C10a–C8a	118.3(2) 118.3	117.9(1) 118.1	117.8(1) 118.1	117.2(2) 116.9	120.1(2) 120.0

[a]Measured and calculated values are shown as upper and lower rows, respectively.

3.1.2. Vertical Distortions

Since anthracene **3** possesses no substituent at the 9- and 10-position, this structure will be excluded from further discussion regarding vertical distortions. For vertical distortions, each torsion angle (α) from respective bonds C1–Cl1//C9–R and C8–Cl2//C9–R for anthracene **4** and C4–H4//C10–R and C5–H5//C10–R for anthracene **5** were evaluated (Table 3-3). However, the trend in the graph will only display the larger dihedral angle from those unsymmetrical geometries, respectively. This is intended to simplify interpretation and harmonize the data using similar sources among all anthracenes. As a result, anthracenes **4** promote dihedral angles with over 30° angles and a steady increase for α, giving the precise order of **4a** < **4b** ≈ **4c** < **4d** (Figure 3-4a). Conversely, only 0–2° of dihedral angle was observed for the **5** series, indicating that coplanar structures were maintained due to minimal steric repulsion from distant substituents.

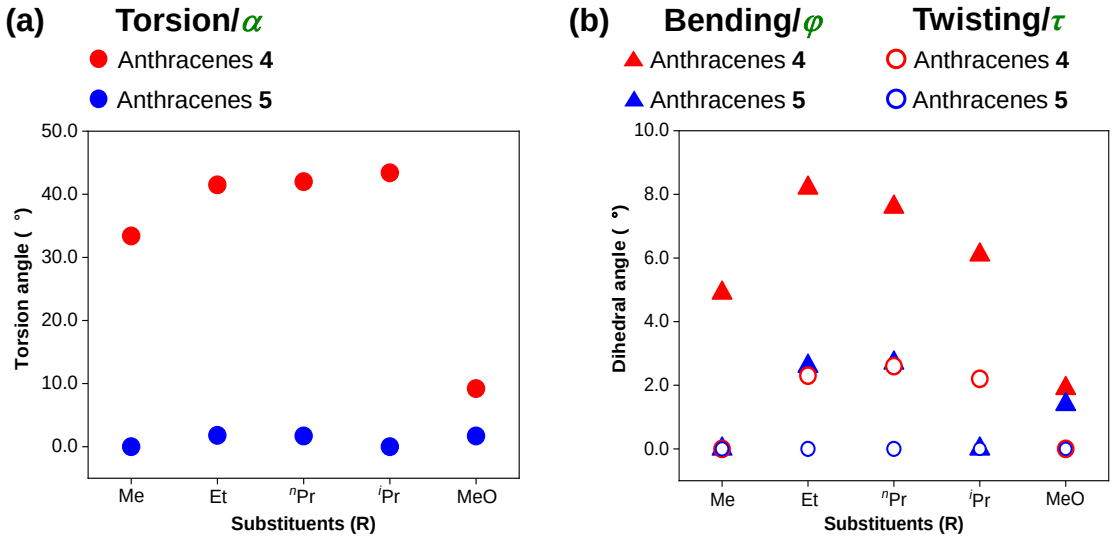

Figure 3-4. Summary of vertical distortion's trend as bulkiness increases in *peri*-position of anthracenes **4–5**.

Table 3-3. Torsion angle evaluating vertical distortion on anthracenes **4**–**5**.[a]

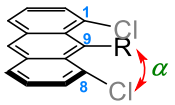

4

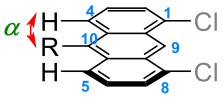

5

R	
Me	**a**
Et	**b**
^{n}Pr	**c**
^{i}Pr	**d**
MeO	**e**

Parameters		**4a**	**4b**	**4c**	**4d**	**4e**
Dihedral angle (º)	C1–Cl1 with C9-R	31.5(1)	36.7(1)	—	—	8.1
		33.4	37.2	37.7	41.4	9.1
	C8–Cl2 with C9–R/α	31.6(1)	40.1(1)	—	—	8.1
		33.4	41.5	42.0	43.4	9.2
		5a	**5b**	**5c**	**5d**	**5e**
	C4–H4 with C10-R/α	0.6	0.3	0.8	5.9	1.4
		0	1.8	1.7	0	1.7
	C5–H5 with C10–R	0.6	1.0	1.4	7.5	1.6
		0	1.8	1.7	0	1.7

[a]Measured and calculated values are shown as upper and lower rows, respectively.

Table 3-4. Bending and Twisting angle evaluating vertical distortion on anthracenes **4** and **5**.[a]

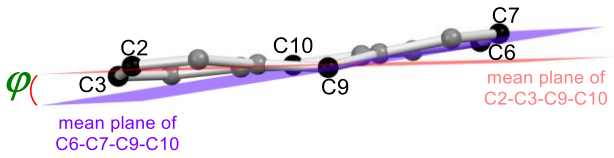

bending on the central ring

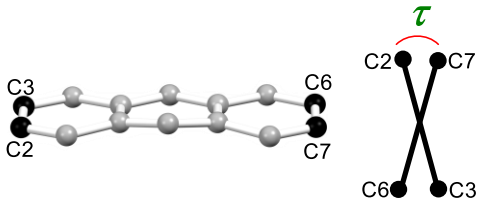

twisting across the central ring

Parameters		**4a**	**4b**	**4c**	**4d**	**4e**	**5a**	**5b**	**5c**	**5d**	**5e**
Dihedral angle (º)	φ	4.9	6.9	—	—	1.8	6.9	1.1	0.4	1.9	2.2
		4.9	8.2	7.6	6.1	1.9	4.9	2.6	2.7	0	1.4
	τ	1.5	4.6	—	—	0	0	0.5	0.5	1.9	2.2
		0	2.3	2.6	2.2	0	0	0	0	0	0

[a]Measured and calculated values are shown as upper and lower rows, respectively.

Additional parameters of vertical distortion derived from the bending and twist angles were studied according to the literature.[1] However, the bending angle interpretation will slightly differ from those illustrated in Figure 3-1, as it is based on the best planes created by terminal carbons of the outer six-membered ring and two carbon atoms in the central ring (Table 3-4).[6] For the bending angle (φ) on the central ring, 9-ethyl and 9-propylanthracenes **4b** and **4c** revealed high values among series **4**. The decreasing trend of φ in both series is presumably due to the participating atoms that created φ experiencing horizontal strain and elongation of the bond length intensively. Meanwhile, the most significant twisting angle (τ) was only owned by 9-ethyl **4b**, 9-propyl **4c**, and 9-isopropylantracene **4d**, as they showed around 2 degrees from calculated data (Table 3-4).

3.2. Magnetic Properties by NICS

To confirm the effect of substituent repulsion on aromaticity, NICS calculations were conducted on the central ring, which is indeed the most distorted ring (Table 3-5).

Table 3-5. NICS values (ppm) at the central ring of anthracene **3–5**.[a]

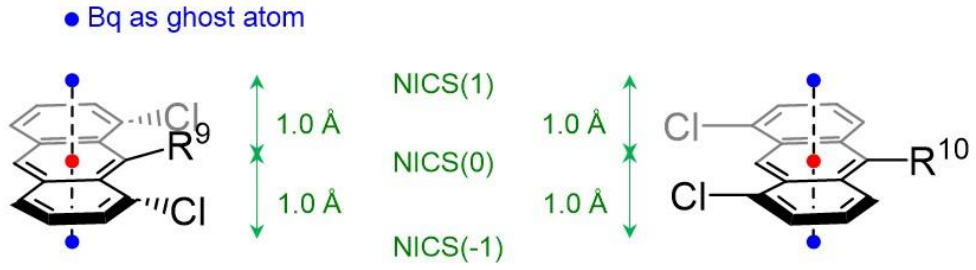

9-Substituted **10-Substituted**

$R^9 = R^{10}$		Anthracene **3** and **4**			Anthracene **5**		
		NICS(-1)	NICS(0)	NICS(1)	NICS(-1)	NICS(0)	NICS(1)
H		−12.8	−11.4	−12.8	—	—	—
Me	**a**	−12.2	−11.0	−12.5	−12.6	−11.2	−12.6
Et	**b**	−11.9	−10.8	−13.1	−12.7	−11.4	−12.8
^{n}Pr	**c**	−11.9	−10.9	−13.3	−12.7	−11.2	−12.8
^{i}Pr	**d**	−11.3	−10.7	−12.9	−12.6	−11.3	−12.6
MeO	**e**	−12.2	−10.2	−12.9	−12.8	−12.3	−13.0

[a]NICS are performed using the GAIO method at B3LYP-D3/6-311G+(d,p) level of theory.

For the most planar structure of anthracene **3**, the NICS(0) value was −11.4 ppm, and both NICS(-1) and NICS (1) shifted to a lower field of −12.8 ppm, indicating an increase in aromaticity. Since unsymmetrical rings trigger magnetically inequivalent sides of the ring, NICS(0) **3** becomes essential as a standard value to compare the deviation of NICS(0) for **4** and **5**. Hence, the variation of NICS(0) values across all anthracenes is considered tolerable.

To assess how the imposed steric repulsion affects aromaticity, two different perspectives of NICS(1) and NICS(-1) must be thoroughly analyzed. First, NICS(1) data reveal that the upper part of the ring, where the ghost atom "Bq" is positioned near the outward-pointing substituents, exhibits diatropic ring currents (values ranged from −12.5 to −13.1 ppm). While this quickly indicates a higher aromaticity character for all anthracenes **4** in comparison to **5**, the influence of molecular orbitals from nearby alkyl groups is likely to play a role. As seen from the side view of optimized structures, the unsymmetrical arrangement of substituents on the ring creates a convex outer surface on the upper part of the ring and a concave inner surface on the bottom, in which the former can add electron density to ghost atom in NICS(1) (Figure 3-5).

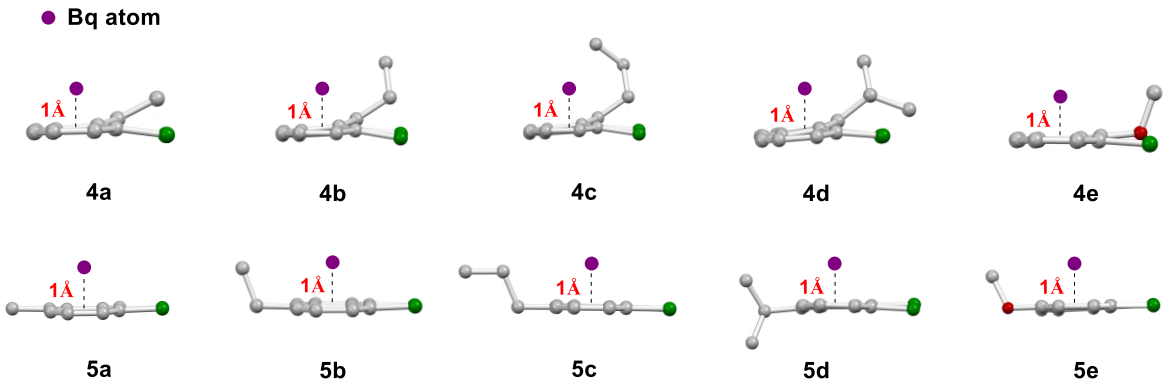

Figure 3-5. The side-view from optimized structures calculated at B3LYP-D3/6-311G+(d,p) level of theory of anthracenes **4–5**. Bq atom positioned 1 Å above the plane for NICS(1) illustrates the close disturbance from nearby substituents.

Secondly, the examination of the NICS(-1) for the lower part of the ring, which experiences minimal interference from substituents, reveals opposite outcomes. Although appeared almost insignificant different from NICS(1), assessing aromaticity via NICS(-1) will bring anthracene **5** as the framework with greater aromatic character than **4** in a general observation (Table 3-5).

Regarding the trend in bulkiness, 9-alkylated anthracenes **4** show a decrease in aromaticity following the upper shift of NICS(-1) as the size of the alkyl group increased. These findings suggest that steric repulsion between *peri*-substituents effectively distorts the coplanarity of the anthracene framework, leading to a decrease in aromatic character by magnetic evaluation.

It is essential to state that inaccuracies may arise in the NICS(-1) and NICS(1) values due to the uniform bending of the molecules away from planarity in the central ring. This bending may increase the distance to the NICS(1) ghost atom above the convex surface to more than 1 Å. In contrast, the distance to the NICS(-1) ghost atom, positioned below the concave surface, reliably decreases to less than 1 Å. Nonetheless, the computation was executed carefully, ensuring that the NICS(0) Bq atom was aligned parallel to the formed plane of the central ring.

4. Reactivity

4.1. Diels–Alder Reaction

To evaluate the non-electronic activation of the anthracene ring by inter-substituent repulsion, the Diels–Alder reaction using maleic anhydride as a dienophile was selected. Initially, it was considered that a less hindered structure with a solid electronic effect would result in a more electron-rich central ring, potentially making it highly reactive. Thus, I prioritized the optimization of compound **5e**, as its outcomes will provide valuable insights into the behavior of other anthracene compounds.

Based on the optimized results presented in Table 3-6, using a nonpolar solvent at a moderately low temperature was found to be the most effective condition. When polar solvents were used, the conversion of maleic anhydride to maleic anhydride was promoted, resulting in a lower product yield. In contrast, the nonpolar solvent proved to be more advantageous as it facilitated the formation of solid cycloadducts, thereby, simultaneously reducing the likelihood of the retro-Diels–Alder reaction.

Table 3-6. Optimization reaction using **5e** to form cycloadduct **8e**.[a]

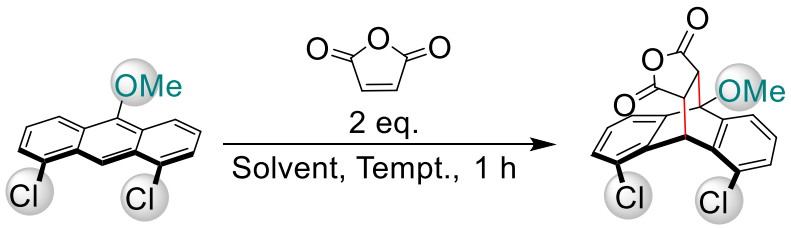

5e **8e**

Entry	Solvent	Temp./ ºC	Yield/%	Recovery/%
1	DMF	100	0	98
2	THF	80	17	70
3	1,4-Dioxane	100	0	98
4	Benzene	80	50	15
5	Toluene	100	25	49

[a]Conditions: **5e** (0.3 mmol), maleic anhydride (0.6 mmol, 2 eq.), solvent (2 mL).

Under the optimum conditions in hand, anthracenes **4** and **5** underwent the Diels–Alder reaction without any detectable by-products, and the higher the bulkiness of the substituent is, the greater the yield of the adduct is (Table 3-7). Furthermore, all 9-alkylanthracenes **4** exhibit higher reactivity than their 10-alkyl-substituted counterparts **5**, corresponding to the distortion degree. Interestingly, the substitution of the electron-donating methoxy group resulted in a lower yield against the alkyl-substituted anthracenes. Especially for the anthracene-bearing bulkier alkyl group, a marked difference was observed. According to these outcomes, it is safe to propose that the effect of electronic donation has a less notable impact.

Table 3-7. Evaluation of reactivity by Diels–Alder reaction on anthracene **3–5** forming cycloadducts **6–8**.[a]

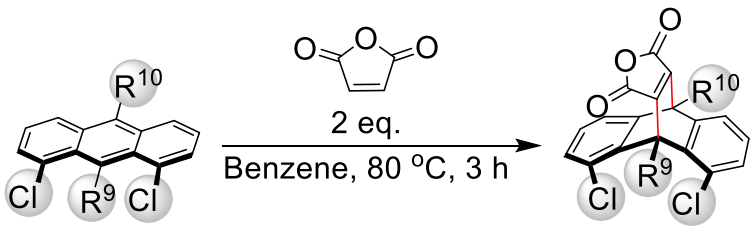

3–5 **6–8**

Entry	Anthracenes			Cycloadducts		Recovery/%
	R^9	R^{10}			Yield/%	
1	H	H	**3**	**6**	43	46
2	Me	H	**4a**	**7a**	79	15
3	Et	H	**4b**	**7b**	75	20
4	^{n}Pr	H	**4c**	**7c**	80	12
5	^{i}Pr	H	**4d**	**7d**	91	5
6	MeO	H	**4e**	**7e**	75	18
7	H	Me	**5a**	**8a**	50	35
8	H	Et	**5b**	**8b**	63	20
9	H	^{n}Pr	**5c**	**8c**	58	30
10	H	^{i}Pr	**5d**	**8d**	75	12
11	H	MeO	**5e**	**8e**	53	36

[a]Conditions: Anthracenes (0.3 mmol), maleic anhydride (0.6 mmol, 2 eq.), solvent (2 mL).

4.2. Reaction Monitoring via Pseudo-First-Order Reaction

Pseudo-first-order rate constants of the Diels–Alder reaction were compared to evaluate the reactivity of anthracenes **3–5** in detail, where ten equivalents of maleic anhydride were employed. In these experiments, the decrease of the anthracenes was monitored by the ^{1}H NMR per designated time until its 75% consumption, and $CDCl_3$ was used as a solvent because of the necessity to dissolve excess amounts of dienophile (Figure 3-6a and 3-6b). Substituted anthracenes **4** and **5** underwent reactions faster than **3**, and 9-substituted anthracenes **4** reacted faster than their 10-substituted analogs **5**, indicating that more distorted anthracenes revealed higher reactivity. In the given observation, rate constant (k) indicates the order of reactivity from the lowest to the highest as **4e** < **4d** < **4c** < **4a** < **4b** by 5-minutes-interval of measurements

(Figure 3-6c).

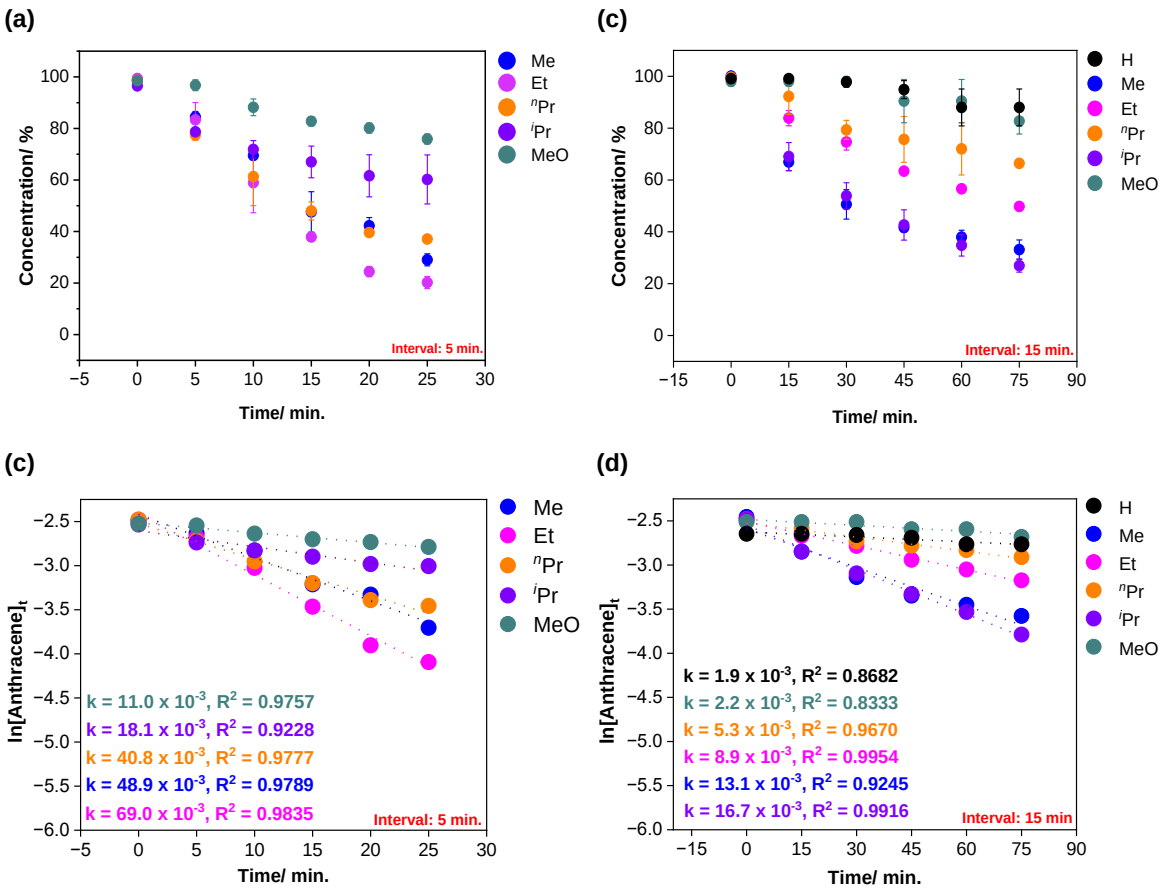

Figure 3-6. Reaction monitoring via Pseudo-First-Order reaction on Diels–Alder reaction.

For **4** series, it would be appropriate to assess reactivity by considering two standpoints: the activation effects due to ring distortion and possible inhibition by steric hindrance. Consequently, **4b**, with its modest distortion and less steric congestion, could exhibit the highest reaction rate constant against the other substituents, whereas **4c** and **4d** were understandable and might be suppressed due to intense steric hindrance. Meanwhile, the least distorted with the smallest substituent of **4a** came in second place by balancing the nature of its geometrical features.

Conversely, the 10-substituted anthracenes **5** followed the reactivity order: **3** < **5e** < **5c** < **5b** < **5a** < **5d**, with a longer duration of 15-minute intervals needed to achieve 75% substrate consumption (Figure 3-6d). We can recognize that in the **5** series, steric hindrance

predominantly affects the rate constant because this framework has less steric distortion, regardless of the bulkiness of substituents. On a related note, 10-isopropylanthracene **5d**, which shows a remarkable horizontal distortion in Figure 3-4, exhibited the highest reaction rate constant contrary to **4d**, in which rate constants of both **4d** and **5d** were almost comparable (18.1 and 16.7, respectively). These results suggest that Diels–Alder reaction of anthracenes with a bulky group strictly follows kinetic control caused by steric hindrance rather than thermodynamic control induced by steric distortion. Interestingly, **4e** and **5e**, possessing an electron-donating methoxy group, exhibited lower reactivity despite likely contributing greater electron density to the ring than the alkylated derivatives. Therefore, an electronic evaluation is necessary to understand methoxy-substituted anthracenes' unique behavior better.

4.3. Electronic Evaluation

The reactivity profile of anthracene while undergoing the Diels–Alder reaction was examined by the HOMO and LUMO energies comparison. Accordingly, anthracene **4** was more reactive than anthracenes **3** and **5**, due to its lower energy gap as shown in Figure 3-7. It is worth mentioning that anthracenes **4** and **5** exhibited similar HOMO and LUMO values in the same series, despite the differences in the bulkiness of their substituents and vertical distortions they owned.

By comparing all structures to **3**, both methoxylated **4e** and **5e** showed a slight rise in HOMO level compared to the alkylated series. This indicates that geometrical distortions are more determined than electronic influences. As previously reported, anthracenes that experience greater bending deformation tend to maintain consistent HOMO–LUMO energy gaps, whereas more twisted structures exhibit a gradual decrease in both energy values. Referring to Table 3-4, indeed, **4b–d** owned the highest bending angle and comparable twisting angle to one another. Still, **4d** was also advantaged by a significant torsion angle (see Table 3-3),[13] resulting in the highest HOMO level amongst all anthracenes (HOMO = −5.66 eV).

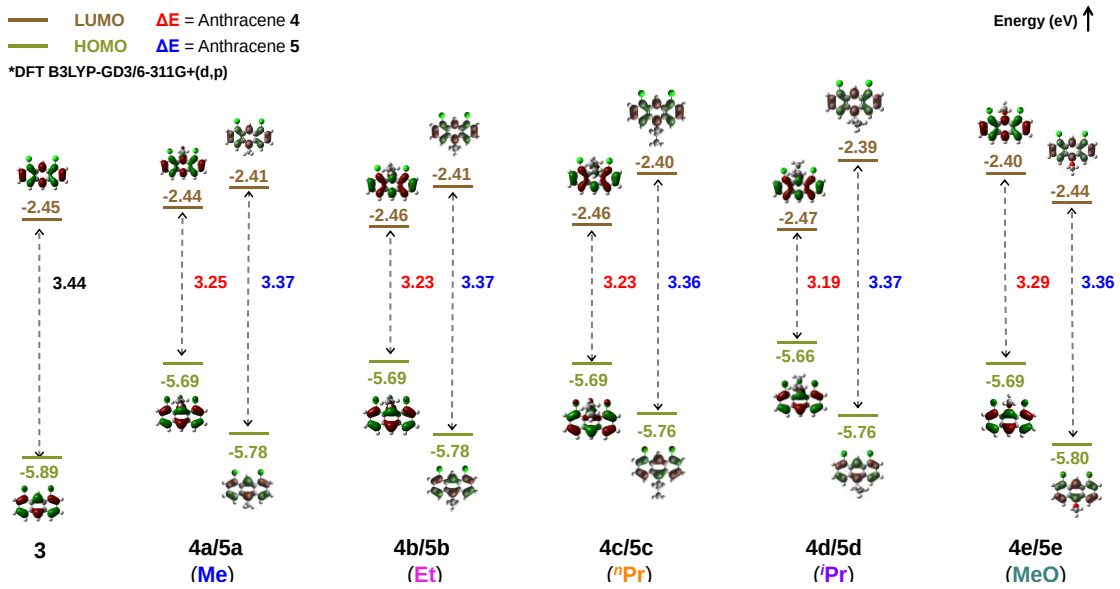

Figure 3-7. HOMO and LUMO levels (eV) of anthracenes **3–5**.

While comparing the interaction between the frontier molecular orbital (FMO) $HOMO_{anthracene}$ and the $LUMO_{maleic\ anhydride}$, the methoxy derivatives resulted in a higher energy gap (ΔE) than the bulkier isopropyl derivative for both frameworks (Figure 3-8). This result strengthens the proposition that the anthracene framework is less influenced by the electron-donating property of the methoxy group.

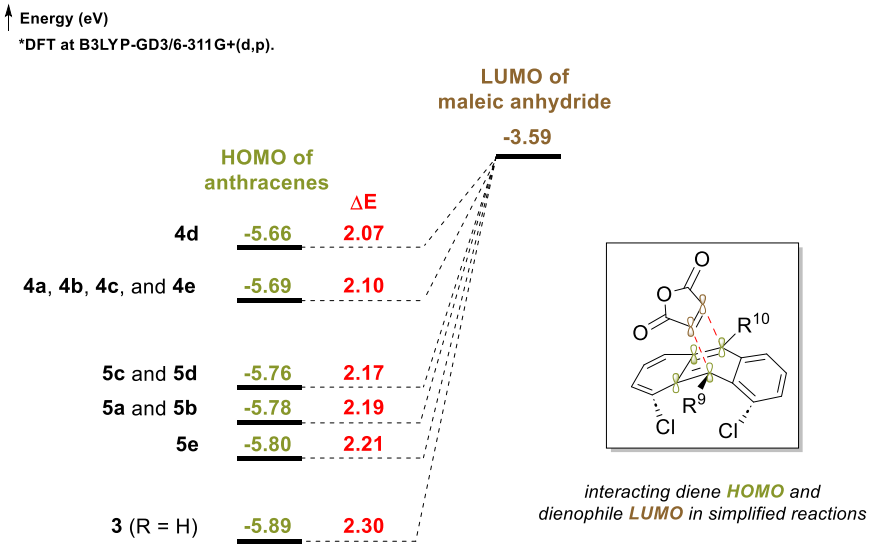

Figure 3-8. Energy diagram (eV) between $HOMO_{anthracenes}$ and $LUMO_{maleic\ anhydride}$ treated as separate reactants.

4.4. Single Point Analysis on Transitional State

To effectively analyze the irregular reactivity order of alkylated anthracenes **4** and **5**, as shown in Figure 3-6, I focus on their planarity-disoriented characteristics by conducting a robust computational analysis assessing asynchronicity (incipient bond distances) and Gibbs free energy ($\Delta G^{\ddagger}$ and $\Delta G°$). This analysis is based on a precise single-point evaluation of the optimized transition state (TS) between anthracene and maleic anhydride, providing clear insights into the underlying mechanisms (Table 3-8). The energy profiles for reactants (anthracene and maleic anhydride), transitional states, and cycloadditions product were gathered and plotted using DFT/B3LYP with basic set 6-311+G(d,p), in which TS structure was reassured by showing only one imaginary frequency.

The asynchronous degree is generally used to describe a favorable Diels–Alder reaction, stating that the shorter the difference of the incipient bond distance value, the greater the overlapping molecular orbital, leading to a smooth response.[14] The position of the substituent displays a harmonized increase for incipient bond distances in alkylated anthracene **4** (*m*) and **5** (*n*), respectively (Table 3-8). The difference between *m* and *n* ($\Delta m/n$) of **TS–4** was 0.1 Å longer than that of **TS–5**, in which **TS–4d** shows the immense $\Delta m/n$ value (0.66 Å). Given this result, a considerable $\Delta m/n$ value indicates a possibility of another reaction route, namely stepwise cycloaddition. Therefore, a particularly low reaction rate of **4d** might be due to the alternative reaction mechanism.

On the other side, the activation energy barrier to reach the transition state revealed moderate variations in $\Delta G^{\ddagger}$ in both **TS 4** and **5** series. Interestingly, such a small substituent of methyl gave a notable lowest activation energy of **TS–4a** ($\Delta G^{\ddagger}$ = 7.8 kcal/mol) and energy barrier for product formation ($\Delta G°$ = −20.9 kcal/mol), indicating how kinetically and thermodynamically favored this reaction should be. This is supported by the smoothness reaction observed in a pseudo-first-order experiment. The methoxy-substituted anthracenes **TS–4e** and **TS–5e** appeared the highest activation barrier energy, stating that the electronic

character of the electron-donating group was less aided in the reaction.

Table 3-8. Single Point Analysis on Transitional State Properties.

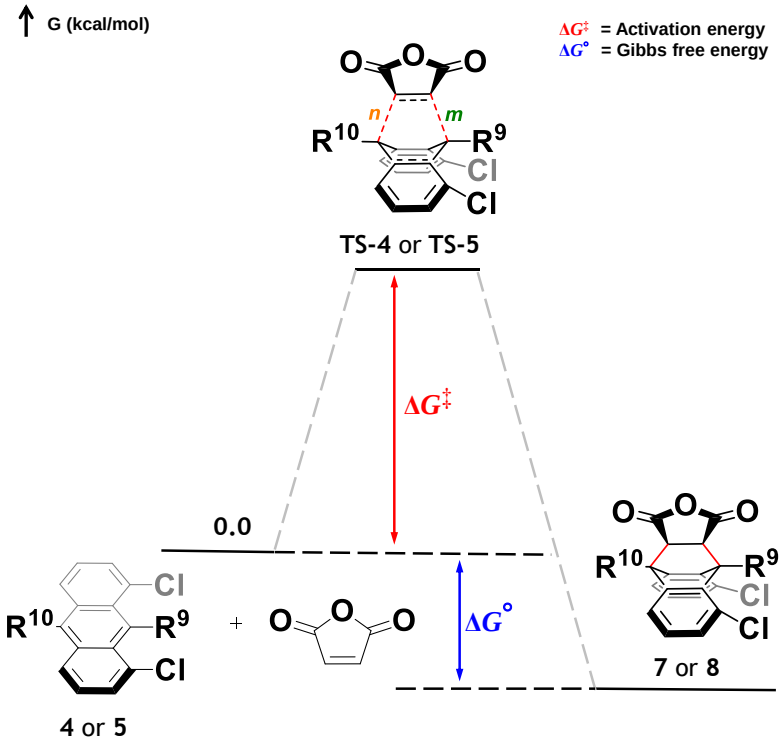

TS	Distance (Å)			G (kcal/mol)	
	m	*n*	*Δm/n*	ΔG ‡	ΔG°
TS–4a	2.48	2.07	0.42	7.8	−20.9
TS–4b	2.42	2.07	0.35	13.1	−15.5
TS–4c	2.41	2.07	0.34	12.5	−15.6
TS–4d	2.65	1.98	0.66	12.8	−15.2
TS–4e	2.43	2.00	0.42	17.2	−9.3
TS–5a	2.14	2.33	0.19	10.2	−19.5
TS–5b	2.12	2.34	0.22	11.2	−15.5
TS–5c	2.12	2.33	0.22	11.2	−15.2
TS–5d	2.08	2.43	0.35	10.6	−18.2
TS–5e	2.12	2.27	0.15	15.5	−12.7

5. Conclusion

This research provides the first experimental and computational evaluation of steric repulsion in the de-aromatization of *peri*-substituted anthracene framework. As a result of comparison with 10-substituted analogs, 9-substituted 1,8-dichloroanthracenes revealed significant dearomaticity features in the most distorted structures, both horizontal and vertical (Figure 3-9). However, the aromaticity assessments on magnetic and electronic did not appear as evidence as geometric ones. The study on the reactivity of anthracenes in the Diels–Alder reaction with maleic anhydride demonstrated that alkylated anthracenes (**4a–d** and **5a–d**) had higher reactivities than methoxy anthracenes (**4e** and **5e**). This highlights the effectiveness of non-electronic activation through ring distortion, suggesting a complex interplay of steric effects in reactivity against electronic influence. Although the impact of steric hindrance adds complexity to the reactivity evaluation, these insights are crucial for guiding future research. By acknowledging the role of steric repulsion as an activation strategy, the challenges of modifying aromatic compounds and exploring new avenues for practical activation approaches.

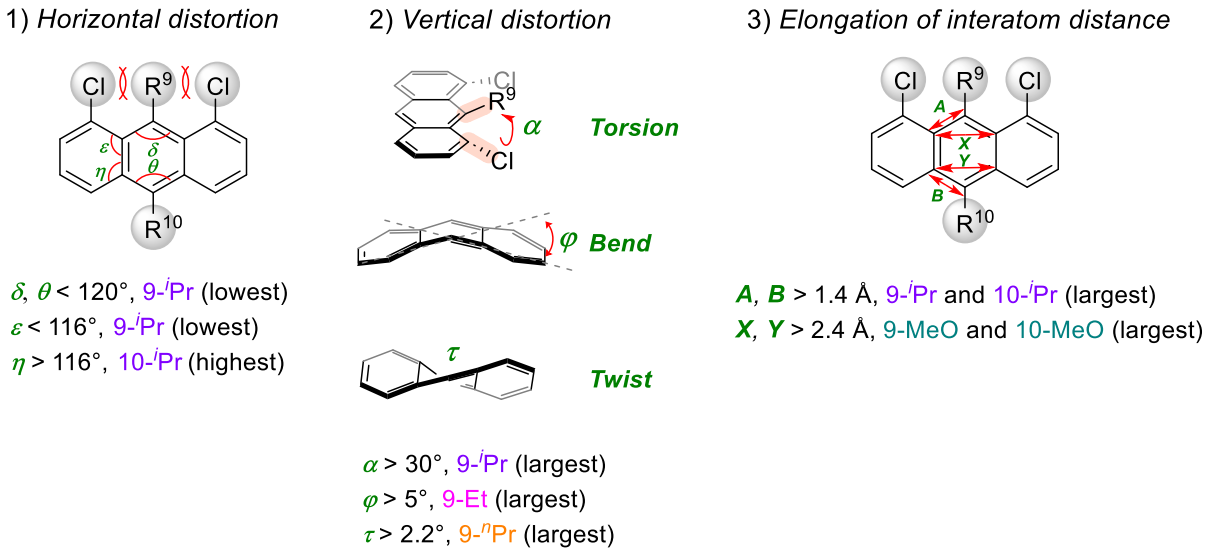

Figure 3-9. Three observing distortions of the anthracene ring.

6. Experimental Section

All reagents were purchased from commercial sources and used without further purification. TLC on commercial aluminum-backed plates of silica gel 60 F254 was used to monitor the progress of the reactions. ^{1}H and ^{13}C-NMR spectra were recorded on a Bruker DPX-400 spectrometer (400 MHz and 100 MHz, respectively) in $CDCl_3$, C_6C_6, and DMSO-d_6 using TMS as an internal standard. DEPT experiments reassured the assignments of the ^{13}C-NMR. IR spectra were recorded with a JASCO FT/IR-4200 spectrometer equipped with an ATM detector. The melting points were recorded on an SRS-Optimelt automated melting point system. Diffraction data were collected at 103 K under a cold N_2-gas stream on a Rigaku XtaLAB Synergy-S/Mo system (λ=0.71073 Å (Mo-Kα)). High-resolution mass spectra (HRMS) were obtained from a Bruker compact mass spectrometer set at APCI-positive mode.

A single crystal of anthracenes was prepared using the slow evaporation method. Approximately 10 mg of the compound was dissolved in organic solvents (1 ml) and placed in a clean dry glass vial. Hexane was used as the solvent for crystal **4b**, while $CHCl_3$ was used to form crystals **4e**, **5b**, **5c**, **5d**, and **5e**. Furthermore, crystal data for **3** (CCDC 925781)[11a], **4a** (CCDC 1002160)[8] and **5a** (CCDC 1868360)[8] were extracted from reported works.

All related calculations were performed using the Gaussian 09 package.[15] Geometries of anthracenes were optimized using B3LYP-D3/6-311G+ (d,p) level of theory, and the structures were verified to be minima via frequency. GIAO NMR shifts were employed to extract NICS values.

a. Preparation of anthrone (**2A** and **2B**)

1,8-Dichloroanthraquinone **1** (11 g, 40 mmol) and $SnCl_2$•$2H_2O$ (27 g, 120 mmol, 3 equiv.) were dissolved in a mixed solvent of acetic acid and 1 M HCl (v/v = 4/1, 200 mL), and the resultant mixture was heated at 115 °C for 2 d. After cooling to room temperature, the reaction was quenched with H_2O (30 mL). The precipitates were collected by filtration under reduced

pressure and were washed with saturated $NaHCO_3$ aqueous solution (30 mL). Further purification was performed by column chromatography on SiO_2 (eluted with hexane/EtOAc = 90/10). Formation of **2A** and **2B** was confirmed by comparison of spectroscopic data with those in the literature.[7]

1,8-dichloro-9-anthrone (**2A**)

Colorless solid (Rf = 0.23), 4.1 g, 40%. ^{1}H NMR (400 MHz, $CDCl_3$) δ 7.44 (dd, J = 7.6, 1.2 Hz, 2H), 7.40 (dd, J = 7.6, 7.6 Hz, 2H), 7.31 (dd, J = 7.6 Hz, 1.2 Hz, 2H), 4.21 (s, 2H).

4,5-dichloro-9-anthrone (**2B**)

Yellow solid (Rf = 0.80), 6.2 g, 60%. ^{1}H NMR (400 MHz, $CDCl_3$) δ 8.30 (dd, J = 7.9, 1.3 Hz, 2H), 7.72 (dd, J = 7.9, 1.3 Hz, 2H), 7.46 (dd, J = 7.9, 7.9 Hz, 2H), 4.26 (s, 2H).

b. Preparation of Alkylanthracenes (**4a–d** and **5a–d**) (Paths *i* and *ii*)

To a solution of Grignard reagent (6 mmol) prepared from haloalkane and Mg in Et_2O (25 mL), 1,8-dichloro-9-anthrone (**2A**) (524 mg, 2 mmol) was added, and the resultant mixture was stirred at room temperature for 9 h. After quenching the reaction with 1 M NH_4Cl aqueous solution (10 mL, 10 mmol), the organic layer was separated, and the aqueous layer was extracted with CH_2Cl_2 (50 mL × 3). The combined organic layer was dried over $MgSO_4$ and concentrated under reduced pressure to afford 9-alkylated 4,5-dichloro-9-anthrol as a yellow oil.

To a solution of the crude product in benzene (20 mL), thionyl chloride (1.2 mL, 16 mmol) and pyridine (1.35 mL, 16 mmol) were added, and the mixture was stirred at room temperature for 3 h. After quenching with H_2O (20 mL), the organic layer was separated, and the aqueous layer was extracted with CH_2Cl_2 (50 mL × 3). The combined organic layer was dried over $MgSO_4$ and concentrated under reduced pressure to give alkylated anthracene **4**. Further purification was performed by column chromatography on SiO_2 using hexane/EtOAc = 90/10 as an eluent. When 4,5-dichloro-10-anthrone (**2B**) was used, experiments were conducted similarly. In the case of EtMgBr, **2A** (1.5 mmol) and **2B** (4 mmol) were used to prepare **4b** and

5b, respectively. In the cases of **4d** and **5d**, commercially available 1 M ^{i}PrMgCl solution (4 mL, 4 mmol) was used. The formation of alkyl anthracenes **4** and **5** was confirmed by comparison of spectroscopic data with those in the literature, respectively.

1,8-Dichloro-9-methylanthracene (**4a**)[8]

Brown solid, 265 mg (yield 51%). ^{1}H NMR (400 MHz, $CDCl_3$) δ 3.39 (s, 3H), 7.32 (dd, J = 8.5, 7.2 Hz, 2H), 7.60 (dd, J = 7.2, 1.2 Hz, 2H), 7.85 (dd, J = 8.5, 1.2 Hz, 2H), 8.24 (s, 1H). CCDC No. 1002160.[11b]

1,8-Dichloro-9-ethylanthracene (**4b**)[8]

Yellowish green solid, 239 mg (yield 58%). ^{1}H NMR (400 MHz, $CDCl_3$) δ 0.99 (t, J = 7.6 Hz, 3H), 4.24 (q, J = 7.6 Hz, 2H), 7.32 (dd, J = 8.4, 7.2 Hz, 2H), 7.58 (d, J = 7.2 Hz, 2H), 7.86 (d, J = 8.4 Hz, 2H), 8.23 (s, 1H). CCDC No. 2342446.

1,8-Dichloro-9-propylanthracene (**4c**)[9]

Yellow solid, 302 mg (yield 52%). ^{1}H NMR (400 MHz, $CDCl_3$) δ 0.63 (dd, J = 7.2, 7.2 Hz, 3H), 1.36 (dq, J = 14.8, 7.2 Hz, 1H), 1.36 (dq, J = 14.8, 7.2 Hz, 1H), 4.18 (t, J = 7.2 Hz, 2H), 7.32 (dd, J = 8.5, 7.2 Hz, 2H), 7.57 (dd, J = 7.2, 1.4 Hz, 2H), 7.86 (dd, J = 8.5, 1.4 Hz, 2H), 8.22 (s, 1H).

1,8-Dichloro-9-isopropylanthracene (**4d**)

Yellowish brown oil, 374 mg (yield 65%). ^{1}H NMR (400 MHz, C_6D_6) δ 1.77 (d, J = 7.2 Hz, 6H), 4.46 (sept, J = 7.2 Hz, 1H), 6.82 (dd, J = 8.4, 7.2 Hz, 2H), 7.38 (dd, J = 7.2, 1.2 Hz, 2H), 7.41 (dd, J = 8.4 Hz, 1.2 Hz, 2H), 7.76 (s, 1H); 13C NMR (100 MHz, C6D6) δ 25.7 (CH3), 34.8 (CH), 124.7 (CH), 128.7 (CH), 129.9 (CH), 131.5 (CH), 132.7 (C), 133.3 (C), 134.1 (C), 144.9 (C); IR (KBr/cm^{-1}) 772; HRMS (APCI–TOF) Calcd. for $[M+H]^+$ $C_{17}H_{15}Cl_2$: 289.0545, found 289.0565.

1,8-Dichloro-10-methylanthracene (**5a**)[8]

Yellow solid, 395 mg (yield 76%). ^{1}H NMR (400 MHz, $CDCl_3$) δ 3.12 (s, 3H), 7.45 (dd, J = 9.0, 7.1 Hz, 2H), 7.64 (dd, J = 7.1, 1.0 Hz, 2H), 8.23 (dd, J = 9.0, 1.0 Hz, 2H), 9.27 (s, 1H).

CCDC No. 1868360.[11b]

1,8-Dichloro-10-ethylanthracene (**5b**)

Yellow solid, 968 mg (yield 88%), mp 107–109 °C. ^{1}H NMR (400 MHz, $CDCl_3$) δ 1.43 (t, J = 7.6 Hz, 3H), 3.61 (q, J = 7.6 Hz, 2H), 7.43 (dd, J = 8.8, 7.2 Hz, 2H), 7.62 (dd, J = 7.2, 1.2 Hz 2H), 8.19 (dd, J = 8.8, 1.2 Hz, 2H), 9.24 (s, 1H); ^{13}C NMR (100 MHz, $CDCl_3$) δ 15.7 (CH3), 21.9 (CH2), 119.9 (CH), 123.7 (CH), 125.6 (CH), 125.7 (CH), 129.5 (C), 130.4 (C), 133.5 (C), 138.4 (C); IR (KBr/cm^{-1}) 771; HRMS (APCI–TOF) Calcd. for $[M+H]^+$ $C_{16}H_{13}Cl_2$: 275.0389, found 275.0402. CCDC No. 2342406.

1,8-Dichloro-10-propylanthracene (**5c**)

Yellow solid, 400 mg (yield 70%), mp 174–176 °C. ^{1}H NMR (400 MHz, DMSO-d_6) δ 1.08 (t, J = 7.2 Hz, 3H), 1.73 (tq, J = 8.0, 7.2, 2H), 3.62 (t, J = 8.0 Hz, 2H), 7.60 (dd, J = 7.2, 8.8 Hz, 2H), 7.82 (d, J = 7.2 Hz, 2H), 8.41 (d, J = 8.8 Hz, 2H), 9.08 (s, 1H); ^{13}C NMR (100 MHz, DMSO-d_6) δ 14.2 (CH3), 24.7 (CH2), 29.8 (CH2), 117.9 (CH), 124.6 (CH), 126.2 (CH), 126.4 (CH), 128.5 (C), 130.3 (C), 131.6 (C), 138.0 (C); IR (KBr/cm^{-1}) 773; HRMS (APCI–TOF) Calcd. for $[M+H]^+$ $C_{17}H_{15}Cl_2$: 289.0545, found 289.0549. CCDC No. 2342445.

1,8-Dichloro-10-isopropylanthracene (**5d**)[9]

Yellow solid, 602 mg (yield quant.). ^{1}H NMR (400 MHz, $CDCl_3$) δ 1.74 (d, J = 7.6 Hz, 6H), 4.56 (sept, J = 7.6 Hz, 1H), 7.41 (dd, J = 9.2, 7.1 Hz, 2H), 7.62 (d, J = 7.1 Hz, 2H), 8.41 (d, J = 9.2 Hz, 2H), 9.33 (s, 1H). CCDC No. 2342446.

c. Preparation of methoxyanthracene (**4e** and **5e**)

To a suspension of sodium hydride (380 mg, 15.5 mmol) in THF (25 mL), 1,8-dichloro-9-anthrone (**2A**) (800 mg, 3.1 mmol) was slowly added, and then dimethyl sulfate (0.32 mL, 3.4 mmol) was added. The mixture was heated under reflux at 80 °C for 12 h and then quenched with H_2O (5 mL). The mixture was extracted with CH_2Cl_2 (50 mL × 3). The organic layer was dried over $MgSO_4$ and concentrated under reduced pressure. The residue was subjected to column chromatography on SiO_2 using hexane/EtOAc = 80/20 as an eluent. The same

procedure was conducted when 4,5-dichloro-9-anthrone (**2B**) was used. The formation of **4e** and **5e** was confirmed by comparison of spectroscopic data with those in the literature.[10]

1,8-dichloro-9-methoxyanthracene (**4e**)

Yellow solid (526 mg, 2.0 mmol, yield 63%). ^{1}H NMR (400 MHz, $CDCl_3$) δ 3.93 (s, 3H), 7.35 (dd, J = 8.4, 7.2 Hz, 2H), 7.58 (dd, J = 7.2, 1.2 Hz, 2H), 7.87 (dd, J = 8.4, 1.2 Hz, 2H), 8.25 (s, 1H). CCDC No. 2342447.

1,8-Dichloro-10-methoxyanthracene (**5e**)

Yellow needles, 1.18 g (yield quant.). ^{1}H NMR (400 MHz, $CDCl_3$) δ 4.14 (s, 3H), 7.43 (dd, J = 8.8, 7.2 Hz, 2H), 7.64 (dd, J = 7.2, 1.2 Hz, 2H), 8.24 (dd, J = 8.8, 1.2 Hz, 2H), 9.08 (s, 1H). CCDC No. 2342404.

d. Preparation of 1,8-dichloroanthracene (**3**)

To a suspension of sodium borohydride (1.1 g, 28.8 mmol, 8 equiv.) in THF (40 mL), 1,8-dichloroanthraquinone (1) (1 g, 3.6 mmol) was slowly added. The mixture was heated at 75 °C for 20 h and quenched with H_2O (10 mL). The mixture was extracted with EtOAc (50 mL × 3). The organic layer was dried over MgSO4 and concentrated under reduced pressure. The residual solid was washed with MeOH (20 mL). Further purification was performed by column chromatography on SiO_2 using hexane/EtOAc = 90/10 as an eluent to afford 1,8-dichloroanthracene (**3**) (488 mg, 2.0 mmol, yield 55%) as a yellow solid. ^{1}H NMR (400 MHz, $CDCl_3$) δ 7.42 (dd, J = 8.4, 7.2 Hz, 2H), 7.64 (d, J = 7.2 Hz, 2H), 7.95(d, J = 8.4 Hz, 2H), 8.48 (s, 1H), 9.27 (s, 1H). CCDC No. 925781.[11a]

e. Diels–Alder reactions on anthracenes **3–5**

To a solution of anthracene **3** (54 mg, 0.3 mmol) in benzene (2 mL), maleic anhydride (59 mg, 0.6 mmol) was added. The mixture was heated at 80 °C in a sealed tube for 3 h, and then the solvent was removed under reduced pressure. The residual product was further purified by column chromatography on SiO_2 using hexane/EtOAc = 90/10 as an eluent to afford 1,8-dichloro-9,10,11,15-tetrahydro-9,10[3′,4′]-furanoanthracene-12,14-dione (**6**) (45 mg, yield

43%) as a colorless solid, mp 223–225 °C. ^{1}H NMR (400 MHz, DMSO-d_6) δ 3.75 (dd, J = 9.2, 3.2 Hz, 1H), 3.82 (dd, J = 9.2, 3.2 Hz, 1H), 5.08 (d, J = 3.2 Hz, 1H), 5.60 (d, J = 3.2 Hz, 1H), 7.25–7.40 (m, 5H), 7.50 (d, J = 7.3 Hz, 1H); ^{13}C NMR (100 MHz, DMSO-d_6) δ 38.1 (CH), 44.5 (CH), 46.5 (CH), 47.1 (CH), 123.9 (CH), 124.2 (CH), 127.2 (CH), 127.7 (CH), 128.6 (CH), 129.1 (C), 129.2 (CH), 129.6 (C), 135.5 (C), 137.1 (C), 141.4 (C), 143.5 (C), 170.7 (C), 170.9 (C); IR (KBr/cm^{-1}) 1868, 1783, 1226, 758; HRMS (APCI–TOF) Calcd. for $[M+H]^+$ $C_{18}H_{11}Cl_2O_3$: 345.0080, found 345.0084.

When other anthracenes **4** and **5** were used as substrates, experiments were conducted in the same way.

1,8-Dichloro-9,10,11,15-tetrahydro-9-methyl-9,10[3′,4′]-furanoanthracene-12,14-dione (**7a**)

Pale yellow solid, 81 mg (yield 79%), mp 188–190 °C. ^{1}H NMR (400 MHz, DMSO-d_6) δ 2.85 (s, 3H), 3.62 (d, J = 9.2 Hz, 1H), 3.72 (dd, J = 9.2, 3.2 Hz, 1H), 4.94 (d, J = 3.2 Hz, 1H), 7.2–7.3 (m, 4H), 7.35 (dd, J = 7.2, 1.6 Hz, 1H), 7.50 (dd, J = 6.7, 1.9 Hz, 1H); ^{13}C NMR (100 MHz, DMSO-d_6) δ 22.5 (CH3), 45.5 (CH), 47.8 (CH), 49.9 (C), 53.5 (CH), 124.1 (CH), 124.8 (CH), 128.7 (CH), 129.0 (CH), 129.7 (C), 129.8 (C), 130.9 (CH), 131.1 (CH), 136.5 (C), 137.8 (C), 142.1 (C), 145.1 (C), 170.1 (C), 170.8 (C); IR (KBr/cm^{-1}) 1864, 1799, 1219, 772; HRMS (APCI–TOF) Calcd. for $[M+H]^+$ $C_{19}H_{13}Cl_2O_3$: 359.0236, found 359.0242.

1,8-Dichloro-9,10,11,15-tetrahydro-9-ethyl-9,10[3′,4′]-furanoanthracene-12,14-dione (**7b**)

Colorless solid, 84 mg (yield 75%), mp 296–298 °C. ^{1}H NMR (400 MHz, DMSO-d_6) δ 1.35 (dd, J = 6.8, 6.8 Hz, 3H), 3.23–3.33 (m, 2H), 3.80 (dd, J = 9.6, 3.6 Hz, 1H), 3.89 (d, J = 9.6 Hz, 1H), 4.91 (d, J = 3.6 Hz, 1H), 7.20–7.27 (m, 4H), 7.32 (dd, J = 6.8, 1.2 Hz, 1H), 7.52 (dd, J = 6.8, 2.0 Hz, 1H); ^{13}C NMR (100 MHz, DMSO-d_6) δ 12.7 (CH3), 23.3 (CH2), 45.5 (CH), 46.6 (CH), 46.9 (CH), 53.4 (C), 124,6 (CH), 125.0 (CH), 128.6 (CH), 128.9 (CH), 129.3 (C), 129.4 (C), 130.7 (CH), 131.2 (CH), 136.9 (C), 137.6 (C), 142.8 (C), 146.0 (C), 169.8 (C), 171.1 (C); IR (KBr/cm^{-1}) 1799, 1774, 1220, 771; HRMS (APCI–TOF) Calcd. for $[M+H]^+$ $C_{20}H_{15}Cl_2O_3$: 373.0393, found 373.0411.

1,8-Dichloro-9,10,11,15-tetrahydro-9-propyl-9,10[3′,4′]-furanoanthracene-12,14-dione (**7c**)

Colorless solid, 93 mg (yield 80%), mp 235–237 °C. ^{1}H NMR (400 MHz, DMSO-d_6) δ 1.18 (dd, J = 7.2, 7.2 Hz, 3H), 1.57–1.61 (m, 1H), 1.83–1.88 (m, 1H), 3.23–3.29 (m, 1H), 3.55–3.61 (m, 1H), 3.79 (dd, J = 9.6, 3.6 Hz, 1H), 3.89 (d, J = 9.6 Hz, 1H), 4.91 (d, J = 3.6 Hz, 1H), 7.18–7.27 (m, 4H), 7.31 (d, J = 6.4 Hz, 1H), 7.51 (dd, J = 6.4, 2.4 Hz, 1H); ^{13}C NMR (100 MHz, DMSO-d_6) δ 14.5 (CH3), 20.6 (CH2), 32.7 (CH2), 45.5 (CH), 46.6 (CH), 47.7 (CH), 52.8 (C), 124.6 (CH), 125.1 (CH), 128.5 (CH), 128.9 (CH), 129.3 (C), 129.4 (C), 130.7 (CH), 131.2 (CH), 137.2 (C), 137.6 (C), 142.6 (C), 145.9 (C), 169.7 (C), 171.1 (C); IR (KBr/cm^{-1}) 1774, 1220, 771; HRMS (APCI–TOF) Calcd. for $[M+H]^+$ $C_{21}H_{17}Cl_2O_3$: 387.0549, found 387.0559.

1,8-Dichloro-9,10,11,15-tetrahydro-9-isopropyl-9,10[3′,4′]-furanoanthracene-12,14-dione (**7d**)

White solid, 105 mg (yield 91%), mp 230–232 °C. ^{1}H NMR (400 MHz, DMSO-d_6) δ 1.52 (d, J = 6.4 Hz, 6H), 3.95 (dd, J = 9.6, 2.8 Hz, 1 H, *This signal is overlapping with nearest –CH signal), 3.96 (d, J = 9.6 Hz, 1 H), 4.74 (sept, J = 6.4 Hz, 1H), 4.83 (d, J = 2.8 Hz, 1H), 7.10–7.15 (m, 2H), 7.19–7.23 (m, 2H), 7.29 (d, J = 7.2 Hz, 1H), 7.44 (dd, J = 7.2 Hz, 1H); ^{13}C NMR (100 MHz, DMSO-d_6) δ 22.9 (CH3), 23.3 (CH3), 27.0 (CH), 45.7 (CH), 46.8 (CH), 47.5 (CH), 59.0 (C), 124.4 (CH), 125.4 (CH), 128.0 (CH), 128.1 (CH), 129.0 (C), 129.3 (C), 130.4 (CH), 130.9 (CH), 139.7(C), 140.2 (C), 144.0 (C), 147.9 (C), 169.8 (C) 170.9 (C); IR (KBr/cm^{-1}) 1796, 1219, 775; HRMS (APCI–TOF) Calcd. for $[M+H]^+$ $C_{21}H_{17}Cl_2O_3$: 387.0549, found 387.0585.

1,8-Dichloro-9,10,11,15-tetrahydro-9-methoxyl-9,10[3′,4′]-furanoanthracene-12,14-dione (**7e**)

Colorless solid, 80 mg (yield 75%), mp 294–296 °C. ^{1}H NMR (400 MHz, DMSO-d_6) δ 3.84 (s, 3H), 3.85 (dd, J = 9.4, 3.4 Hz, 1H. *This signal is overlapping with –OCH3 signal), 4.39 (d, J = 9.4 Hz, 1H), 4.91 (d, J = 3.4 Hz, 1H), 7.17–7.25 (m, 4H), 7.29 (dd, J = 7.0, 1.2 Hz, 1H), 7.50 (dd, J = 6.4, 2.0 Hz, 1H); ^{13}C NMR (100 MHz, DMSO-d_6) δ 43.9 (CH), 46.3 (CH), 46.5 (CH), 55.4 (CH3), 84.2 (C), 124.0 (CH), 124.1 (CH), 128.2 (C), 128.8 (CH), 128.9 (CH), 129.0 (C),

130.3 (CH), 131.2 (CH), 135.7(C), 136.5 (C), 140.8 (C), 143.4 (C), 168.3 (C), 170.9 (C); IR (KBr/cm^{-1}) 1790, 1219, 776; HRMS (APCI–TOF) Calcd. for $[M+H]^+$ $C_{19}H_{13}Cl_2O_4$: 375.0185, found 375.0217.

1,8-Dichloro-9,10,11,15-tetrahydro-10-methyl-9,10[3′,4′]-furanoanthracene-12,14-dione (**8a**) Colorless solid, 54 mg (yield 50%), mp 236–238 °C. ^{1}H NMR (400 MHz, DMSO-d_6) δ 2.18 (s, 3H), 3.46 (d, J = 9.2 Hz, 1H), 3.85 (dd, J = 9.2, 3.6 Hz, 1H), 5.65 (d, J = 3.6 Hz, 1H), 7.3–7.45 (m, 6H); ^{13}C NMR (100 MHz, DMSO-d_6) δ 14.9 (CH3), 37.6 (CH), 45.3 (C), 47.9 (CH), 50.9 (CH), 121.7 (CH), 121.8 (CH), 127.2 (CH), 127.7 (CH), 128.5 (CH), 128.9 (C), 129.0 (CH), 129.7 (C), 135.5 (C), 137.5 (C), 143.8 (C), 146.1 (C), 170.1 (C), 170.6 (C); IR (KBr/cm^{-1}) 1798, 1079, 780; HRMS (APCI-TOF) Calcd. for $[M+H]^+$ $C_{19}H_{13}Cl_2O_3$: 359.0236, found 359.0269.

1,8-Dichloro-9,10,11,15-tetrahydro-10-ethyl-9,10[3′,4′]-furanoanthracene-12,14-dione (**8b**) Colorless solid, 70 mg (yield 63%), mp 205–207 °C. ^{1}H NMR (400 MHz, DMSO-d_6) δ 1.28 (dd, J = 7.2, 7.2 Hz, 3H), 2.65–2.7 (m, 2H), 3.09 (d, J = 11.2 Hz, 1H), 3.74 (dd, J = 11.2, 2.0 Hz, 1H), 5.34 (d, J = 2.0 Hz, 1H), 7.07–7.25 (m, 5H), 7.31 (d, J = 6.4 Hz, 1H); ^{13}C NMR (100 MHz, DMSO-d_6) δ15.8 (CH3), 21.2 (CH2), 46.6 (CH), 48.6 (CH), 52.3 (CH), 62.3 (C), 121.7 (CH), 122.1 (CH), 125.5 (CH), 126.1 (CH), 126.3 (CH), 127.1 (CH), 128.1 (C), 130.1 (C), 138.9 (C), 141.7 (C), 146.4 (C), 154.4 (C), 167.0 (C), 171.3 (C); IR (KBr/cm^{-1}) 1777, 1227, 773; HRMS (APCI-TOF) Calcd. for $[M+H]^+$ $C_{20}H_{15}Cl_2O_3$: 373.0393, found 373.0376.

1,8-Dichloro-9,10,11,15-tetrahydro-10-propyl-9,10[3′,4′]-furanoanthracene-12,14-dione (**8c**) Colorless solid, 87 mg (yield 58%), mp 216–218 °C. ^{1}H NMR (400 MHz, DMSO-d_6) δ 1.24 (dd, J = 7.2, 7.2 Hz, 3H), 1.73–1.93 (m, 2H), 2.41–2.47 (m, 1H), 2.71–2.77 (m, 1H), 3.65 (d, J = 9.2 Hz, 1H), 3.90 (dd, J = 9.2, 3.6 Hz, 1H), 5.65 (d, J = 3.6 Hz, 1H), 7.26–7.38 (m, 6H); ^{13}C NMR (100 MHz, DMSO-d_6) δ 14.5 (CH3), 17.8 (CH2), 29.4 (CH2), 37.5 (CH), 46.7 (C), 47.0 (CH), 48.3 (CH), 121.8 (CH), 122.5 (CH), 126.9 (CH), 127.5 (CH), 128.3 (CH), 129.0 (CH), 129.2 (C), 129.7 (C), 135.9(C), 138.3 (C), 144.3 (C), 144.7 (C), 169.7 (C), 170.6 (C); IR (KBr/cm^{-1}) 1710, 1218, 772; HRMS (APCI-TOF) Calcd. for $[M+H]^+$ $C_{21}H_{17}Cl_2O_3$: 387.0549,

found 387.0590.

1,8-Dichloro-9,10,11,15-tetrahydro-10-isopropyl-9,10[3′,4′]-furanoanthracene-12,14-dione (**8d**)

Colorless solid, 87 mg (yield 75%), mp 274–276 °C. ^{1}H NMR (400 MHz, DMSO-d_6) δ 1.50 (d, J = 7.2 Hz, 3H), 1.61 (d, J = 7.2 Hz, 3H), 3.31–3.36 (m, 1H, *This signal assumed to be overlapping with the H2O signal), 3.73 (d, J = 9.2 Hz, 1H), 3.77 (dd, J = 9.2, 3.6 Hz, 1H), 5.70 (d, J = 3.6 Hz, 1H), 7.28–7.44 (m, 5H), 7.72 (d, J = 7.2 Hz, 1H); ^{13}C NMR (100 MHz, DMSO-d_6) δ 17.8 (CH3), 19.5 (CH3), 25.5 (CH), 37.6 (CH), 48.1 (CH), 48.4 (CH), 53.2 (C), 123.5 (CH), 124.8 (CH), 127.0 (CH), 127.6 (CH), 127.8 (CH), 128.9 (CH), 129.4 (C), 129.7 (C), 135.7(C), 138.5 (C), 141.8 (C), 142.7 (C), 169.2 (C), 170.3 (C); IR (KBr/cm^{-1}) 1783, 1224, 778; HRMS (APCI-TOF) Calcd. for $[M+H]^+$ $C_{21}H_{17}Cl_2O_3$: 387.0549, found 387.0529.

1,8-Dichloro-9,10,11,15-tetrahydro-10-methoxyl-9,10[3′,4′]-furanoanthracene-12,14-dione (**8e**)[10]

Pale yellow solid, 60 mg (yield 53%), mp 263–265 °C. ^{1}H NMR (400 MHz, DMSO-d_6) δ 3.99 (s, 3H), 4.02 (dd, J = 9.2, 3.6 Hz, 1H), 4.25 (d, J = 9.2 Hz, 1H), 5.55 (d, J = 3.6 Hz, 1H), 7.29–7.49 (m, 6H); ^{13}C NMR (100 MHz, DMSO-d_6) δ 36.7 (CH), 45.6 (CH), 47.1 (CH), 54.2 (CH3), 81.1 (C), 120.7 (CH), 120.8 (CH), 127.4 (CH), 127.8 (CH), 128.4 (CH), 129.1 (CH), 129.2 (C), 129.3 (C), 133.7 (C), 136.2 (C), 142.6 (C), 143.3 (C), 168.2 (C), 170.3 (C); IR (KBr/cm^{-1}) 1782, 1224, 773; HRMS (APCI-TOF) Calcd. for $[M+H]^+$ $C_{19}H_{13}Cl_2O_4$: 375.0185, found 375.0220.

f. Reaction Monitoring on Pseudo-First-Order

To a solution of maleic anhydride (50 mg, 0.5 mmol) in $CDCl_3$ (0.5 mL), anthracene **3–5** (0.05 mmol) was added, and the mixture was carefully transferred to the NMR tube. The residue was recollected by dissolving with another $CDCl_3$ (0.1 ml) and transferred to the NMR tube. After adding 1,1,2,2-tetrachloroethane as an internal standard, the NMR tube was heated at 60 °C. The progress of the reaction was monitored by ^{1}H NMR spectroscopy at intervals of several minutes. This procedure was conducted in three replications for each anthracene to

afford an average value.

7. References

1. Armon, A. M.; Bedi, A.; Borin, V.; Schapiro, I.; Gidron, O. *Eur. J. Org. Chem*. **2021**, *39*, 5424−5429.
2. Dobrowolski, M. A.; Cyrański, M. K.; Merner, B.L.; Bodwell, G. J.; Wu, J. I.; Schleyer P. V. R. *J. Org. Chem*. **2008**, *73*, 8001−8009.
3. Biswas, S.; Qiu, C. S.; Dawe, L. N.; Zhao, Y.; Bodwell, G. J. *Angew. Chem. Int. Ed*. **2019**, *58*, 9166−9170.
4. (a) Bodwell, G. J.; Fleming, J. J.; Miller, D. O. *Tetrahedron* **2001**, *57*, 3577−3585; (b) Aida, Y.; Nogami, J.; Sugiyama, H.; Uekusa, H.; Tanaka, K. *Chem. Eur. J*. **2020**, *26*, 12579−12588.
5. Qiao, X.; Padula, M. A.; Ho, D. M.; Vogelaar, N. J.; Schutt, C. E.; Pascal, R. A. *J. Am. Chem. Soc*. **1996**, *118*, 741−745.
6. Dobrowolski, M. A.; Cyrański, M. K.; Wróbel, Z. *Phys. Chem. Chem. Phys*. **2016**, *18*, 11813−11820.
7. House, H.; Ghali, N. I.; Haack, J. L.; Vanderveer, D. *J. Org. Chem.* **1980**, *145*, 1807−1817.
8. Yamashita, M.; Yamamoto, Y.; Akiba, K. Y.; Hashizume, D.; Iwasaki, F.; Takagi, N.; Nagase, S. *J. Am. Chem. Soc*. **2005**, *127*, 4354−4371.
9. Toyota, S.; Onishi, H.; Kawai, Y.; Morimoto, T.; Miyahara, H.; Iwanaga, T.; Wakamatsu, K. *Org. Lett*. **2009**, *11*, 321−324.
10. Meek, J. S.; Koh, L. L.; *J. Org. Chem*. **1968**, *33*, 2942−2946.
11. (a) Muller, P.; Fronczek, F. R.; Smith, S. J.; Mako, T.; Levine, M. *Acta Crystallogr. Sec. C.* **2013**, *69*, 199−203.; (b) Niermeier, P.; Lamm, J. H.; Peters, J. H.; Neumann, B.; Stammler, H. G.; Mitzel, N. W. *Synthesis* **2019**, *50*, 1623−1632.
12. Haddon, R. C. *Acc. Chem. Res*. **1988**, *21*, 243−249.

13. (a) Sinha, R. K.; Pradhan, B.; Wategaonkar, S.; Singh, B. P.; Kundu, T. *J. Chem. Phys*. **2007**, *126*, 114312−114319; (b) Xia, C. J.; Fang, C. F.; Zhao, P.; Xie, S. J.; Liu, D. S. *Phys. Lett. A*. **2009**, *41*, 3787−3794; (c) Kasemthaveechok, S.; Abella, L.; Crassous, J.; Autschbach, J.; Favereau, L. *Chem. Sci*. **2022**, 13, 9833−9847; (d) Sicard, L.; Lucas, F.; Jeannin, O.; Bouit, P. A. Rault-Berthelot, J.; Quiton, C.; Poriel, C. *Angew. Chem. Int. Ed*. **2020**, *59*, 110662−11072.

14. (a) Yamabe, S.; Dai, T.; Minato, T. *J. Am. Chem. Soc.* **1995**, *117*, 10994–10997; (b) Linder, M.; Brinck, T. *Org. Biomol. Chem*. **2009**, *7*, 1304–1311; (c) Vermeeren, P.; Hamlin, T. A.; Bickelhaupt, F. M. *Phys. Chem. Chem. Phys*. **2021**, *23*, 20095–20106.

15. Gaussian 09, Revision A.02, M. J. Frisch, G. W. Trucks, H. B. Schlegel, G. E. Scuseria, M. A. Robb, J. R. Cheeseman, G. Scalmani, V. Barone, B. Mennucci, G. A. Petersson, H. Nakatsuji, M. Caricato, X. Li, H. P. Hratchian, A. F. Izmaylov, J. Bloino, G. Zheng, J. L. Sonnenberg, M. Hada, M. Ehara, K. Toyota, R. Fukuda, J. Hasegawa, M. Ishida, T. Nakajima, Y. Honda, O. Kitao, H. Nakai, T. Vreven, J. A. Montgomery Jr., J. E. Peralta, F. Ogliaro, M. Bearpark, J. J. Heyd, E. Brothers, K. N. Kudin, V. N. Staroverov, T. Keith, R. Kobayashi, J. Normand, K. Raghavachari, A. Rendell, J. C. Burant, S. S. Iyengar, J. Tomasi, M. Cossi, N. Rega, J. M. Millam, M. Klene, J. E. Knox, J. B. Cross, V. Bakken, C. Adamo, J. Jaramillo, R. Gomperts, R. E. Stratmann, O. Yazyev, A. J. Austin, R. Cammi, C. Pomelli, C. Ochterski, J. W. Martin, R. L. Morokuma, K. Zakrzewski, V. G. Voth, P. Salvador, J. J. Dannenberg, S. Dapprich, A. D. Daniels, O. Farkas, J. B. Foresman, J. V. Ortiz, J. Cioslowski, D. J. Fox, Gaussian, Inc., Wallingford CT, **2016**.